

# Site U1304<sup>1</sup>

Expedition 303 Scientists<sup>2</sup>

## Chapter contents

Background and objectives .....	1
Operations .....	2
Lithostratigraphy .....	3
Biostratigraphy .....	5
Paleomagnetism .....	8
Composite section .....	8
Geochemistry .....	9
Physical properties .....	11
References .....	12
Figures .....	14
Tables .....	53

## Background and objectives

The objective at Integrated Ocean Drilling Program Site U1304 was to obtain a high-resolution (high sedimentation rate) Pliocene–Quaternary environmental record from a location within the central Atlantic ice-raftered debris (IRD) belt, at a water depth sufficient to sample North Atlantic Deep Water (NADW). A partially enclosed basin at the southern limit of the Gardar Drift just to the north of the Charlie Gibbs Fracture Zone provided a suitable location with water depth of 3024 m (Fig. F1). This basin lies to the east of the Reykjanes Ridge on oceanic crust associated with magnetic Anomaly 5 (~10 Ma). The site is located 217 km (117 nmi) west-northwest of Deep Sea Drilling Project Site 611 (Fig. F1), drilled in 1983 on the southern rim of the Gardar Drift. The mean sedimentation rate (in the Brunhes Chron) at Site 611 was found to be 2.7 cm/k.y. The sedimentation rates at Site U1304 are greater by a factor of about six, thereby achieving the objective of recovering a high-sedimentation-rate record in deep water at the southern limit of the Gardar Drift.

Seismic data for positioning of Site U1304 were collected during the *Knorr* KN166-14 cruise in summer 2002. The local bathymetry was determined by SeaBeam survey (Fig. F2). Seismic reflection profiles were collected with the Lamont-Doherty Earth Observatory portable high-resolution acquisition system. A crossing ship track (Fig. F3) yielded high-quality multichannel seismic profiles (Fig. F4) that indicated that the site is optimally positioned in a thick (>900 ms two-way traveltime) well-stratified sediment pile.

A piston core from this location (Core HU91-045-080P) collected during the 1991 cruise of the *Hudson* indicated moderate to high sedimentation rates (~10–15 cm/k.y.), good preservation of siliceous and calcareous microfossils, and the attributes for yielding isotopic and paleomagnetic (paleointensity) age control (Fig. F5). This has been confirmed by another piston core (KN166-14-13JPC) collected during the site survey cruise for Expeditions 303 and 306 conducted by the *Knorr*. Core KN166-14-13JPC, a 23.6 m core, extends into marine isotope Stage (MIS) 6 based on relative paleointensity and susceptibility correlations. Notwithstanding significant top-core stretching in Core KN166-14-13JPC, sedimentation rates appear to be ~10–20 cm/k.y., with elevated sedimentation rates during interglacial stages. Diatom mats are associated with MIS 5 in Core HU91-045-080P and in Core KN166-14-13JPC. Similar diatom mats, dominated by *Thalassiothrix longissima*, have

<sup>1</sup>Expedition 303 Scientists, 2006. Site U1304. In Channell, J.E.T., Kanamatsu, T., Sato, T., Stein, R., Alvarez Zarikian, C.A., Malone, M.J., and the Expedition 303/306 Scientists. Proc. IODP, 303/306: College Station TX (Integrated Ocean Drilling Program Management International, Inc.). doi:10.2204/iodp.proc.303306.104.2006

<sup>2</sup>Expedition 303 Scientists' addresses.



been observed within MIS 5e in Core EW9303-17 (Bodén and Backman, 1996). Core EW9303-17 is located in 3233 mbsl water depth on the west side of the Reykjanes Ridge at 57°N, 37°W, ~500 km (270 nmi) north-northwest of Site U1304.

The presence of diatom mats in the Quaternary of the North Atlantic has not been widely documented. Their occurrence is apparently localized to a narrow subarctic convergence zone between the cold, less saline surface water associated with the Labrador Sea current and the warmer North Atlantic current (see Bodén and Backman, 1996). This narrow convergence zone in the modern North Atlantic meanders northward, crisscrossing the mid-oceanic ridge (Ruddiman and Glover, 1975), and lies close to both Site U1304 and Core EW9303-17.

Diatom mat deposition at Site U1304 was found to be episodic and discontinuous but present throughout the recovered sequence that spans the entire Quaternary. Although some thicker meter-scale mats are present, most are less than a few centimeters in thickness and are intercalated with clays and silts. If diatom deposition can be tied to the subarctic convergence zone, the 1.8 m.y. record recovered at Site U1304 will provide an unprecedented environmental record of movements of the convergence zone during the Quaternary. Good preservation of foraminifers, nannofossils, and diatoms and the potential for paleomagnetic and isotopic age control means that the environmental record comprising sea-surface and bottom-water characteristics, and detrital (Heinrich-type) stratigraphy, can be integrated into a paleointensity-assisted stratigraphy (PAC).

## Operations

### Transit from Site U1303 to Site U1304

After completing operations at Site U1303, the ship departed for proposed Site LAB6A on the Eirik Drift at 1315 h on 6 October 2004. On the morning of 7 October, the daily forecast for Eirik Drift area indicated that a low-pressure system over northwestern Canada was moving eastward and was projected to affect the LAB6A area by the afternoon of 9 October. Eventual storm maximum was predicted to have winds reaching 40–50 kt with gusts to 65 kt by 11 October. After considering the possibility of 4–5 days of weather downtime waiting for the storm to pass, as well as the potential danger to the vessel presented by this system, we decided to alter course to the closest other primary site, GAR2A, at 0840 h on 7 October. We arrived at Site U1304 (GAR2A) at 0630 h on 9 October.

### Hole U1304A

Hole U1304A was spudded with the advanced piston corer (APC) system at 1345 h, returning a full core barrel. Thus, we were unable to establish a seafloor depth. Piston coring continued to 239.0 meters below seafloor (mbsf), taking 26 cores with an average recovery of 105.6% (Table T1). Nonmagnetic core barrels were used for Cores 1H–19H. Core 19H was a partial stroke of the APC, which required employing the drillover procedure to free the core barrel. Consequently, subsequent cores were obtained with standard steel core barrels without running the Tensor tool to reduce the risk of a downhole hardware failure during the drilling-over process. The drillover technique was used for Cores 19H–22H and 24H–26H. Coring operations ceased when the formation became too stiff to continue and shattering of core liners became common. Operations in Hole U1304A concluded when the bit cleared the seafloor at 1945 h on 10 October 2004.

### Hole U1304B

The vessel was offset 20 m southeast of Hole U1304A, and the bit was positioned 5 m shallower than for Hole U1304A (3075.0 meters below rig floor [mbrf]). Hole U1304B was spudded with the APC at 2105 h on 10 October 2004. The recovery of the initial core was 8.14 m, which suggested a seafloor depth of 3065 meters below sea level (mbsl) (3076.3 mbrf; 9.1 m shallower than the precision depth recorder depth), albeit with a nearly full core. Piston coring advanced the hole to a final depth of 242.4 mbsf with an average recovery of 104.0% (Table T1). Nonmagnetic core barrels were used through Core 19H, and subsequent cores were obtained with the standard core barrels without the Tensor tool. Cores 20H and 26H were advanced by recovery, and drillover was used to obtain Cores 20H, 21H, 24H, and 25H. Operations in Hole U1304B ended when the bit cleared the seafloor at 0215 h on 12 October.

### Hole U1304C

The ship was offset 20 m southeast of Hole U1304B, and Hole U1304C was spudded with the APC at 0445 h on 12 October 2004. Based on the 4.6 m recovery in the initial core, the calculated seafloor depth is 3064.5 mbsl (3075.4 mbrf). Piston coring advanced to 69.6 mbsf, when operations had to be terminated because of deteriorating weather conditions. The passage of a cold front during the early morning hours of 12 October was accompanied by wind gusts as high as 50 kt, a steady 20–25 kt wind, and 16–18 ft seas, which caused vessel heave to exceed 4 m. These



conditions made it difficult to successfully land the core barrel without prematurely parting the shear pin of the corer and compromising the quality of the cores. At 1425 h, the bit was pulled clear of the seafloor, ending operations in Hole U1304C.

### Hole U1304D

From 1430 to 1745 h, the ship remained positioned at the site with the drill string suspended above the seafloor waiting for the weather to abate. At 1745 h, the vessel was offset 20 m southeast of Hole U1304C, and Hole U1304D was spudded at 1830 h on 12 October 2004. The hole was drilled with a center bit to 52.0 mbsf, where coring was initiated. The hole was APC cored from 52.0 to 243.9 mbsf with an average recovery of 97.3%, with the exception of the interval from 180.3 to 181.3 mbsf, which was drilled (i.e., not cored). Nonmagnetic core barrels were used through Core 14H, and subsequent cores were obtained with the standard steel core barrels without the deployment of the Tensor tool. Cores 14H and 20H were advanced by recovery, and drillover was used to obtain Cores 15H–17H and 19H–21H. After recovering the drill string and disassembling the bottom-hole assembly for transit, we departed for Site U1305 (LAB6A) at 1230 h on 14 October.

## Lithostratigraphy

Four holes were drilled at Site U1304 to a total depth of 244 mbsf (264 meters composite depth [mcd]) (**T1**). All cores were recovered using the APC. Recovery was excellent in Holes U1304A and U1304B but decreased in Holes U1304C and U1304D because of worsening weather conditions (see “**Operations**”).

The sediments at Site U1304 are predominantly interbedded nannofossil oozes and diatom oozes, with less common intervals of clay and silty clay, which also contain abundant nannofossils and/or diatoms (Figs. **F6**, **F7**, **F8**). The color of the sediments throughout the section is various shades of gray. Most contacts between nannofossil ooze and clay intervals are gradational, although sharp contacts are also observed. The contacts between diatom ooze beds and the other lithologies are generally sharp. Redeposited beds of silt- and sand-sized particles are rare throughout the hole, and disturbed units related to mass-transport processes (e.g., slumps and debris flows) are also rare. Thus, the section cored at Site U1304 apparently represents a relatively continuous pelagic section. The sediments at Site U1304 have been designated as a single unit, composed of Holocene–Upper Pliocene sediments. The various lithologies throughout the hole are generally interbedded on a scale of centimeters to decimeters (see

“**Site U1304 visual core descriptions**” in “Core Descriptions”). These frequent changes of lithology at this scale do not allow for effective subdivision into multiple units or subunits.

## Description of units

### Unit I

Intervals: Sections 303-U1304A-1H-1, 0 cm, to 26H-CC, 25 cm; 303-U1304B-1H-1, 0 cm, to 26H-CC, 10 cm; 303-U1304C-1H-1, 0 cm, to 8H-CC, 13 cm; and 303-U1304D-1H-1, 0 cm, to 21H-CC, 05 cm

Depths: Hole U1304A: 0–239.46 mbsf, Hole U1304B: 0–242.45 mbsf, Hole U1304C: 0–69.38 mbsf, and Hole U1304D: 52.0–243.74 mbsf (0–263.8 mcd)

Age: Holocene–Late Pliocene

Unit I is composed predominantly of interbedded nannofossil ooze (Fig. **F6**) and diatom ooze (Figs. **F7**, **F8**). Additional lithologies recognized are nannofossil ooze with clay, nannofossil ooze with silty clay, nannofossil ooze with diatoms, nannofossil ooze with foraminifers, diatom ooze with clay, diatom ooze with nannofossils, clay, silty clay, silty clay nannofossil ooze, silty sand with diatoms, and foraminifer sand. The colors of the nannofossil ooze are generally gray (5Y 6/1 and 5Y 5/1), dark gray (5Y 4/1), greenish gray (5GY 5/1), and olive-gray (5Y 4/2 and 5Y 6/2) (Fig. **F6**). The diatom ooze is highly laminated and displays an even wider range of colors including gray (5Y 6/1 and 5Y 5/1), greenish gray (5GY 5/1), dark greenish gray (5GY 4/1), dark olive-gray (5Y 4/2), light olive-gray (5Y 6/2 and 7Y 6/2), and pale yellow (5Y 7/3) (Figs. **F7**, **F8**). Colors of the other lithologies are predominantly gray (5Y 6/1 and 5Y 5/1), dark gray (5Y 4/1), and very dark gray (e.g., Fig. **F6**). In contrast to these gray colors, the upper 13 cm of sediments in Hole U1304B (interval 303-U1304B-1H-1, 0–13 cm), which occurs just below the sediment/water interface, is brown nannofossil ooze and has a zone of iron oxide laminae from 9 to 11 cm. Intervals of similar brown sediment with this iron-rich zone were observed in the uppermost sediments of Sites U1302 and U1303 and, in fact, have been previously observed in the uppermost meter of seafloor sediments in numerous cores taken throughout the world ocean (e.g., McGahey and Damuth, 1973; Damuth, 1977, and references therein).

Contacts between the various lithologies are generally gradational, except for contacts between diatom ooze and other lithologies, which are sharp (Figs. **F6**, **F8**). However, sharp contacts between the other lithologies are rare. Bioturbation is ubiquitous throughout this unit in all lithologies except the dia-



tom oozes. Most sediments are moderate to heavily burrowed and are recognized by subtle centimeter-scale color mottling or by millimeter-scale pyritic burrow fills. In a few cases, discrete burrows or discrete macroscopic pyritized burrows were observed.

Intervals of laminated diatom ooze comprise much of the section in Unit I. The intervals in which the diatom ooze dominates the lithology are 30–60, 85–115, and 180–265 mcd (Fig. F9). The beds of diatom ooze generally show millimeter-scale laminations, which are more apparent in sections split by saw blades. In contrast, sections split by pulling a wire through the core tends to destroy the millimeter-scale structure because of the resistance of the diatom mats to the wire (Figs. F7, F8). Nearly all individual beds of diatom ooze are centimeter or decimeter scale, and individual beds are commonly separated by laminae and thin beds of nannofossil ooze. Only in interval 303-U1304A-19H-1, 0 cm, to 19H-CC, 21 cm (171.0–175.0 mbsf), are beds thicker than 1 m, and here the entire core is composed of diatom ooze.

Beds of discrete silt- and sand-sized particles are rare throughout Unit I. Where present, these beds are only centimeters thick and are predominantly composed of foraminifer sand. These beds appear to be formed by winnowing by bottom currents. Redeposited sediments formed by mass-transport processes are also rare throughout Unit I. Interval 303-U1304B-19H-3, 107–138 cm, contains a deposit of deformed, folded nannofossil ooze and diatom ooze, which is interpreted as a 31 cm thick intraformational slump deposit (Fig. F10). Interval 303-U1304B-24H-6, 136 cm, to 24H-CC, 21 cm, appears to be a disturbed interval with numerous rock clasts of granule to gravel size and is probably a small debris flow deposit. Interval 303-U1304B-26H-1, 0 cm, to 26H-2, 145 cm, and 26H-4, 65 cm, to 26H-5, 55 cm, also appear to be small slumps or debris flows. Dropstones are absent to rare throughout much of the section, and where present, only a few per 10 cm interval were observed (Fig. F11). Total carbonate contents range from 4 to 71 wt% in these cores (see “Geochemistry” and “Site U1304 smear slides” in “Core descriptions”). Pyrite (usually associated with burrow fills; e.g., Fig. F6) and iron oxide coatings on grains are common and are the only authigenic sediment components observed.

Abundances of terrigenous components, as estimated from smear slides, are quartz, 0%–90%; detrital carbonate, 0%–50%; feldspars, 0%–15%; clay minerals (including chlorite), 0%–70%; heavy minerals (especially hornblende), 0%–1%; and volcanic glass, 0%–3% (note: one slide had 70%). Abundances

of biogenic components, as estimated from smear slides, are nannofossils, 0%–95%; foraminifers, 0%–65%; diatoms, 0%–90%; radiolarians, 0%–1%; and sponge spicules, 0%–1% (see “Site U1304 smear slides” in “Core descriptions”). Figure F12 shows downhole plots for diatoms, quartz, and nannofossils for all smear slides. In general, quartz and diatom contents appear to be relatively low between 50 and 95 mcd. Figure F13 shows downhole plots for coccoliths, diatoms, quartz, detrital carbonate, and clay using only smear slide data from nannofossil ooze layers. Although no strong trends are observed, diatom content in general tends to increase upsection, whereas the quartz content apparently decreases.

## Discussion

The sediments at Site U1304 represent mainly pelagic deposition. This is clearly demonstrated by comparison of digital imaging system core images from Holes U1304A and U1304B. When the same intervals from each hole are compared side by side, individual beds, especially the laminated diatom oozes, correlate extremely well. This correlation indicates the absence of significant reworking of sediments by bottom currents, as well as input of sediment from downslope processes such as turbidity currents and related gravity-controlled mass flows. Thus, we accomplished the objective at Site U1304 to obtain a high-resolution Pliocene–Quaternary pelagic record from within the central Atlantic IRD belt at a water depth sufficient to sample NADW (Fig. F9).

The most striking sediments recovered at Site U1304 are the thick deposits of laminated diatom ooze (Figs. F7, F8, F9). The presence of these thick diatom ooze layers in the Quaternary sediments of the North Atlantic was only recently discovered by Bodén and Backman (1996), who recovered a 3 m section of laminated diatom ooze (termed “LDO” by them) in Ewing Core EW9303-17. The LDO section occurs only in Stage 5e and consists of *Thalassiothrix longissima*. However, this core recovered only MIS 3–6. The occurrence of LDOs is apparently localized to a narrow subarctic convergence zone between the cold, less saline surface water associated with the Labrador Sea Current and the warmer North Atlantic Current. Site U1304 sediments show that thick LDOs have not been accumulating at this site during the latest Quaternary (Fig. F9); however, Site U1304 extends the record of LDO accumulation back to the Late Pliocene and shows that thick LDO successions accumulated periodically at this site since at least that time (Fig. F9). Postcruise studies should reveal whether the LDO deposition can be tied to the sub-



arctic convergence zone and, if so, Site U1304 will provide a 1.8 m.y. record of movements of the convergence zone during the Quaternary.

## Biostratigraphy

Recurring laminated diatom-rich sequences are the most prominent feature in all holes drilled at Site U1304 (Fig. F14). Diatom assemblages are dominated by needle-shaped species of the *Thalassiothrix-Lion-sloma* complex. All other groups investigated (coccoliths, planktonic and benthic foraminifers, radiolarians, and palynomorphs) are present in high to moderate abundance and are well preserved throughout (Tables T2, T3, T4, T5, T6, T7, T8, T9, T10, T11, T12, T13, T14, T15, T16, T17). Biostratigraphic datums mainly derive from coccoliths and are consistent with datums provided by diatoms, planktonic foraminifers, and dinocysts (Fig. F15). Accordingly, the first occurrence (FO) of encrusted *Neogloboquadrina pachyderma* (sinistral) indicates that the composite sequence of Site U1304 should have its base in the Olduvai Subchron. The FO of *Gephyrocapsa caribbeanica* (1.73 Ma) close to the base of the section indicates that the entire Pleistocene is represented. The microfossil assemblages indicate only minor redeposition of sediments at Site U1304.

Preliminary paleoceanographic and paleoclimatic interpretation of the microflora and microfauna reveals large-amplitude changes in surface water temperature and trophic conditions. Diatom layers were formed during both cold and warm phases according to the species composition of diatom and planktonic foraminifer assemblages (Fig. F16). A shift from dominance of autotrophic to dominance of heterotrophic dinocyst taxa is recorded at ~1.2 Ma. This may suggest a general change in trophic conditions of the surface ocean. The presence of the benthic foraminifer *Epistominella exigua* documents recurring pulses of fresh organic matter reaching the seafloor (Fig. F16).

### Calcareous nannofossils

Calcareous nannofossils were examined in all core catcher samples from Holes U1304A–U1304D (Tables T2, T3, T4, T5). Several additional samples were examined to refine the depth of biostratigraphic datums. All samples are characterized by well to moderately well preserved and abundant calcareous nannofossils except Samples 303-U1304A-3H-CC, 18H-1, 0–1 cm, 19H-CC, and 21H-CC; 303-U1304B-13H-CC; 303-U1304C-4H-CC; and 303-U1304D-14H-CC, 15H-CC, and 20H-CC (Fig. F14). The assemblages are dominated by small-sized coccoliths of *Gephyrocapsa* spp. and *Reticulofenestra* spp. Reworked

nannofossils from the Cretaceous–Miocene occur throughout the sections.

Ten Quaternary nannofossil datums defined by Sato et al. (1999) are detected in the sequences at Site U1304 (Fig. F15). The FO of *Emiliania huxleyi* (0.25 Ma) and last occurrence (LO) of *Pseudoemiliania lacunosa* (0.41 Ma), which are situated in Brunhes Chron, are found in Samples 303-U1304A-4H-CC, 303-U1304B-4H-CC, and 303-U1304C-5H-CC and in Samples 303-U1304A-7H-CC, 303-U1304B-8H-CC, 303-U1304C-8H-CC, and 303-U1304D-2H-CC, respectively (Tables T2, T3, T4, T5). Both the LO of *Reticulofenestra asanoi* (0.85 Ma) and the FO of *Gephyrocapsa parallela* (0.95 Ma) are correlated to the interval between the base of the Brunhes Chron and the top of the Jaramillo Subchron of the Matuyama Chron and are detected in Samples 303-U1304A-14H-CC, 303-U1304B-15H-CC, and 303-U1304D-9H-CC, and in Samples 303-U1304A-15H-CC, 303-U1304B-16H-CC, and 303-U1304D-10H-CC, respectively. The FO of *R. asanoi* (1.16 Ma), situated just below the Jaramillo Subchron, occurs in Samples 303-U1304A-17H-CC, 303-U1304B-18H-CC, and 303-U1304D-12H-CC. Large forms of *Gephyrocapsa* spp. occur from 1.45 to 1.21 Ma and are detected in Samples 303-U1304A-18H-7, 50–51 cm, to 20H-CC; 303-U1304B-19H-CC to 21H-CC; and 303-U1304D-13H-CC to 15H-CC. The LO of *Helicosphaera sellii*, which is dated at 1.27 Ma, is found in Samples 303-U1304A-18H-CC, 303-U1304B-20H-CC, and 303-U1304D-15H-CC.

The oldest two nannofossil datums recognized are the FOs of *Gephyrocapsa oceanica* (1.65 Ma) and *G. caribbeanica* (1.73 Ma), situated in Samples 303-U1304A-24H-CC, 303-U1304B-24H-CC, and 303-U1304D-19H-CC. Assemblages found in samples below these datums are characterized by small *Gephyrocapsa* and *Calcidiscus macintyreui* and by the absence of *G. caribbeanica*, *G. oceanica*, and *Discoaster brouweri*. This suggests that the lowermost samples of Holes U1304A, U1304B, and U1304D correspond to the uppermost Pliocene between 1.97 and 1.73 Ma (Fig. F15).

### Planktonic foraminifers

Planktonic foraminifers were examined in all core catcher samples from Holes U1304A–U1304D (Table T6, T7, T8, T9). Diatom-rich sediments were washed, and foraminiferal tests were separated from diatoms by decanting the diatom frustules. A certain proportion of the foraminiferal tests present in the sample were probably lost due to this procedure. Some planktonic foraminiferal assemblages within diatom oozes are dominated by small-sized tests. Within diatom-poor sediments, planktonic foraminifers are



abundant (>50% of all particles >63 µm) and well preserved. Planktonic foraminiferal tests were absent only in Sample 303-U1304D-16H-CC.

The dominant planktonic foraminiferal species are *N. pachyderma* (sinistral), *Globorotalia inflata*, or *Globigerina bulloides*. Most of the *N. pachyderma* (sinistral) tests are encrusted. *N. pachyderma* (sinistral) is almost continuously present downcore (Fig. F14). The FO of encrusted *N. pachyderma* (sinistral) lies between Samples 303-U1304A-26H-CC and 303-U1304B-25H-CC and is assigned to the boundary between the *N. pachyderma* (sinistral) Zone and the *G. inflata* Zone (Weaver and Clement, 1987) at the top of the Olduvai Subchron (Fig. F14). Tests of *N. pachyderma* (sinistral), present in minor amounts in Sample 303-U1304D-21H-CC, are not encrusted. Consequently, Sample 303-U1304D-21H-CC is placed in the *G. inflata* Zone (Weaver and Clement, 1987). The occurrence of the extinct species *Neogloboquadrina atlantica* and *Globigerina decoraperta* in a few sections from Holes U1304B and U1304D was possibly caused by sediment reworking. *Turborotalita quinqueloba* (sinistral and dextral) and *N. pachyderma* (dextral) are abundant, and *Globigerinita glutinata* is rare in many sections. Tropical and subtropical species (*Globigerinoides ruber*, *Globigerinoides trilobus*, *Globigerinella siphonifera*, and *Orbulina universa*) and deep-dwelling species (e.g., *Globorotalia truncatulinoides*) are sporadically present. All of these species are present in the modern North Atlantic.

An alternation of subpolar/polar species (*N. pachyderma* [sinistral]) and temperate species (e.g., *G. bulloides* and *N. pachyderma* [dextral]) occurs throughout the studied core intervals (Table T6, T7, T8, T9). The variable frequency of *G. bulloides* and *G. inflata* suggests changing trophic conditions. The dominance of *G. bulloides* indicates distinct seasonality and phytoplankton blooms (Schiebel and Hemleben, 2002). *Globorotalia inflata* is generally considered a “frontal species,” and its dominance during many intervals indicates a front-dominated hydrography (Fig. F16). Tropical species indicate rare intrusions of warm surface waters by the Gulf Stream. *G. truncatulinoides* is distributed by currents around the subtropical gyres and occasionally to higher latitudes and indicates rare intrusions of subsurface water masses from the south.

### Benthic foraminifers

Benthic foraminifers were examined in all core catcher samples from Holes U1304A–U1304D. *E. exigua* and other small-sized and thin-walled taxa (e.g., *Gavelinopsis*) are most abundant. *Pullenia quinqueloba* and *Pullenia bulloides* are frequent throughout the cores. Occasionally, *Globobulimina* sp. dominates the

benthic foraminiferal assemblage. Agglutinated taxa are rare (Table T10).

The presence of *E. exigua* suggests flux pulses of fresh organic matter formed during phytoplankton blooms (Gooday, 1993). *Globobulimina* is characteristic of high-nutrient, low-oxygen conditions (Lutze, 1980; Jorissen et al., 1995). Both species indicate frequent sedimentation of large amounts of surface-derived organic matter to the seafloor throughout the Pleistocene (Fig. F16).

### Diatoms

Diatom assemblages were investigated in all core catcher samples and several additional samples from Holes U1304A–U1304D (Tables T11, T12, T13, T14). Diatoms are abundant or common throughout the sedimentary sequence (Fig. F14) and are very well to moderately well preserved. Monospecific diatom layers occur at several depths and are mainly composed of needle-shaped diatoms of the *Thalassiothrix-Lioloma* complex. Additionally, some thinner diatom layers composed of other genera are observed. Four silicoflagellate species and the siliceous dinoflagellate *Actiniscus pentasterias* are observed throughout, and sponge spicules occur in some samples.

Four diatom zones following the zonation of Koç et al. (1999) are assigned using three diatom datum events (Fig. F15; Tables T11, T12, T13, T14). The LO of *Proboscia curvirostris*, which defines the base of the *Thalassiosira oestrupii* Zone and the top of the *P. curvirostris* Zone (0.3 Ma, MIS 9; Koç et al., 1999), is found between Samples 303-U1304A-4H-CC and 5H-CC, 303-U1304B-4H-CC and 5H-CC, and 303-U1304C-6H-CC and 7H-CC. The LO of *Neodenticula seminae* (0.84–0.85 Ma, MIS 21; Koç et al., 1999) lies between Samples 303-U1304A-13H-CC and 14H-CC, 303-U1304B-13H-CC and 14H-CC, and 303-U1304D-8H-CC and 9H-CC. The FO of *N. seminae* (1.25–1.26 Ma, MIS 37; Koç et al., 1999) is between Samples 303-U1304A-17H-CC and 18H-CC, 303-U1304B-18H-CC and 19H-CC, and 303-U1304D-12H-CC and 13H-CC. Intervals below the *N. seminae* Zone are placed in the *Fragilaropsis reinholdii* Zone (1.25 through ~1.89 Ma; Koç et al., 1999).

The diatom association at Site U1304 is rich in species (>95 diatom taxa are recognized). The most striking feature is the presence of thick diatom layers in several horizons, mainly composed of needle-shaped forms of the *Thalassiothrix-Lioloma* complex (Tables T11, T12, T13, T14). The occurrence of very thick diatom-rich deposits in the open North Atlantic is possibly related to intensified surface circulation leading to the development of frontal systems (Kemp and Baldauf, 1993; Bodén and Backman, 1996). The diatom mats reveal repeated episodes of



increased primary production between ~1.8 Ma and the Holocene (Fig. F16).

Several thinner diatom mats (<25 cm) are frequent throughout the sediment sequence at Site U1304. These diatom sequences are almost monospecifically composed of *Coscinodiscus* spp. (Samples 303-U1304A-5H-4, 84 cm; 21H-3, 124 cm; and 303-U1304B-1H-6, 30 cm), *Rhizosolenia* spp. (Samples 303-U1304A-23H-1, 148 cm, and 25H-CC), vegetative cells of *Chaetoceros concavicornis* (Samples 303-U1304A-1H-1, 12 cm; 21H-3, 124 cm; and 303-U1304B-1H-6, 30 cm), and resting spores of *Chaetoceros* spp. (Sample 303-U1304C-2H-7, 40 cm). The continuous influence of the warm North Atlantic water masses at the site is indicated by the presence of *Fragilariopsis doliolus*, *Coscinodiscus asteromphalus*, *C. marginatus*, *T. oestrupii* var. *oestrupii*, and *T. oestrupii* var. *venrickae* (Andersen et al., 2004). The influence of colder northern water masses is indicated by the occurrence of *Actinocyclus curvatulus*, forms of *Rhizosolenia hebetata*, and vegetative cells of *Thalassiosira gravida*, which is typical of subarctic and arctic waters (Andersen et al., 2004). The co-occurrence of both warm and cold assemblages suggests the existence of a hydrographic front between subpolar and temperate water masses near Site U1304 during the Pleistocene.

## Radiolarians

Radiolarians were examined in all core catcher samples from Holes U1304A and U1304B (Table T15). In general, radiolarians are abundant to common and preservation is good (Table T15). In the diatomaceous oozen, only a few radiolarians are present because of dilution by diatoms (Fig. F14).

Abundant species and species groups are *Cycladophora davisiana davisiana*, *Stylochlamidium venustum*, *Spongodiscus* spp., and *Actinomma leptodermum*. *Pylospira* sp., *P. octopyle*, and *Pseudodictyophimus* sp. are abundant in the laminated diatomaceous oozen. Several species of theoperids, pterocorythids, aristostrobiids, and cannabotryids also occur in these samples, and species diversity is generally high. *A. leptodermum* is common to abundant in calcareous oozen of the middle part of Holes U1304A and U1304B and is relatively rare in the diatom oozen.

*C. davisiana davisiana* occurs almost throughout Holes U1304A and U1304B. The sequences are therefore assigned to the Upper Pliocene–Pleistocene *C. davisiana davisiana* Zone of Goll and Bjørklund (1989).

## Palynomorphs

Palynological assemblages were examined in core catcher samples from Holes U1304A and U1304D.

Samples were extremely difficult to process because of the abundance of diatoms. Two sampling protocols were used. Sediment samples from Hole U1304A were processed using heavy liquid separations, allowing palynological observations in all samples (Table T16). This preparation may result in underestimation of the palynomorph abundances because the small organic particles might be trapped and entrained within the diatom network. Sediment samples from Hole U1304D were processed without heavy liquid separation. In this case, the abundant diatom remains made palynological examination possible only in samples containing a very high number of dinocysts (Table T17).

Many samples from Holes U1304A and U1304B contain diversified palynological assemblages with extremely abundant dinocysts (Fig. F14). In some samples, the dinocyst concentration is higher than  $10^4$  cysts/cm<sup>3</sup>. Most assemblages are dominated by *Brigantedinium* spp. cysts, which are produced by heterotrophic *Protoperidinium* dinoflagellates feeding on diatoms and are common in estuarine and epicontinental domains as well as upwelling areas. Abundant *Protoperidinium* dinoflagellates in the open ocean constitutes a peculiarity that could be related to the extremely high diatom production (Fig. F14).

The composition of dinocyst assemblages suggests three ecostratigraphic zones (Fig. F15):

1. The upper part of Holes U1304A (Samples 303-U1304A-1H-CC to 9H-CC; i.e., down to ~100 mcd) and U1304D (Samples 303-U1304D-1H-CC to 4H-CC, i.e., down to ~98 mcd) are dominated by *Brigantedinium*.
2. In the middle part of Hole U1304A (Samples 303-U1304A-10H-CC to 19H-CC) and Hole U1304D, *Brigantedinium* spp. is often common or abundant but does not always dominate the assemblage. Autotrophic Gonyaulacales dinoflagellates may also be abundant, such as *Impagidinium aculeatum*, *Operculodinium centrocarpum*, *Spiniferites membranaceus*, or *Nematosphaeropsis labyrinthica*.
3. In the lower part of the Holes U1304A (Samples 303-U1304A-20H-CC to 26H-CC) and U1304B, below ~200 mcd, the dinocyst concentration is lower. The assemblages are dominated by Gonyaulacales *I. aculeatum*, *O. centrocarpum*, or *Filisphaera filifera*, whereas *Brigantedinium* is a minor component.

In the three zones mentioned above, large changes in concentration and species composition of assemblages suggest large-amplitude variability in sea-surface conditions including temperature, salinity, and nutrient availability.

The dinocyst assemblages contain a few species that are biostratigraphically useful. *I. velorum* and *F.*



*filifera* record their LO in the North Atlantic at ~0.4 and 0.7 Ma, respectively (cf. de Vernal et al., 1992). The presence of *I. velorum* in Sample 303-U1304A-8H-CC suggests an age of at least 0.4 Ma at 89 mcd, and the presence of *F. filifera* in Sample 12H-CC indicates an age of ~0.7 Ma at 131 mcd (Fig. F15).

The palynological assemblages include small numbers of palynomorphs of terrestrial or terrigenous origin. There are few to common *Pinus* pollen grains, which are wind transported over very long distances. Reworked palynomorphs are rare in examined samples, except in Sample 303-U1304A-15H-CC (Fig. F14).

## Paleomagnetism

The natural remanent magnetization of the archive half-core sections of Site U1304 were measured and then remeasured after alternating-field (AF) demagnetization in peak fields of up to 20 mT. Cores 303-U1304A-1H through 7H and 17H through 26H were AF demagnetized at peak fields of 10 and 20 mT. Cores 303-U1304A-8H through 13H were AF demagnetized at peak fields of 20 mT. Cores 303-U1304A-14H through 16H were AF demagnetized at 10 mT. It appears that the viscous magnetization component was removed and the characteristic magnetization revealed at peak fields of 10 mT; therefore, all subsequent sections from Holes U1304B, U1304C, and U1304D were only demagnetized to that level.

The magnetization intensity before and after AF demagnetization and the inclination and declination obtained after AF demagnetization are shown in Figures F17, F18, F19. Data associated with intervals identified as drilling slurry, affected by drilling disturbance, or exceptionally coarse grained deposits (see “[Lithostratigraphy](#)”) were culled. Intensities are in the  $10^{-1}$  A/m range for most intervals (Fig. F18). Intervals rich in diatom oozes (see “[Lithostratigraphy](#)”) are, however, less strongly magnetized, with intensities in the  $10^{-3}$  A/m range. Based on the differences in both intensity and direction before and after demagnetization, it appears that viscous magnetization components are removed after AF demagnetization at peak fields of 10 mT. Little difference in magnetization direction or intensity is observed between 10 and 20 mT, suggesting that the characteristic magnetic directions are generally adequately defined by the 10 mT step. Inclinations associated with both normal and reversed polarity intervals vary around the expected values (approximately  $\pm 69^\circ$ ) for a geocentric axial dipole (Fig. F18). Declinations are consistent within core. Tensor tool-corrected declinations reveal clear polarity zone boundaries (Fig. F19). Holes U1304A and U1304B

document an almost continuous sequence recording the Brunhes and much of the Matuyama Chronozones, the Jaramillo Subchronozone and Cobb Mountain Subchronozone, and a fraction of the Olduvai Subchronozone. The polarity transition at the top of the Olduvai polarity subchronozone is observed near the base of the recovered sections at ~260–265 mcd (Table T18).

For a few intervals, polarity interpretations are ambiguous. In the diatom ooze at 195–204 mcd, below the Cobb Mountain Subchronozone, AF demagnetization at peak fields of 10 or 20 mT did not succeed in removing a normal polarity magnetic overprint (Fig. F18). In Hole U1304A, the lower Jaramillo polarity transition is apparent in declination (Fig. F19) but is poorly defined in inclination. Hole U1304B clearly shows the transition from normal to reversed polarity in both declination and inclination. Overall, Holes U1304A and U1304B give very consistent records of past polarity changes when plotted versus meters composite depth.

Hole U1304C only penetrated part of the Brunhes Chronozone with poor core quality due to heavy swell (see “[Operations](#)” and “[Lithostratigraphy](#)”). Drilling in Hole U1304D continued through to the Olduvai normal subchronozone. Holes U1304C and U1304D document a discontinuous record due to a number of disturbed sections caused by poor weather conditions.

No geomagnetic excursions were recorded in sediments from the Brunhes Chronozone. Short intervals of normal polarity are recognized in Holes U1304A and U1304B during the Matuyama Chronozone below the Cobb Mountain Subchronozone. These might reflect the Gardar and/or the Gilsa geomagnetic events previously identified at Ocean Drilling Program Leg 162 Sites 983 and 984 (Channell et al., 2002). Tables T18 and T19 summarize the depths (mbsf and mcd) of polarity zone boundaries identified in the different holes at Site U1304 and their correlation to the geomagnetic polarity timescale (Cande and Kent, 1995).

## Composite section

Cores were initially depth-shifted on the basis of magnetic susceptibility data collected with the “Fast Track” magnetic susceptibility core logger (MSCL) soon after recovery. The correlation was refined once density, natural gamma radiation (NGR), and color reflectance data were available from the multisensor track (MST) and archive multisensor track. Magnetic susceptibility and NGR proved most useful for correlating between holes at Site U1304. Features in the magnetic susceptibility and NGR profiles are well



aligned between Holes U1304A and U1304B, as these cores were not significantly stretched, squeezed, or disturbed during the coring process (e.g., Fig. F20). The offsets and composite depths are listed in Table T20. Good weather conditions during the early occupation of Site U1304 led to excellent recovery in both Holes U1304A and U1304B. Weather deteriorated as coring in Hole U1304C began, and the condition of the recovered cores was generally poor. Because of the highly disturbed nature of Cores 303-U1304C-2H, 3H, and 7H, it was not possible to correlate this core to the other holes. Ship heave also disrupted some of the cores from Hole U1304D, resulting in no correlation for Core 303-U1304D-4H. In the deeper sections of Hole U1304D, core quality was variable and some sections are well correlated with Holes U1304A and U1304B, whereas others are clearly disturbed.

The sections of core used for the splice are identified in Table T21. The spliced composite section mainly consists of sections from Holes U1304A and U1304B. We generally avoided using sections from Holes U1304C and U1304D because of core disturbance. Two short segments from Cores 303-U1304D-18H and 19H were needed in the splice to fill core breaks in Holes U1304A and U1304B. The cores from Site U1304 provide a continuous stratigraphic sequence to ~258.1 mcd with a single potential break in an 8 m thick diatom mat at the base of Cores 303-U1304A-19H, 303-U1304B-19H, and 303-U1304D-14H and the tops of Cores 303-U1304A-20H, 303-U1304B-20H, and 303-U1304D-15H (Figs. F20, F21). These cores were appended to one another at ~199.3 mcd because partial strokes in Cores 303-U1304A-19H and 303-U1304D-14H failed to cover the break between Cores 303-U1304B-19H and 20H.

A growth factor (GF) of 1.12 is calculated by linear regression for all holes at Site U1304, indicating a 12% increase in mcd relative to mbsf (Fig. F22). We used this value of GF to calculate corrected meters composite depth (cmcd) presented in Table T20 to aid in the calculation of mass accumulation rates.

We calculated sedimentation rates using paleomagnetic and biostratigraphic datums. Dinocyst datums were not used because they represent minimum ages. Linear regression provides a mean sedimentation rate of 17.8 cm/k.y. for the last 0.78 m.y. (i.e., Brunhes Chronozone) (Fig. F23). Sedimentation rates decrease to 12.2 cm/k.y. for the interval from 0.78 to 1.77 Ma, representing the period from the Brunhes/Matuyama boundary to the top of the Olduvai Subchronozone. If only paleomagnetic datums are used, the interval sedimentation rates are more variable during the upper Matuyama (0.78–1.77 Ma), ranging from 10.6 to 13.9 cm/k.y. (Table T22).

## Geochemistry

### Volatile hydrocarbons

Headspace gas analysis was performed as a part of the standard protocol required for shipboard safety and pollution prevention monitoring. A total of 25 headspace samples from Hole U1304A (sampling resolution of one per core) were analyzed (Table T23; Fig. F24). Methane ( $C_1$ ) is the only hydrocarbon detected at this site. The  $C_1$  concentration in Hole U1304A is relatively constant and ranges from 2.2 to 5.2 ppmv. The maximum  $C_1$  concentration is 5.2 ppmv at 154 mcd.

### Sedimentary geochemistry

Sediment samples were collected for analysis of solid-phase geochemistry (inorganic carbon and elemental C and N) at a resolution of approximately two samples per core in Hole U1304A. Figure F25 shows calcium carbonate ( $CaCO_3$ ) concentrations. Total organic carbon (TOC) content, N elemental concentrations, and C/N ratios are shown in Figure F26. Results of coulometric and elemental analyses are listed in Table T24.

$CaCO_3$  contents range from 4.6 to 71.3 wt% and are higher than ~30 wt% in the upper sediment intervals (Fig. F25).  $CaCO_3$  content variability increases below 120 mcd. Extremely low  $CaCO_3$  contents are found at 197, 228, and 260 mcd. These minima coincide with the depths of diatom ooze layers (see Fig. F9); therefore, a reasonable interpretation for low  $CaCO_3$  content is dilution by biogenic siliceous materials.

Sedimentary TOC and total N concentrations were determined on 50 samples from Hole U1304A. TOC is characterized by extremely low concentrations for most intervals at this site (average concentration = 0.4 wt%) (Fig. F26). Total N contents at Hole U1304A range from 0.03 to 0.15 wt% (average = ~0.07 wt%) (Fig. F26). The C/N ratio, which is used to distinguish the origin of organic matter (i.e., marine, degraded marine, or terrestrial) in the sediments (Emerson and Hedges, 1988; Meyers, 1997), indicates that the organic C is mainly derived from marine organic materials produced in the upper water column (Fig. F26). Relatively high C/N values are recognized in a few intervals. Further study employing other methods is necessary to determine the origin of organic C.

### Interstitial water chemistry

Interstitial water samples were extracted from 12 whole-round sediment sections and processed for routine shipboard geochemical analyses. Details of sampling procedure and analytical methods for interstitial water can be found in “Geochemistry” in



the “Site U1302–U1308 methods” chapter. Filtered (0.45 µm) samples were analyzed for pH, salinity, chloride, alkalinity, sulfate ( $\text{SO}_4^{2-}$ ), ammonium ( $\text{NH}_4^+$ ), silica ( $\text{H}_4\text{SiO}_4$ ), boron ( $\text{H}_3\text{BO}_3$ ), iron ( $\text{Fe}^{2+}$ ), manganese ( $\text{Mn}^{2+}$ ), and major cations ( $\text{Na}^+$ ,  $\text{K}^+$ ,  $\text{Mg}^{2+}$ ,  $\text{Ca}^{2+}$ ,  $\text{Li}^+$ ,  $\text{Sr}^{2+}$ , and  $\text{Ba}^{2+}$ ). Concentrations of dissolved chemical elements are shown in Table T25 and Figure F27.

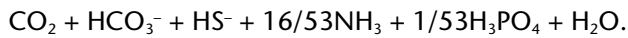
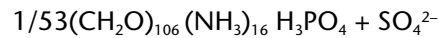
### Chloride, sodium, and pH

Chloride ( $\text{Cl}^-$ ) concentrations increase to ~566 mM in the upper 50 mcd. As at Sites U1302 and U1303, this maximum  $\text{Cl}^-$  concentration at 48 mcd implies the remnant of higher salinity bottom water masses during the Last Glacial Maximum (e.g., Adkins and Schrag, 2003), although a smooth diffusional profile is not observed with discrete maxima at 92 and 186 mcd. Sodium ( $\text{Na}^+$ ) values range from 481 to 496 mM (Fig. F27). The pH profile at Site U1304 increases with depth, ranging from 7.4 to 7.7 (Fig. F27).

### Dissolved silica, alkalinity, sulfate, and ammonium

Dissolved silica concentrations increase with depth from 623 µM near the seafloor to 912 µM at ~60 mcd (Fig. F27). The elevated dissolved  $\text{H}_4\text{SiO}_4$  at Site U1304 is most likely derived from dissolution of biogenic silica in these diatom-rich sediments (see “[Lithostratigraphy](#)” and “[Biostratigraphy](#)”).

Alkalinity monotonically increases with depth from 4.5 to 19.3 mM in the upper 155 mcd, followed by relatively constant values downcore (Fig. F27). In contrast to alkalinity, the sulfate profile shows a progressive decrease from 27.3 mM near the seafloor to <3 mM at the base of the cored interval (Fig. F27). Ammonium increases with depth from 169 µM in the shallowest sample to a maximum of 1400 µM at 243 mcd (Fig. F27). The downhole increases in alkalinity and  $\text{NH}_4^+$  and the decrease in  $\text{SO}_4^{2-}$  most likely represent oxidation of organic materials through  $\text{SO}_4^{2-}$  reduction (Fig. F27):



In this equation, 2 moles of alkalinity (i.e.,  $\text{HCO}_3^-$ ) are produced for every 1 mole of  $\text{SO}_4^{2-}$  that is reduced.

The increase in alkalinity is not consistent with the amount of reduced  $\text{SO}_4^{2-}$ . Assuming seawater concentrations of both alkalinity (2.4 mM) and  $\text{SO}_4^{2-}$  (~28 mM) as initial values, consumption of 24 mM of  $\text{SO}_4^{2-}$  at 186 mcd should result in an increase of ~48 mM of alkalinity (Fig. F27). This deficit suggests alkalinity is being consumed by another reaction, which

is most likely  $\text{CaCO}_3$  precipitation (Morse and Mackenzie, 1990).

### Calcium, lithium, strontium, magnesium, and potassium

Pore water calcium ( $\text{Ca}^{2+}$ ) concentrations decline from approximately the seawater value of ~10.3 mM to 2.7 mM within the upper 60 mcd and decrease gradually downcore (Fig. F27). The ~75% decrease in Ca values is mostly explained by precipitation of  $\text{CaCO}_3$ , which is consistent with the inferred alkalinity consumption in the waters (Fig. F27).

Lithium ( $\text{Li}^+$ ) concentrations at Site U1304 are lower than the seawater value of 28 µM throughout the cored interval (Fig. F27). These low  $\text{Li}^+$  concentrations indicate uptake of  $\text{Li}^+$  into alteration products. The downcore  $\text{Li}^+$  concentration profile shows two minima at 48 and 123 mcd. Gravel counts are relatively high at these depths (see “[Lithostratigraphy](#)”).  $\text{Li}^+$  depletion in interstitial water has been linked to the presence of altered volcanic material in the sediment column (Stoffyn-Egli and Mackenzie, 1984). However, the highest  $\text{Li}^+$  concentrations are seen below 190 mcd, coincident with intervals of thick diatom ooze. Accordingly, the minima in the interstitial water most likely imply incorporation of  $\text{Li}^+$  into altered lithogenic material.

Dissolved strontium ( $\text{Sr}^{2+}$ ) contents in the uppermost sediments are close to the seawater value of 87 µM. Similar to  $\text{Ca}^{2+}$ , the  $\text{Sr}^{2+}$  profile is primarily characterized by a decreasing trend, although it has a minimum concentration at 154 mcd (Fig. F27). The decrease in  $\text{Sr}^{2+}$  may indicate incorporation into diagenetic carbonate. However, like the  $\text{Li}^+$  profile, the minimum  $\text{Sr}^{2+}$  zones are clearly identified at the depths centered at 58 and 123–154 mcd (Fig. F27). Additionally, both  $\text{Sr}^{2+}/\text{Ca}^{2+}$  and  $\text{Li}^+/\text{Ca}^{2+}$  have distinct minima at 154 mcd (Fig. F27). This evidence suggests that some diagenetic process affects  $\text{Li}^+$  and  $\text{Sr}^{2+}$  concentrations in interstitial water. Thus,  $\text{Sr}^{2+}$  may also be incorporated into authigenic minerals other than secondary precipitated  $\text{CaCO}_3$ . In addition, the very low  $\text{Sr}^{2+}$  concentrations indicate that dissolution and recrystallization of biogenic carbonate are not important processes in the cored interval.

As for Sites U1302 and U1303, magnesium ( $\text{Mg}^{2+}$ ) and potassium ( $\text{K}^+$ ) concentrations show correlating profiles (Fig. F27).  $\text{Mg}^{2+}$  concentrations in the uppermost sediments are lower than the seawater value of 52.7 mM. In contrast,  $\text{K}^+$  concentrations in the same depth interval are higher than the seawater value of 10.1 mM.  $\text{Mg}^{2+}$  and  $\text{K}^+$  are probably being consumed in a common diagenetic process (e.g., reaction with silicate minerals).



## Manganese, iron, boron, and barium

Reduction of Mn oxides is indicated by a sharp decrease in manganese ( $Mn^{2+}$ ) concentrations from the shallowest sample to 16 mcd (Fig. F27). Below ~16 mcd,  $Mn^{2+}$  concentrations decrease moderately downhole, reaching a minimum concentration of ~2.8  $\mu M$  at 90 mcd. The downhole  $Mn^{2+}$  profile suggests that  $Mn^{2+}$  reduction occurs in the upper 40 m (Fig. F27).

Iron ( $Fe^{2+}$ ) concentrations are very low, ranging from 4.3 to 31.3  $\mu M$  (Fig. F27). The maximum concentration of 31.3  $\mu M$  is found at 27 mcd. There are two additional maxima at 123 and 212 mcd. Because of low concentrations, it is difficult to interpret the latter two  $Fe^{2+}$  maxima. Boron ( $H_3BO_3$ ) concentrations in the interstitial water samples (Table T25) show a wide variety of values, ranging from 435 to 607  $\mu M$ . Barium ( $Ba^{2+}$ ) concentrations (Table T25) monotonically increase with depth and are very low (<2.0  $\mu M$ ), which is expected due to barite insolubility with the sulfate reduction zone.

## Physical properties

Measurements of physical properties were conducted at Site U1304 following the procedures described in “Physical properties” in the “Site U1302–U1308 methods” chapter. Two measurements of magnetic susceptibility were conducted, along with gamma ray attenuation (GRA) density, NGR, and *P*-wave velocity. Thermal conductivity was measured on whole cores in Hole U1304A with a frequency of one per section for each core. Moisture and density (MAD) properties were also measured on two discrete samples per core, usually at the bottom of Section 1 and the top of Section 6.

### Whole-core magnetic susceptibility measurements

The magnetic susceptibility records derived during coring operations at Site U1304 show a highly variable record that results from lithologic and/or mineralogic changes. Magnetic susceptibility measurements obtained from the Fast Track MSCL and the MST present the same trends and display multiple excursions toward higher values (Fig. F28).

Site U1304 has peak magnetic susceptibility values of ~ $400 \times 10^{-5}$  SI and minimum values approaching the instrument noise level, with most values ranging from  $40 \times 10^{-5}$  to  $160 \times 10^{-5}$  SI. The magnetic susceptibility record shows two main trends at Site U1304 (Fig. F28). The first trend runs approximately from 0 to 115 mcd with average values ranging from  $80 \times 10^{-5}$  to  $120 \times 10^{-5}$  SI. The second trend is seen from

115 to 275 mcd and has average values of  $160 \times 10^{-5}$  to  $140 \times 10^{-5}$  SI. Site U1304 also contains abundant diatom mats that caused the magnetic susceptibility values to approach the noise levels of the MSCL and MST (see “Lithostratigraphy”). These mats had highly variable thickness from centimeter to meter scale.

### GRA density

Bulk density measurements taken at Site U1304 show a similar trend among holes and are variable, ranging from 1.2 to 1.8  $g/cm^3$  (Fig. F29). The bulk density record shows a very similar trend to that of magnetic susceptibility. Bulk density between 0 and 120 mcd averages ~1.4  $g/cm^3$ , whereas the lower interval between 120 and 275 mcd shows a higher average of ~1.5  $g/cm^3$ . The diatom layers cause density values to drop to ~1.2  $g/cm^3$ . Discrete density was also determined from Hole U1304A physical property MAD samples. The discrete measurements match the values produced by the MST (Fig. F29).

### Natural gamma radiation

NGR counts range from 0 to 35 cps with the majority of the values between 7 and 21 cps (Fig. F30). NGR values also mimic the trends seen in the magnetic susceptibility and GRA data. NGR counts average ~7 cps from 0 to 120 mcd and ~14 cps from 120 to 275 mcd.

### *P*-wave velocity

Both *P*-wave logger (PWL) and discrete (*P*-wave sensor number 3 [PWS3]) velocity measurements were performed at Site U1304 when possible. Some core sections could not be measured because of the presence of diatom mats that disrupted the velocity measurements due to severe signal attenuation. Measurements that could be obtained at Site U1304 are fairly consistent, varying between 1500 and 1600 m/s (Fig. F31). There is a general increase in velocity from the top (~1525 m/s) to the bottom (~1580 m/s) of the core. We also see an offset in PWL and PWS3 measurements that is a long-standing problem not unique to Expedition 303.

### Thermal conductivity

Discrete thermal conductivity measurements were made usually on Section 4 of each core at Site U1304 (Table T26). Thermal conductivity is highly variable ranging from 0.7 to 1.1 W/(m·K). There appears to be a slight correlation between thermal conductivity and magnetic susceptibility, GRA, and NGR data sets, but low resolution of the thermal conductivity data does not allow further conclusions.



## Porosity

Porosity was calculated using MST GRA density measurements and spot-checked with porosity results generated from discrete MAD samples. Porosity values are highly variable and range between 60% and 90% (Fig. F32). As expected, porosity shows an inverse relationship to density. Porosity decreases only slightly with depth at Site U1304. This trend may be attributed to the presence of diatom layers causing the interval density values to be reduced to a value lower than that of the surrounding silty clay layers.

## Discussion

The spliced record generated at Site U1304 shows a discontinuity in the magnetic susceptibility, GRA, and NGR records at ~115 mcd (Fig. F33). The discontinuity is characterized by higher values and higher-frequency variability below the discontinuity and lower values and lower-frequency variability above. An age estimate for this discontinuity is ~0.7 Ma (see “[Biostratigraphy](#)” and “[Paleomagnetism](#)”).

Diatom mats interbedded with silty clay layers at Site U1304 influence the magnetic susceptibility and NGR data (Fig. F33). The effect is more readily seen from 0 to 115 mcd where the average magnetic susceptibility and NGR values are lower and contain less variability and where carbonate content averages 43 wt% (see “[Geochemistry](#)”). Although the 115–275 mcd section contains more diatom mats, this is not particularly apparent in the physical property records (see “[Lithostratigraphy](#)”). We assume that the non-diatom-rich sediments between 125 and 275 mcd are better able to mask the presence of the diatoms because of their higher values of magnetic susceptibility and NGR and lower carbonate content (~30 wt%).

## References

- Adkins, J.F., and Schrag, D.P., 2003. Reconstructing last glacial maximum bottom water salinities from deep-sea sediment pore fluid profiles. *Earth Planet. Sci. Lett.*, 216:109–123. doi:[10.1016/S0012-821X\(03\)00502-8](https://doi.org/10.1016/S0012-821X(03)00502-8)
- Andersen, C., Koç, N., and Moros, M., 2004. A highly unstable Holocene climate in the subpolar North Atlantic: evidence from diatoms. *Quat. Sci. Rev.*, 23:2155–2166. doi:[10.1016/j.quascirev.2004.08.004](https://doi.org/10.1016/j.quascirev.2004.08.004)
- Bodén, P., and Backman, J., 1996. A laminated sediment sequence from northern North Atlantic Ocean and its climatic record. *Geology*, 24:507–510. doi:[10.1130/0091-7613\(1996\)024<0507:ALSSFT>2.3.CO;2](https://doi.org/10.1130/0091-7613(1996)024<0507:ALSSFT>2.3.CO;2)
- Cande, S.C., and Kent, D.V., 1995. Revised calibration of the geomagnetic polarity timescale for the Late Cretaceous and Cenozoic. *J. Geophys. Res.*, 100:6093–6095. doi:[10.1029/94JB03098](https://doi.org/10.1029/94JB03098)
- Channell, J.E.T., Mazaud, A., Sullivan, P., Turner, S., and Raymo, M.E., 2002. Geomagnetic excursions and paleointensities in the Matuyama Chron at ODP Sites 983 and 984 (Iceland Basin). *J. Geophys. Res.*, 107. doi:[10.1029/2001JB000491](https://doi.org/10.1029/2001JB000491)
- Damuth, J.E., 1977. Late Quaternary sedimentation in the western equatorial Atlantic. *Geol. Soc. Am. Bull.*, 88:695–710. doi:[10.1130/0016-7606\(1977\)88<695:LQSITW>2.0.CO;2](https://doi.org/10.1130/0016-7606(1977)88<695:LQSITW>2.0.CO;2)
- de Vernal, A., Londeix, L., Mudie, P.J., Harland, R., Morzadec-Kerfourn, M.T., Turon, J.-L., and Wrenn, J.H., 1992. Quaternary organic-walled dinoflagellate cysts of the North Atlantic Ocean and adjacent seas: ecostratigraphy and biostratigraphy. In Head, M.J., and Wrenn, J.H. (Eds.), *Neogene and Quaternary Dinoflagellate Cysts and Arcitarchs*: Salt Lake City (Publisher’s Press), 289–328.
- Emerson, S., and Hedges, J.I., 1988. Processes controlling the organic carbon content of open ocean sediments. *Paleoceanography*, 3:621–634.
- Goll, R.M., and Bjørklund, K.R., 1989. A new radiolarian biostratigraphy for the Neogene of the Norwegian Sea: ODP Leg 104. In Eldholm, O., Thiede, J., Taylor, E., et al., *Proc. ODP, Sci. Results*, 104: College Station, TX (Ocean Drilling Program), 697–737. [PDF]
- Gooday, A.J., 1993. Deep-sea benthic foraminiferal species which exploit phytodetritus: characteristic features and controls on distribution. *Mar. Micropaleontol.*, 22:187–205. doi:[10.1016/0377-8398\(93\)90043-W](https://doi.org/10.1016/0377-8398(93)90043-W)
- Jorissen, F.J., de Stigter, H.C., and Widmark, J.G.V., 1995. A conceptual model explaining benthic foraminiferal microhabitats. *Mar. Micropaleontol.*, 26:3–15. doi:[10.1016/0377-8398\(95\)00047-X](https://doi.org/10.1016/0377-8398(95)00047-X)
- Kemp, A.E.S., and Baldauf, J.G., 1993. Vast Neogene laminated diatom mat deposits from the eastern equatorial Pacific Ocean. *Nature (London, U. K.)*, 362:141–144. doi:[10.1038/362141a0](https://doi.org/10.1038/362141a0)
- Koç, N., Hodell, D.A., Kleiven, H., and Labeyrie, L., 1999. High-resolution Pleistocene diatom biostratigraphy of Site 983 and correlations with isotope stratigraphy. In Raymo, M.E., Jansen, E., Blum, P., and Herbert, T.D. (Eds.), 1999. *Proc. ODP, Sci. Results*, 162: College Station, TX (Ocean Drilling Program), 51–62. [HTML]
- Lutze, G.F., 1980. Depth distribution of benthic foraminifera on the continental margin off NW Africa. “*Meteor*” Forschungsergebnisse Reihe C, 32:31–80.
- McGeary, D.F.R., and Damuth, J.E., 1973. Postglacial iron-rich crusts in hemipelagic deep-sea sediment. *Geol. Soc. Am. Bull.*, 84:1201–1212. doi:[10.1130/0016-7606\(1973\)84<1201:PICIH>2.0.CO;2](https://doi.org/10.1130/0016-7606(1973)84<1201:PICIH>2.0.CO;2)
- Meyers, P.A., 1997. Organic geochemical proxies of paleoceanographic, paleolimnologic, and paleoclimatic processes. *Org. Geochem.*, 27:213–250. doi:[10.1016/S0146-6380\(97\)00049-1](https://doi.org/10.1016/S0146-6380(97)00049-1)
- Morse, J.W., and Mackenzie, F.T., 1990. *Geochemistry of Sedimentary Carbonates*: Amsterdam (Elsevier).
- Ruddiman, W.F., and Glover, L.K., 1975. Sub-polar North Atlantic circulation at 9300 yr BP: faunal evidence. *Quat. Res.*, 5:361–389.



- Sato, T., Kameo, K., and Mita, I., 1999. Validity of the latest Cenozoic calcareous nannofossil datums and its application to the tephrochronology. *Earth Sci.*, 53:265–274.
- Schiebel, R., and Hemleben, C., 2002. Interannual variability of planktic foraminiferal populations and test flux in the eastern North Atlantic Ocean (JGOFS). *Deep-Sea Res., Part II*, 47(9-11):1809–1852.
- Smith, W.H.F., and Sandwell, D.T., 1994. Bathymetric prediction from dense satellite altimetry and sparse shipboard bathymetry. *J. Geophys. Res.*, 99:21803–21824.  
[doi:10.1029/94JB00988](https://doi.org/10.1029/94JB00988)
- Stoffyn-Egli, P., and Mackenzie, F.T., 1984. Mass balance of dissolved lithium in the oceans. *Geochim. Cosmochim. Acta*, 48:859–872. [doi:10.1016/0016-7037\(84\)90107-8](https://doi.org/10.1016/0016-7037(84)90107-8)
- Weaver, P.P.E., and Clement, B.M., 1987. Magnetobiostratigraphy of planktonic foraminiferal datums, DSDP Leg 94, North Atlantic. In Ruddiman, W.F., Kidd, R.B., Thomas, E., et al., *Init. Repts. DSDP*, 94: Washington (U.S. Govt. Printing Office), 815–829.

Publication: XX Month 2006  
MS 303-104



**Figure F1.** Location of Site U1304 relative to Deep Sea Drilling Project (DSDP) Site 611. The Charlie Gibbs Fracture Zone (CGFZ) is indicated. (Bathymetry from Smith and Sandwell, 1994).

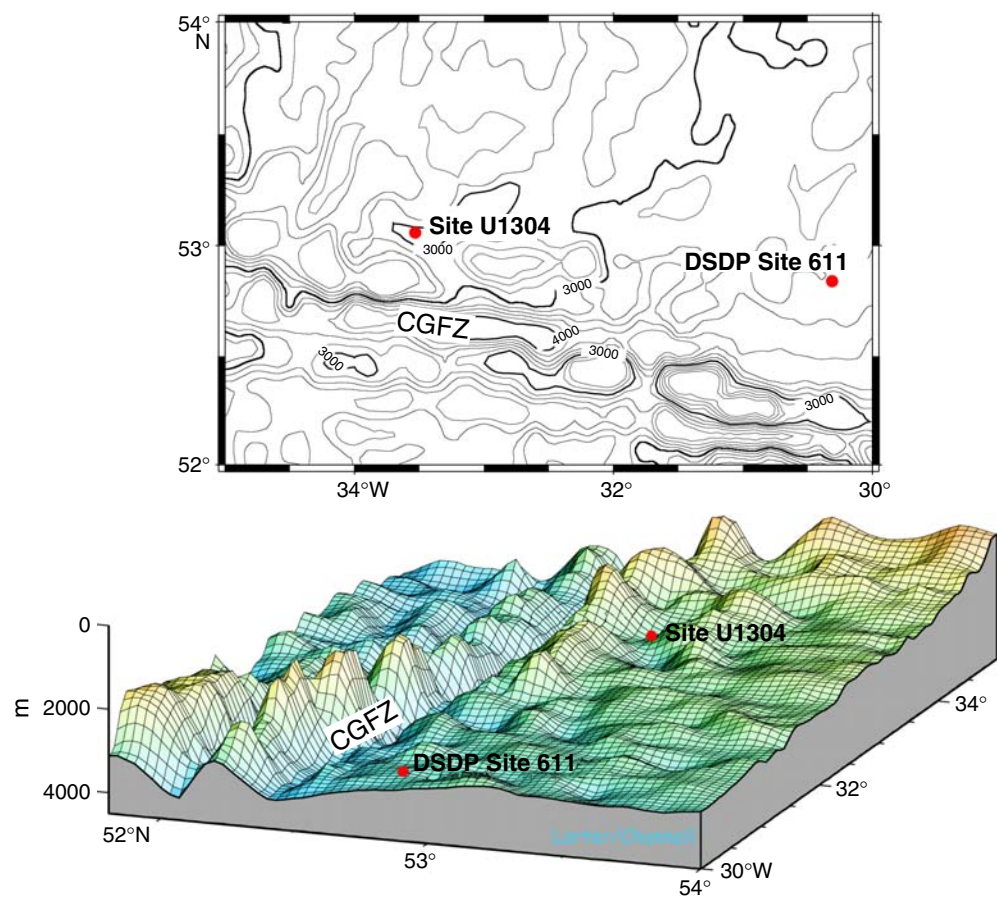
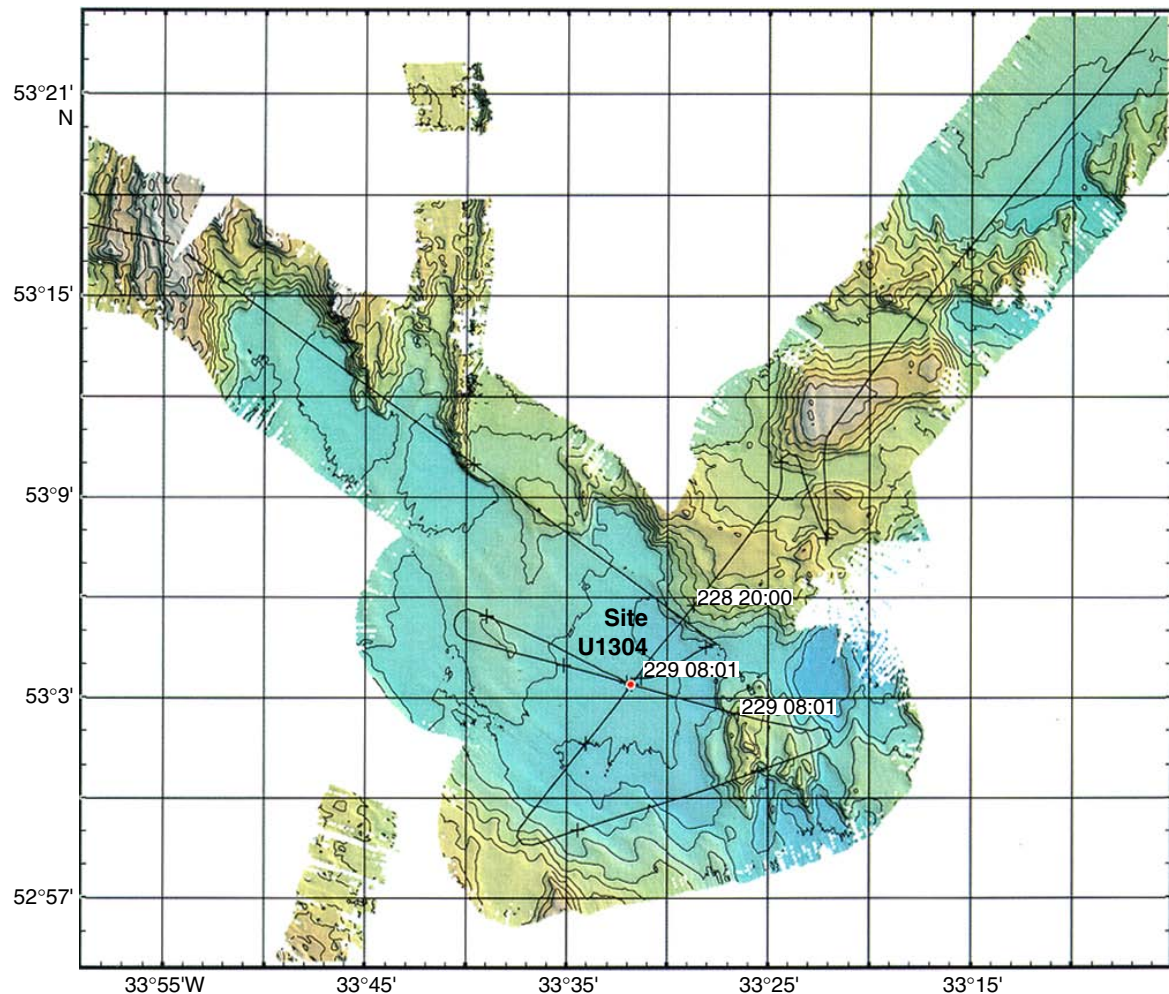
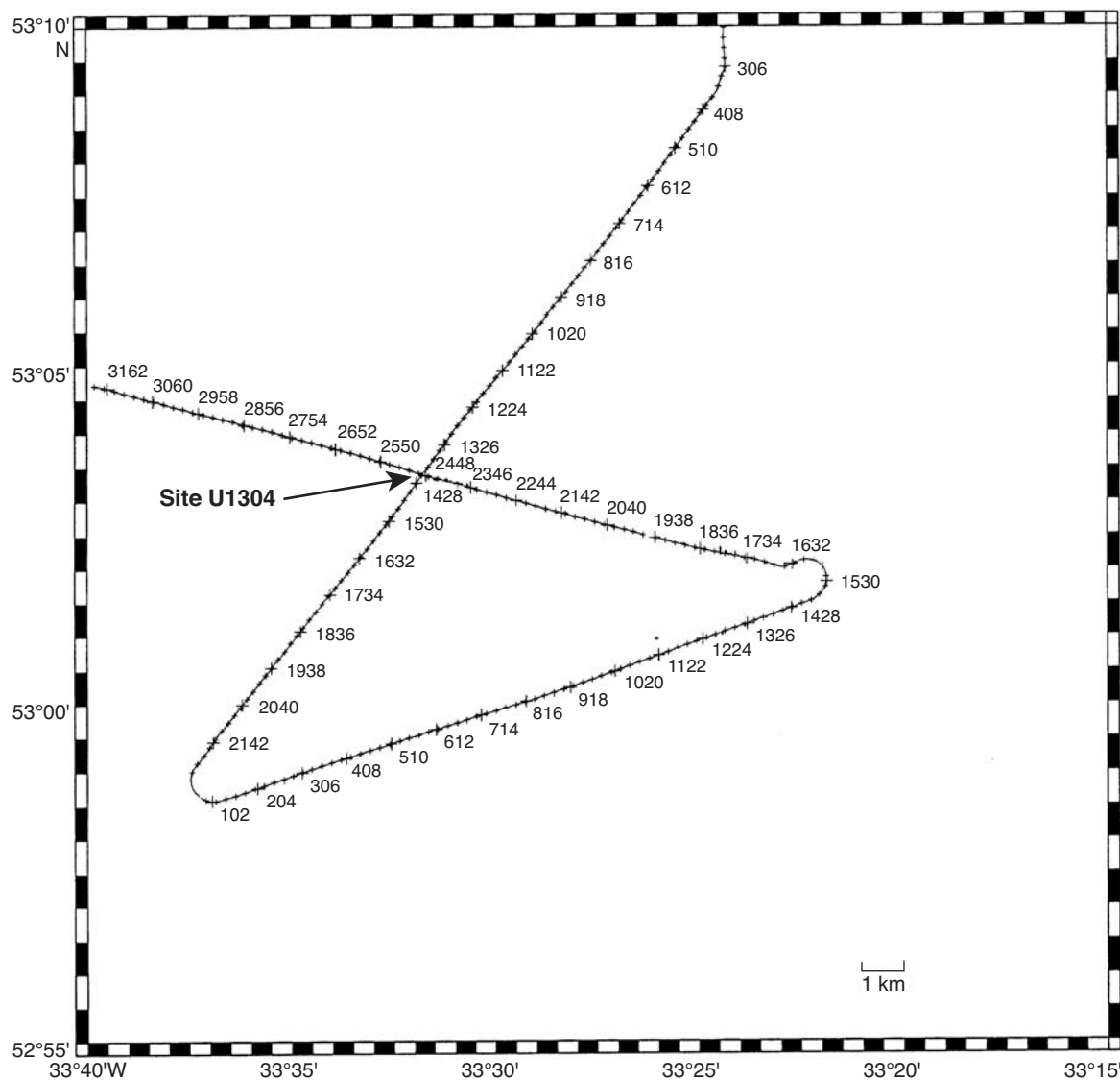


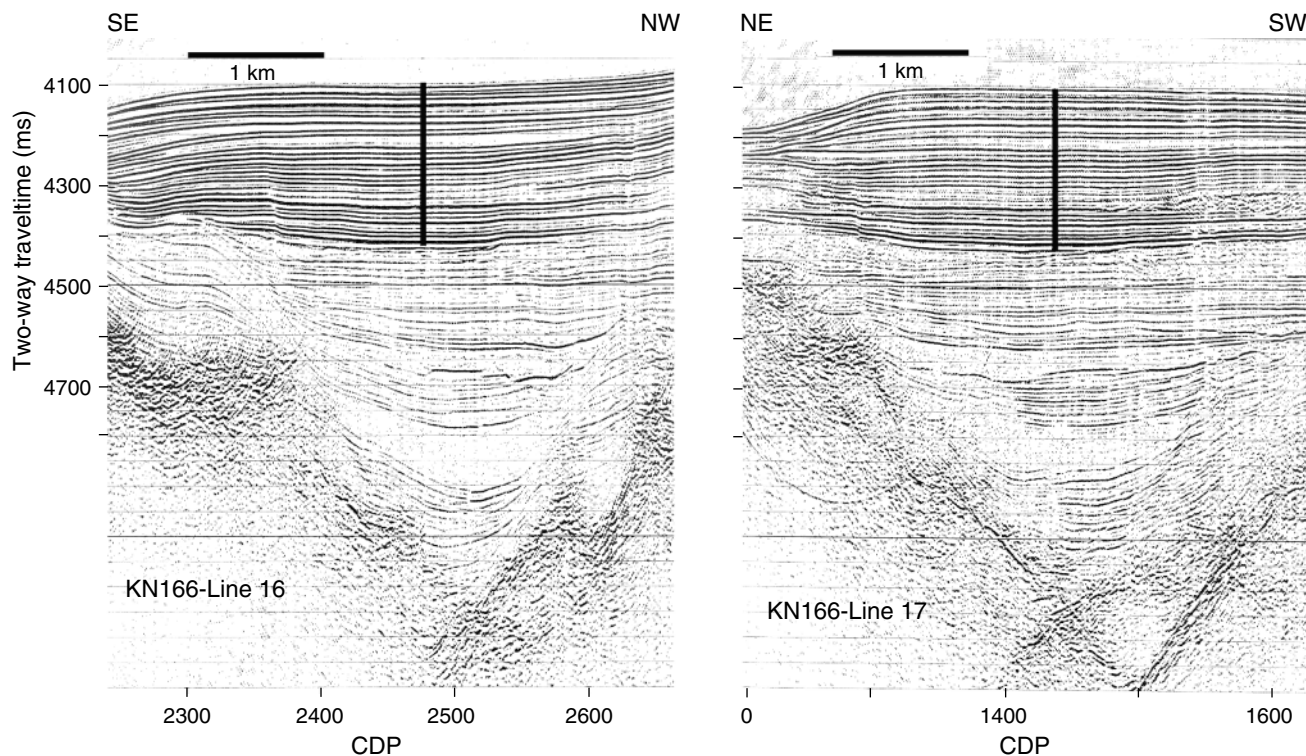
Figure F2. SeaBeam survey over Site U1304 showing ship's track (Mountain et al., unpubl. data).



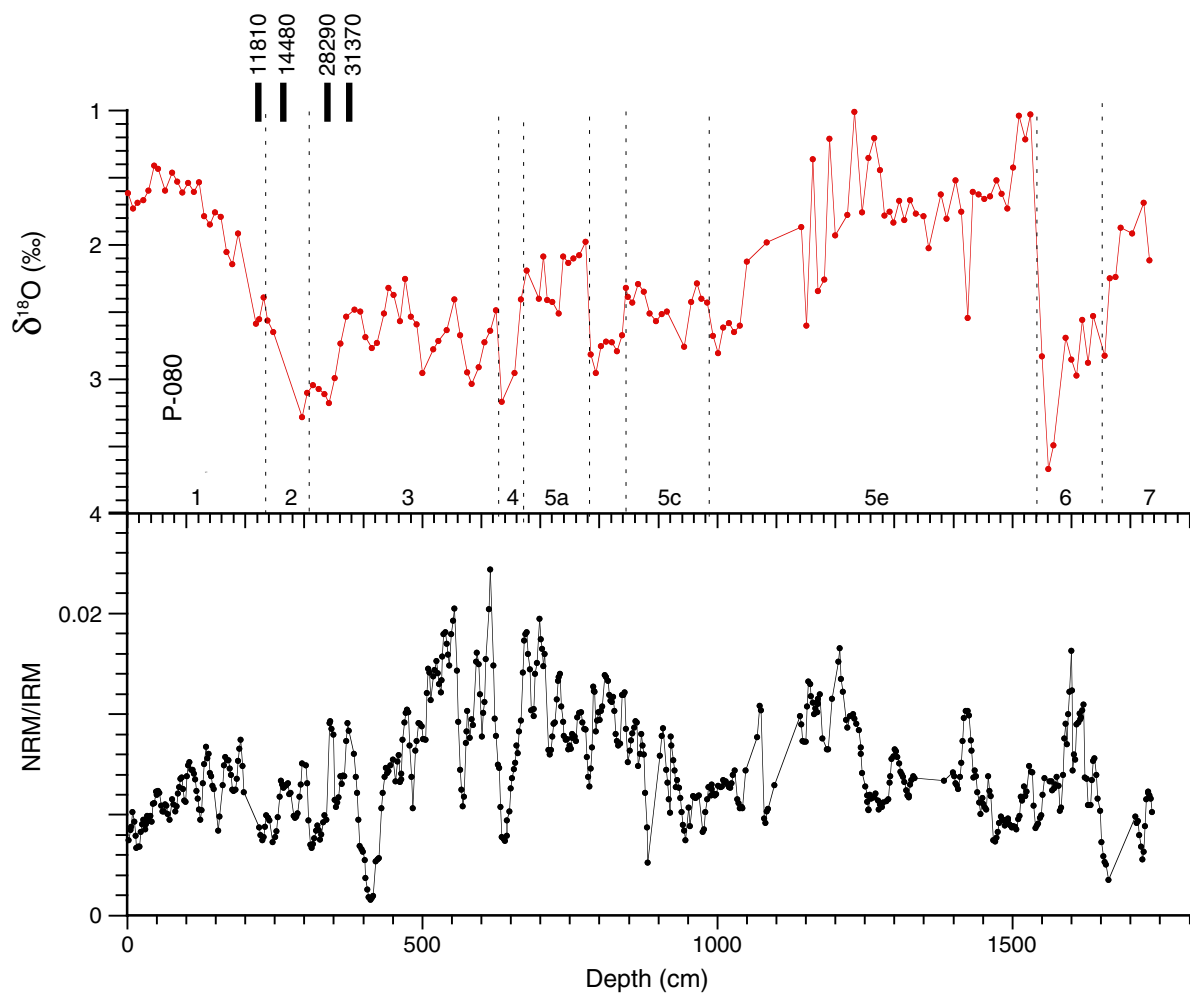
**Figure F3.** Track map for the multichannel seismic survey over Site U1304 (GAR2A). Common depth points (CDP) indicated (Mountain et al., unpubl. data).



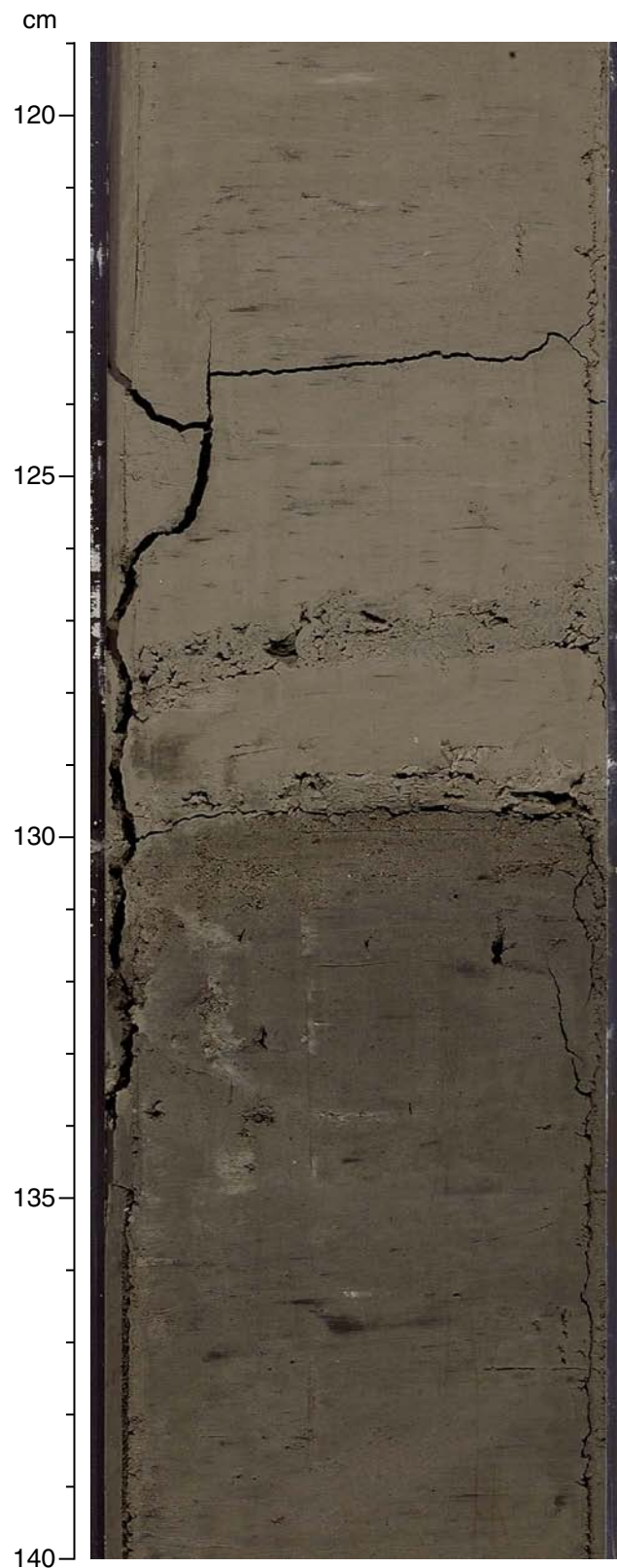
**Figure F4.** Multichannel seismic data for the crossing lines over Site U1304 (GAR2A). The target depth corresponding to 300 ms two-way traveltime is indicated. Common depth points (CDP) are also indicated (Mountain et al., unpubl. data).



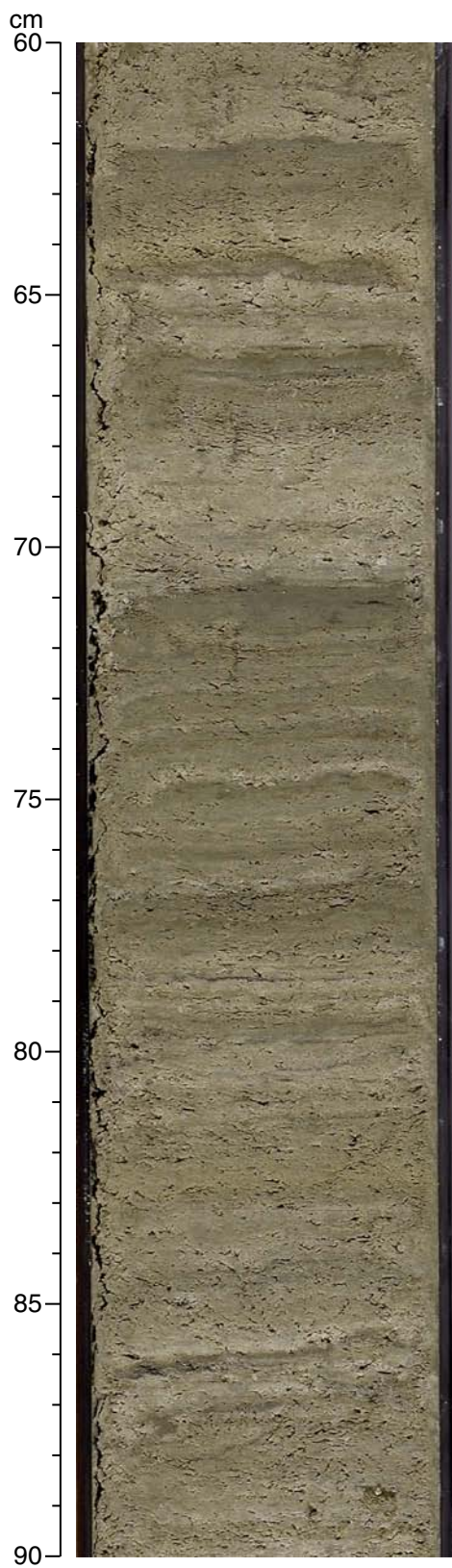
**Figure F5.** Oxygen isotope record, acceleration mass spectrometry  $^{14}\text{C}$  ages, and relative paleointensity data from Core HU91-045-080P (Stoner, Hillaire-Marcel, et al., unpubl.). NRM = natural remanent magnetization, IRM = isothermal remanent magnetization.



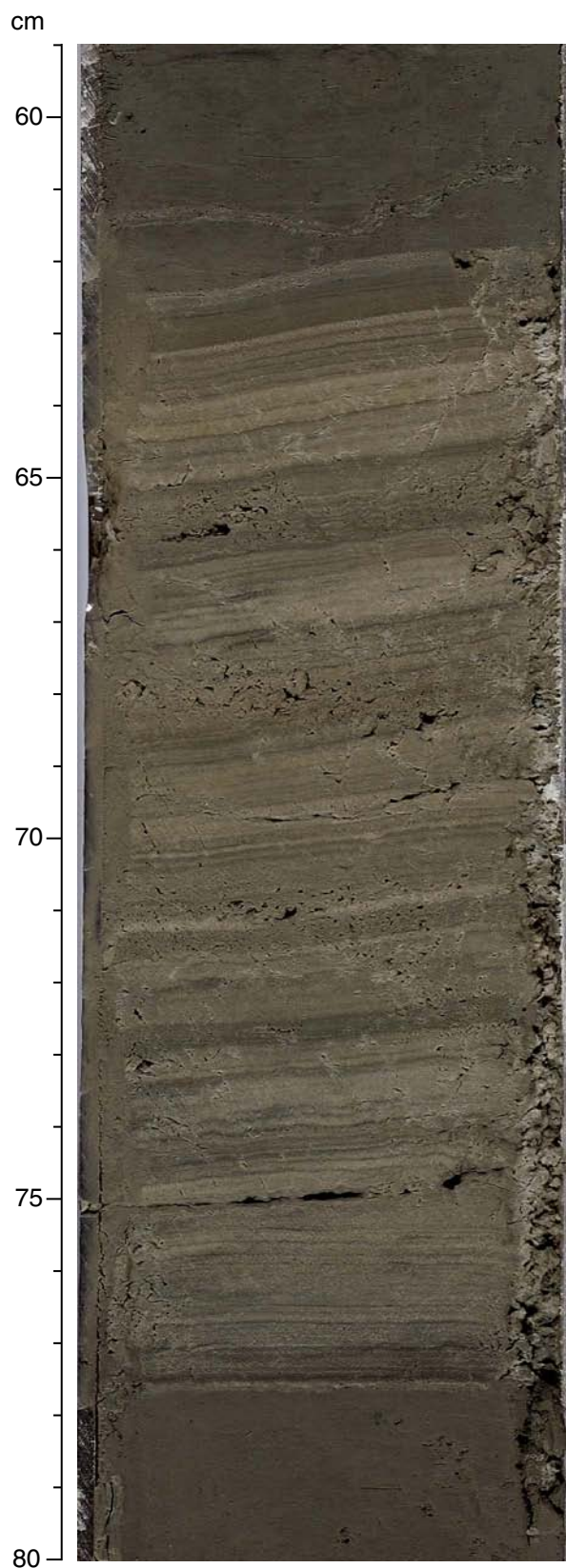
**Figure F6.** Examples of gray nannofossil ooze (119–130 cm) and darker gray silty clay with nannofossils (130–140 cm) (interval 303-U1304D-8H-5, 119–140 cm). Laminae of diatom ooze occur at 127–128 and 129–130 cm. Small black blotches on the clay are pyrite-filled burrows.



**Figure F7.** Laminated diatom ooze in core split with a steel wire (interval 303-U1304B-19H-5, 60–90 cm). Note interbedded laminae of gray nannofossil ooze.

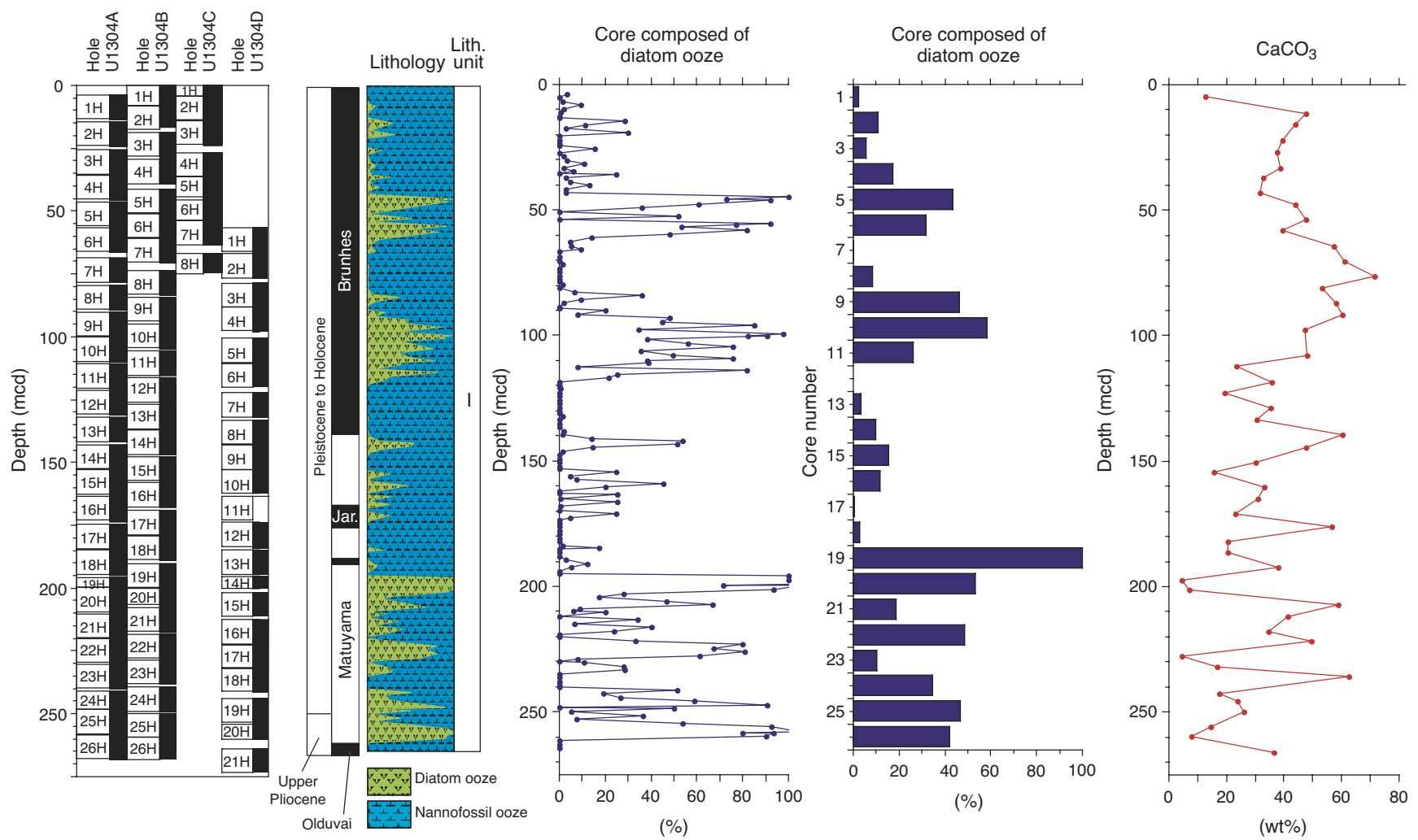


**Figure F8.** Laminated diatom ooze in core split with saw, showing the fine laminae characteristic of these sediments (interval 303-U1304A-24H-4, 59–80 cm).





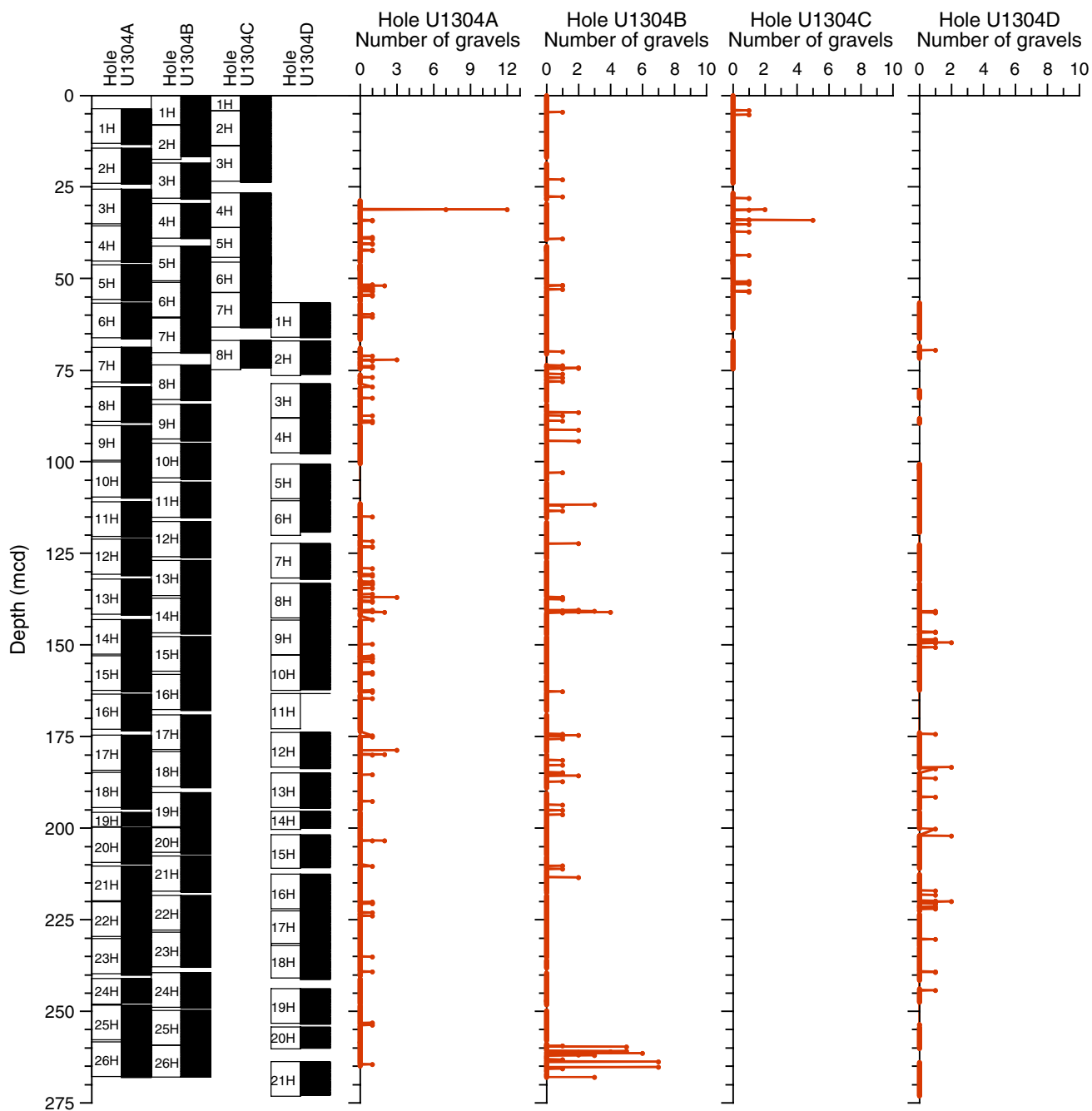
**Figure F9.** Graphic summary of the lithologies recovered in Hole U1304A.



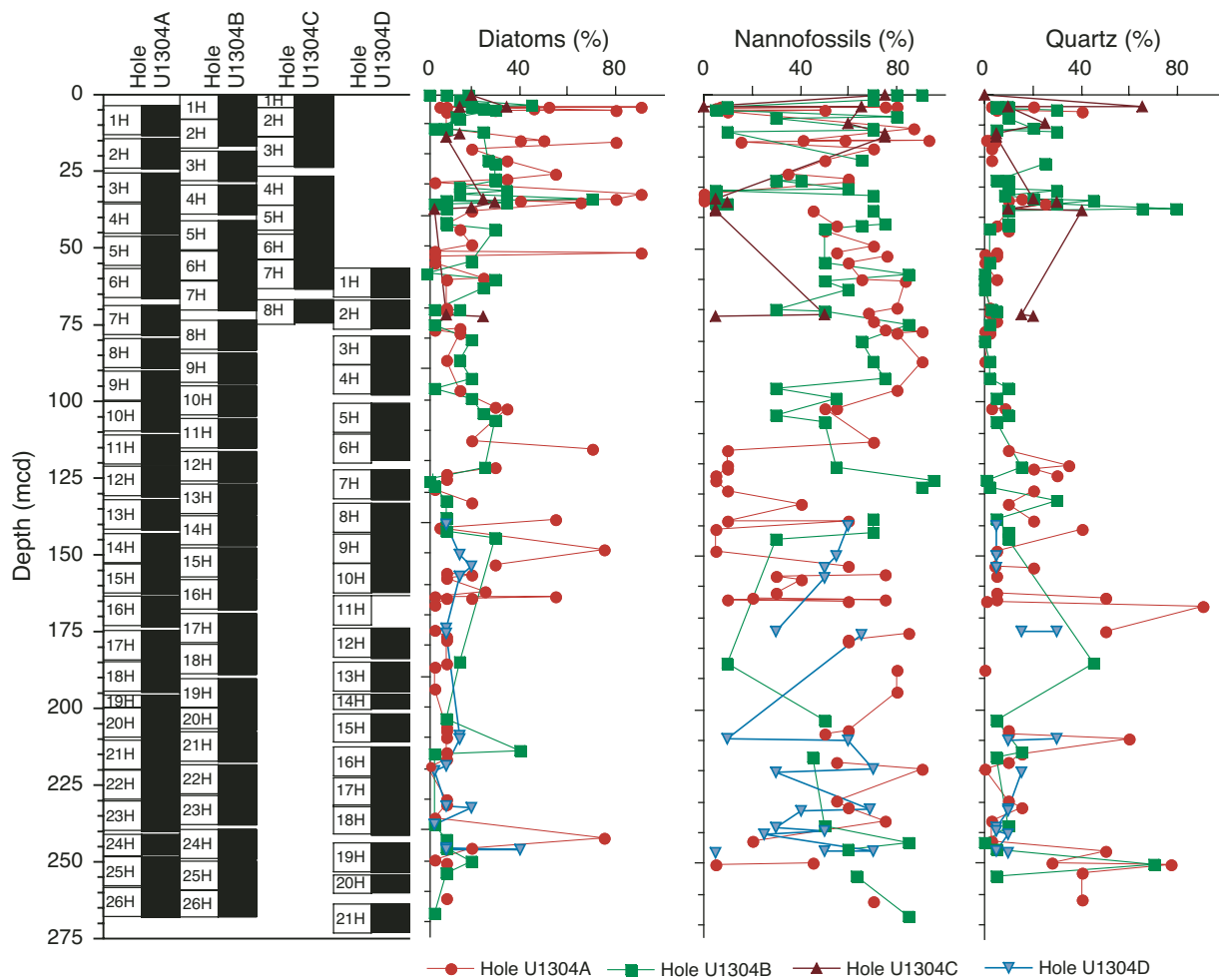
**Figure F10.** Intraformational slump deposit in nannofossil ooze and diatom ooze showing deformed, folded laminae and beds (interval 303-U1304B-19H-3, 104–126 cm)



Figure F11. Abundance of gravel-sized grains (number of grains/10 cm length of core).



**Figure F12.** Abundance of diatoms, quartz, and nannofossils based on all smear slides.



**Figure F13.** Abundance of diatoms, clay, quartz, calcite, and coccoliths from smear slide data from nannofossil ooze layers only.

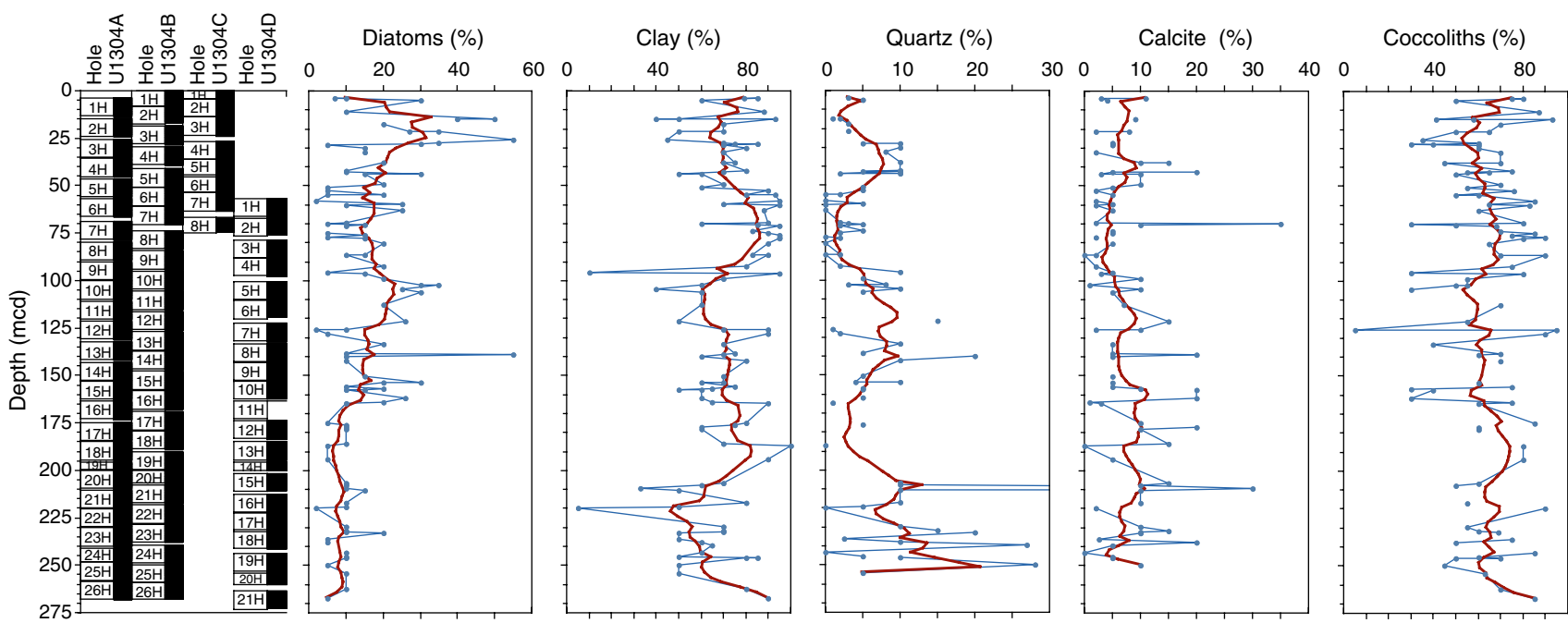


**Figure F14.** Site U1304 downcore relative abundance of calcareous nannofossils, planktonic foraminifers, diatoms, radiolarians, dinocysts, and pollen.

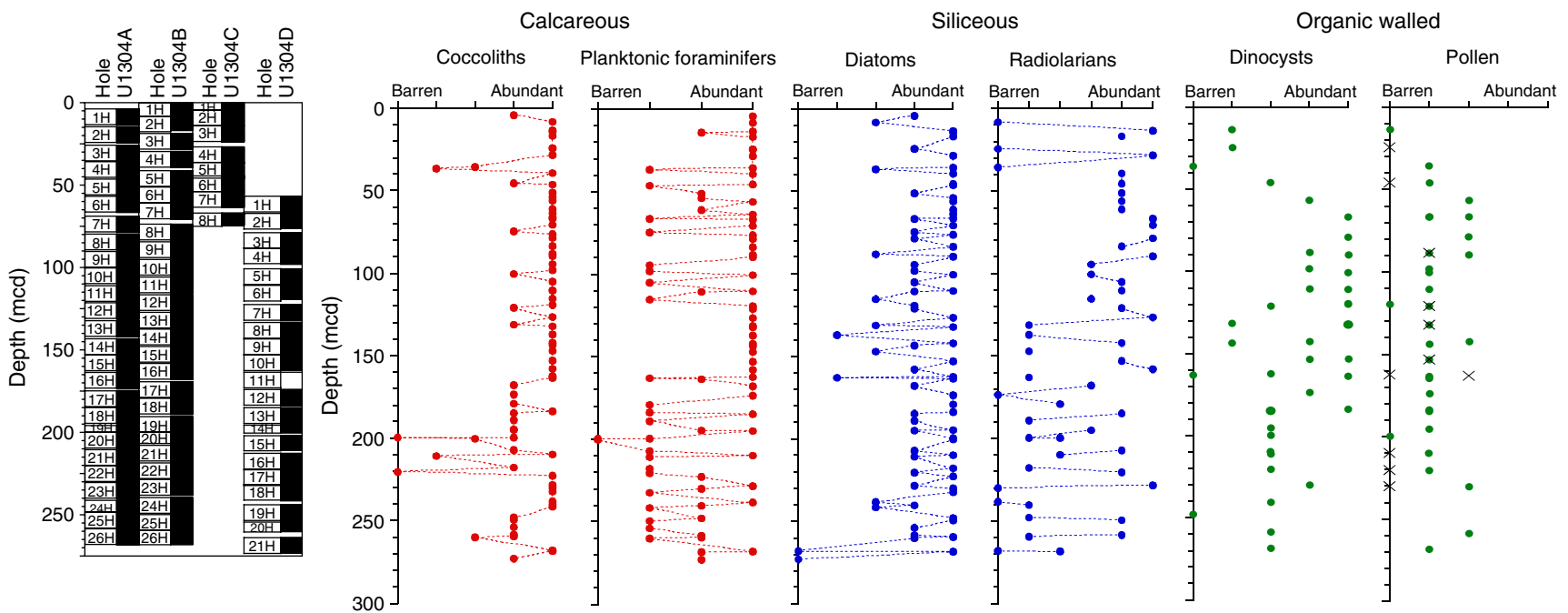


**Figure F15.** Chronostratigraphic correlation of Holes U1304A–U1304D based on calcareous nannofossils, diatoms, planktonic foraminifers, and dinocysts. Relationship to magnetostratigraphy is shown in the left panel. MIS = marine isotope stage, LO = last occurrence, FO = first occurrence.

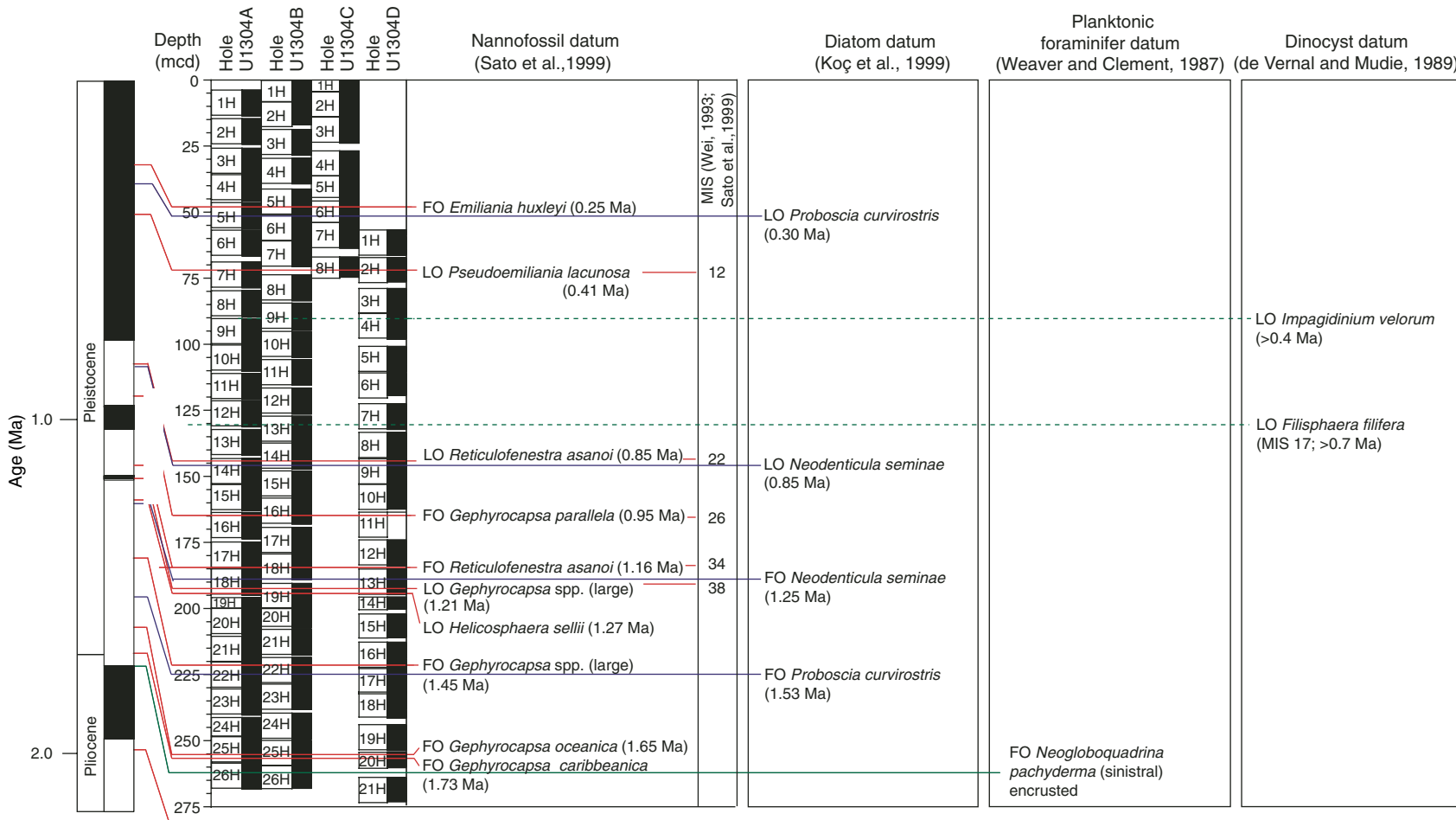


**Figure F16.** Downcore relative abundance of the polar planktonic foraminifer *Neogloboquadrina pachyderma* (sinistral) indicates frequent southward penetration of polar/subpolar surface waters to the position of Site U1304. The concentration of diatoms and the relative abundance of the planktonic foraminifer *Globorotalia inflata* suggest the recurring presence of hydrographic fronts. The benthic foraminifer *Epistominella exigua* may indicate fresh organic matter sedimentation at the seafloor.

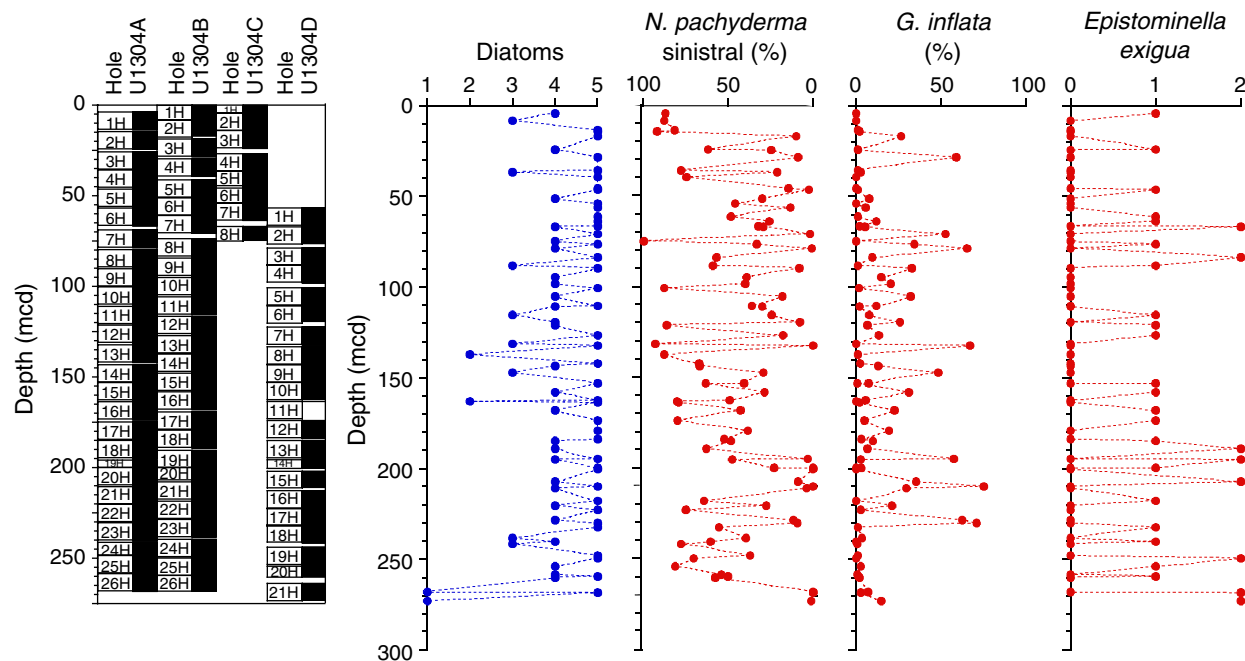


**Figure F17.** Site U1304 magnetization intensity before and after AF demagnetization versus depth. Core recovery is shown in the left panel.

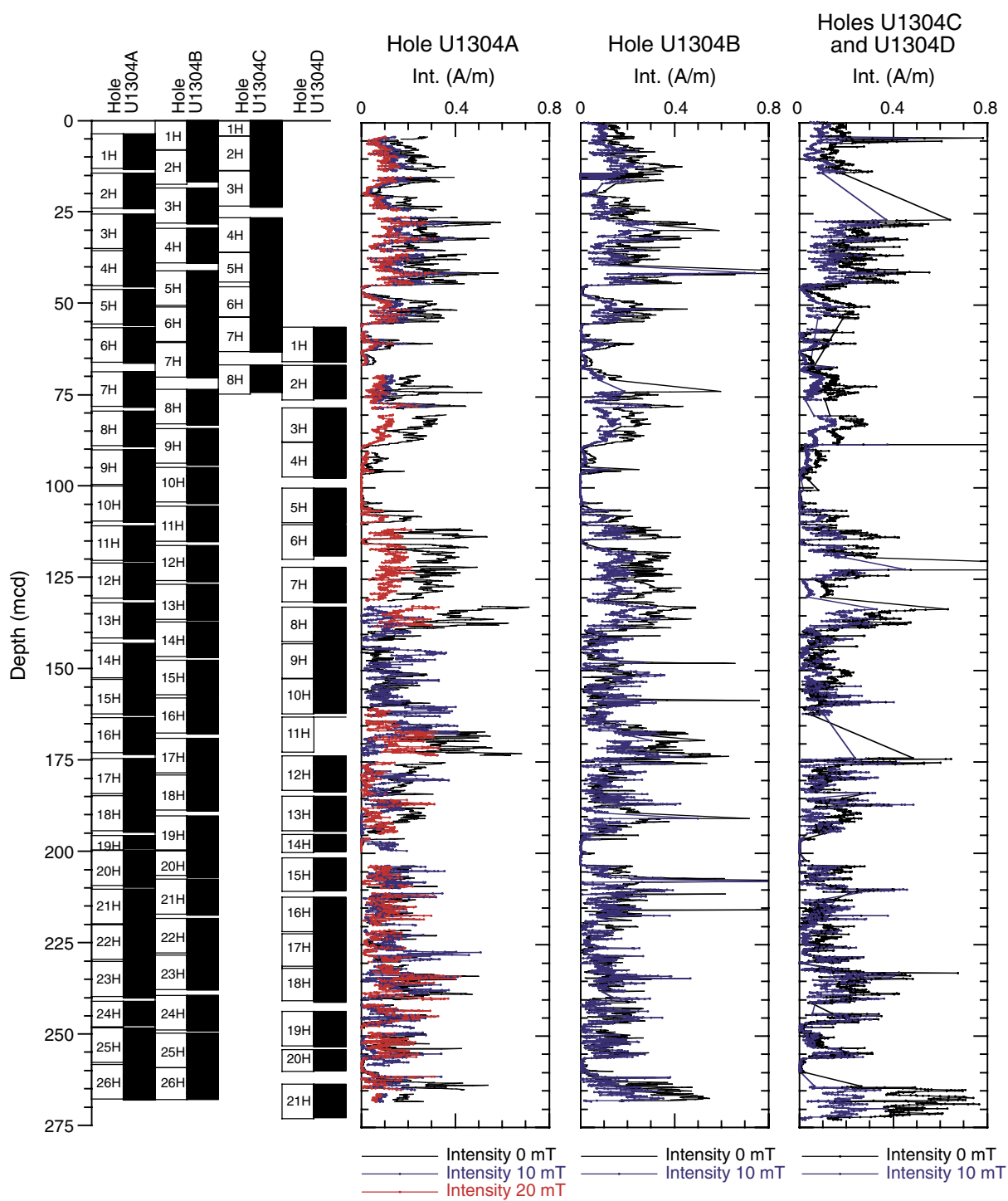


**Figure F18.** Site U1304 inclination of remanent magnetization after AF demagnetization versus depth. Data gaps reflect poor recovery or coring disturbance. Core recovery is shown in the left panel.

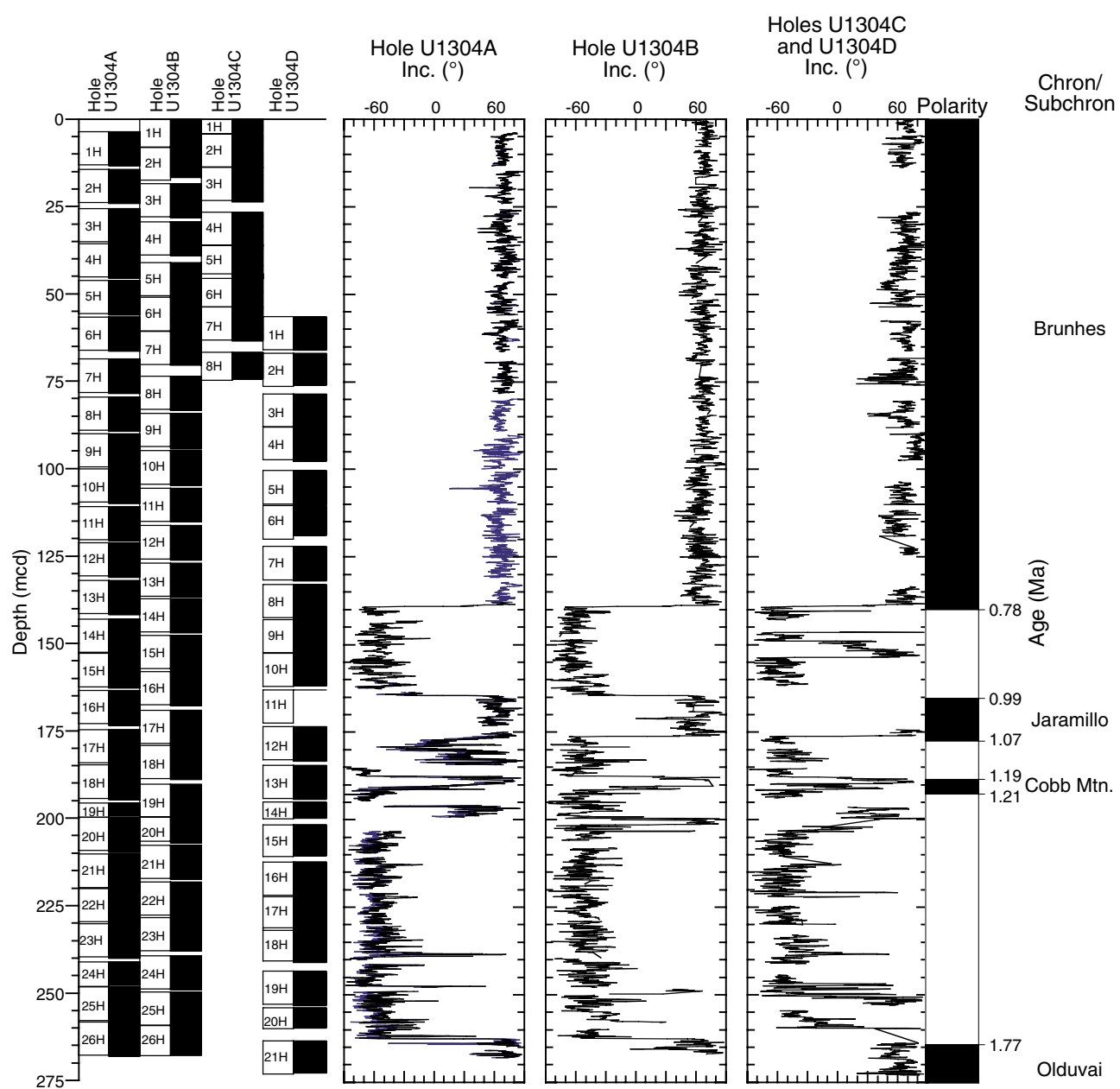


**Figure F19.** Site U1304 Tensor tool corrected declination after AF demagnetization at peak fields of 10 mT (black) or 20 mT (blue) versus depth. Core recovery is shown in the left panel.

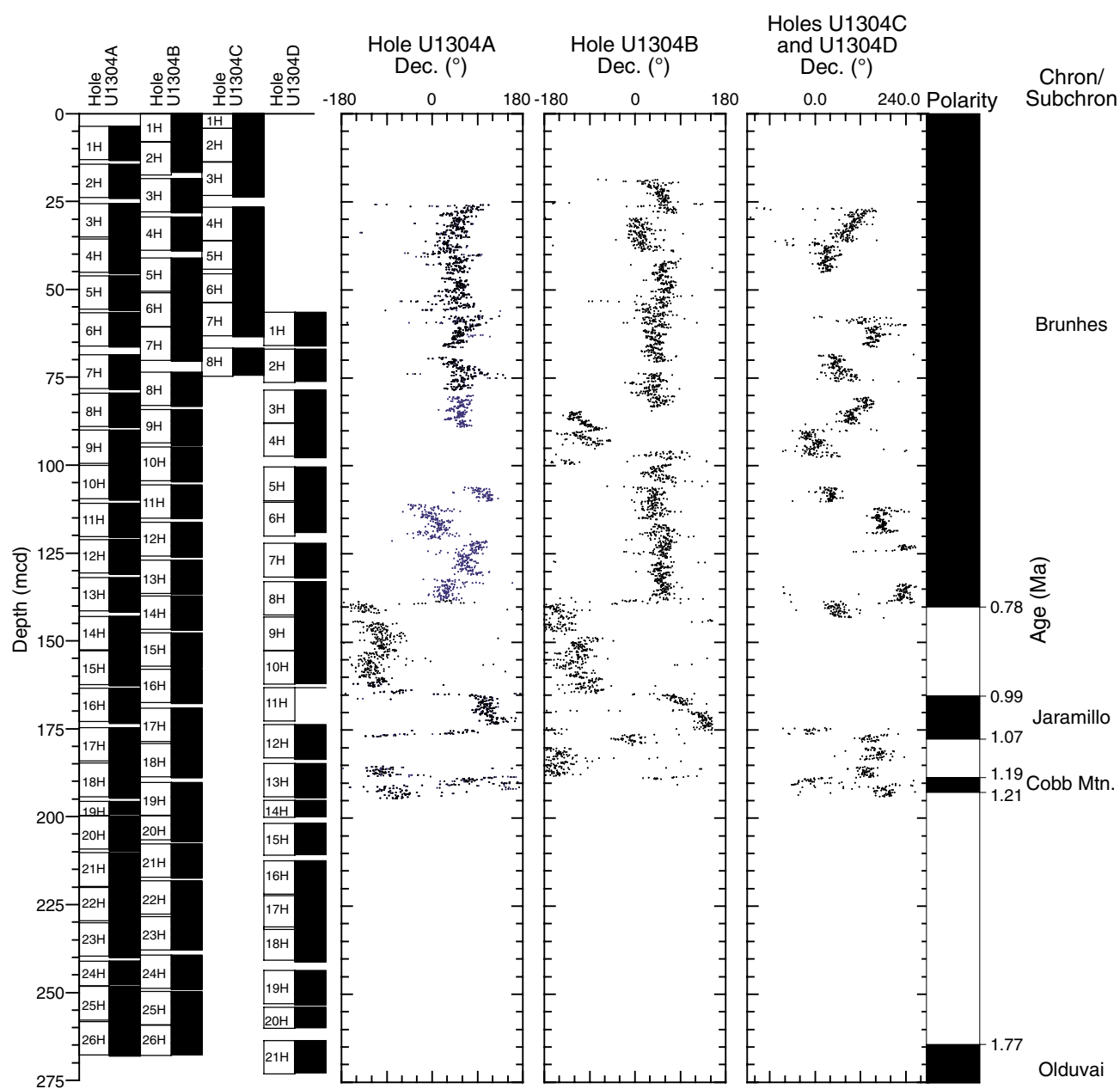


**Figure F20.** Natural gamma radiation (NGR), Site U1304. Upper panel shows composite NGR record indicating which hole was used to form the splice. A. 0–70 mcd. (Continued on next three pages.)

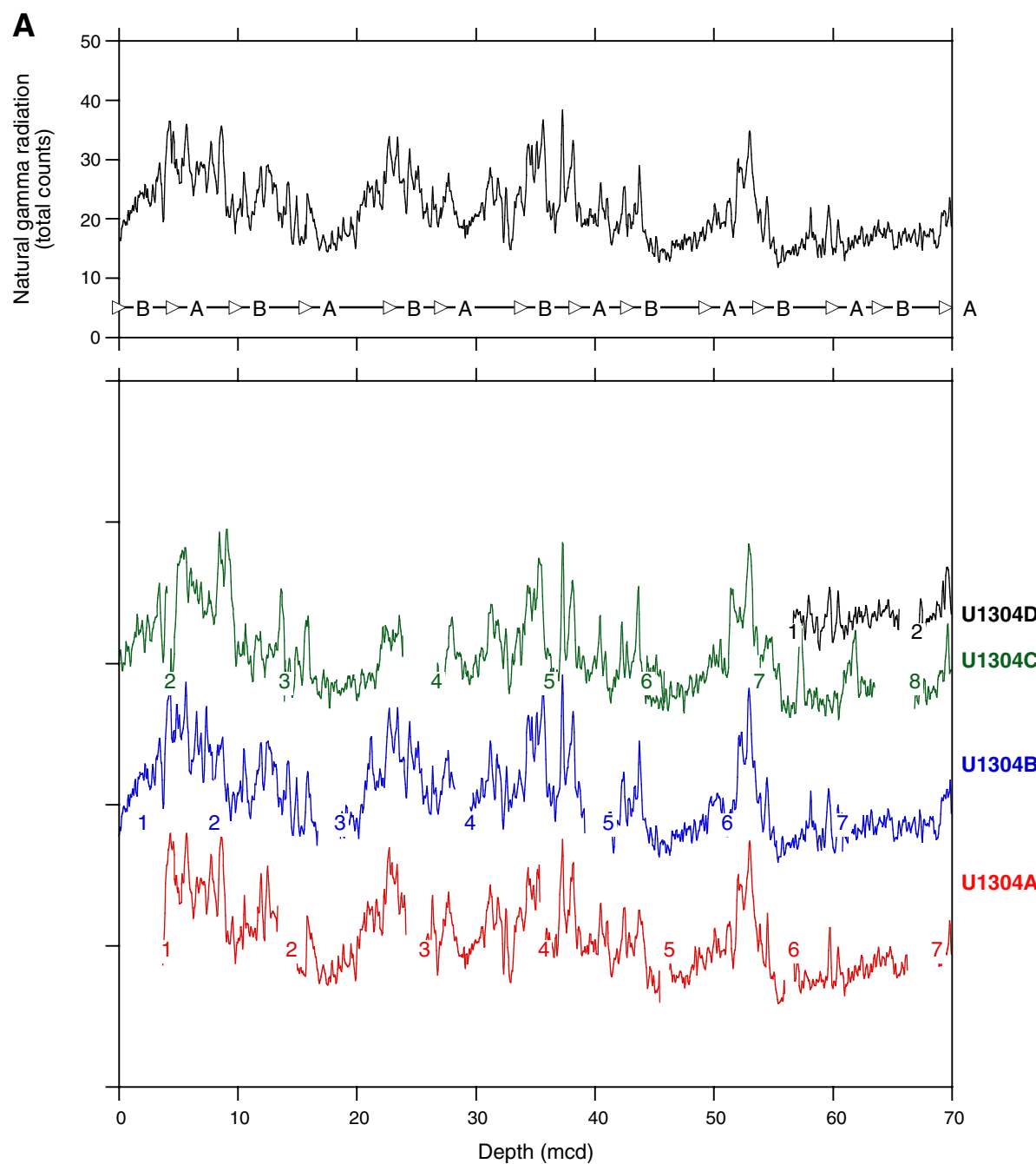


Figure F20 (continued). B. 70–140 mcd.

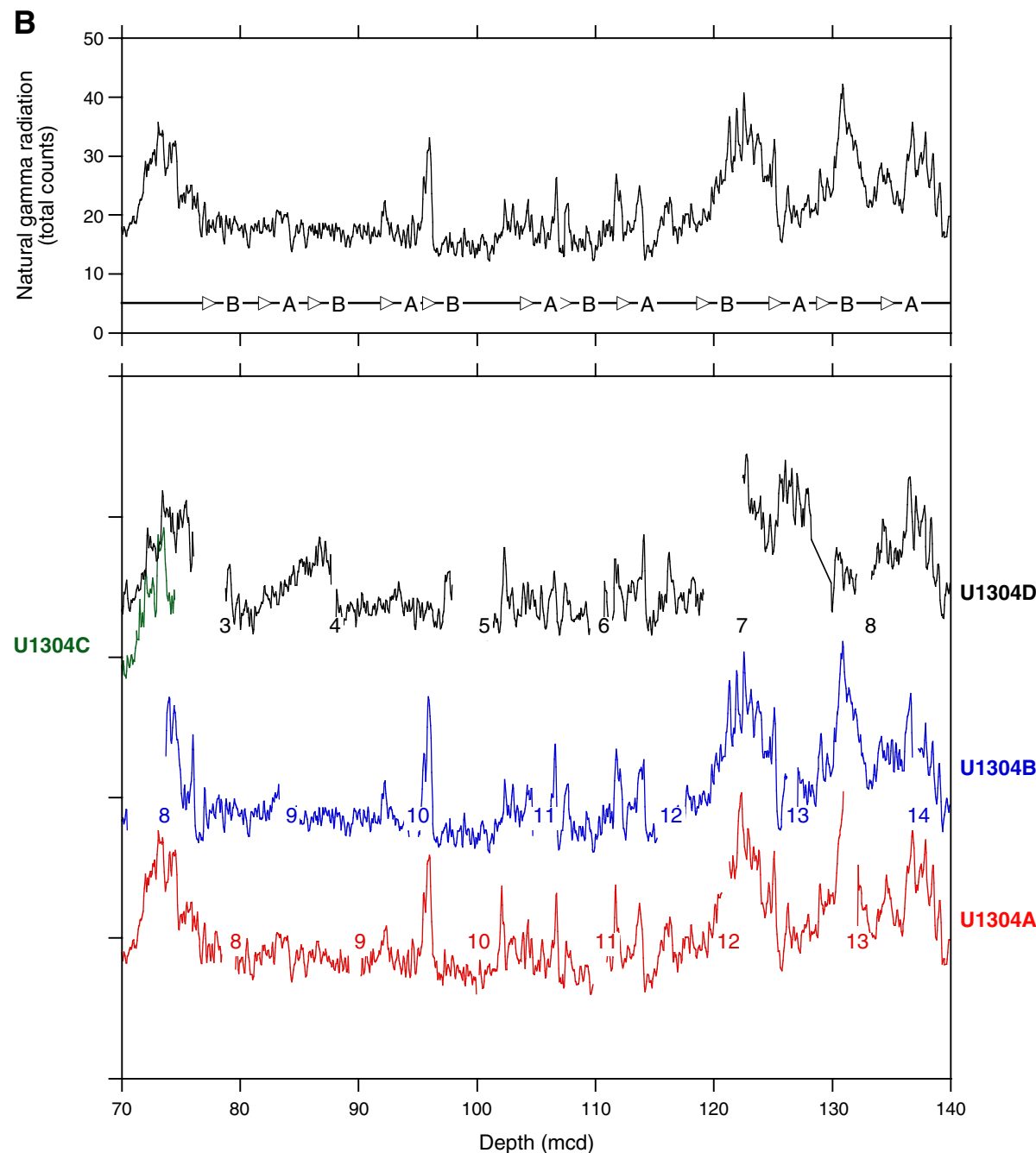


Figure F20 (continued). C. 140–210 mcd.

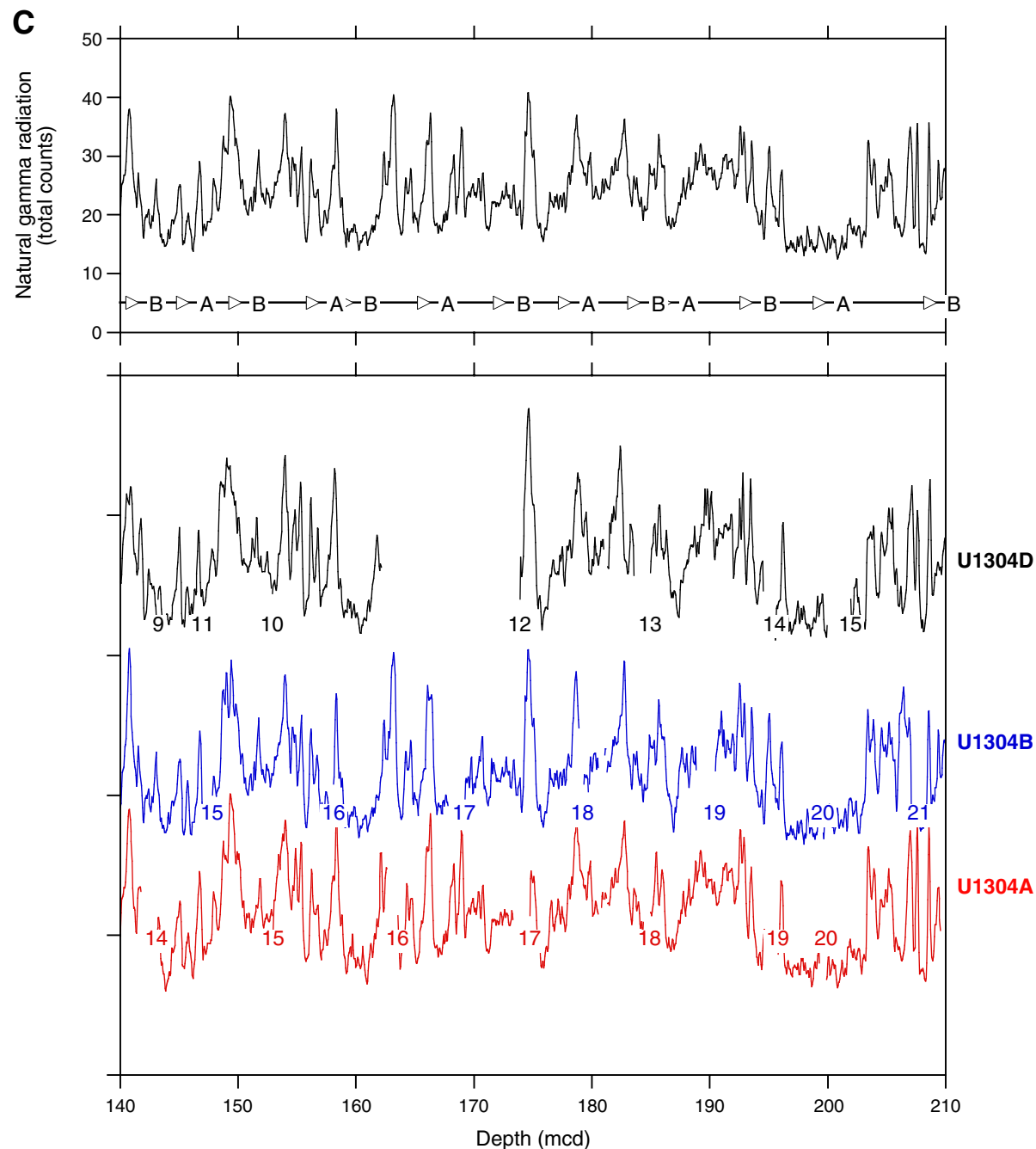
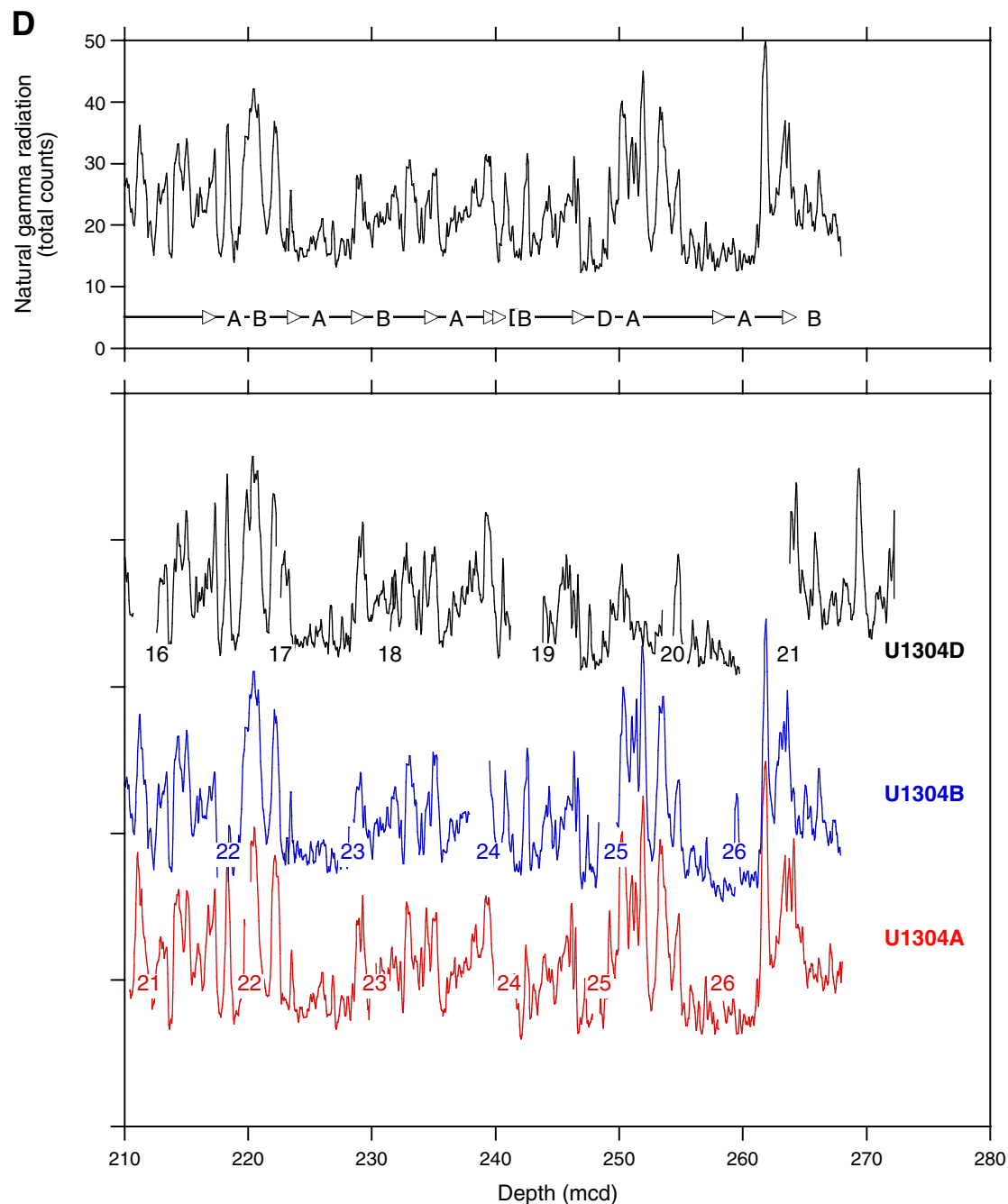


Figure F20 (continued). D. 210–280 mcd.



**Figure F21.** Magnetic susceptibility (MS), Site U1304. Upper panel shows composite MS record indicating which hole was used to form the splice. Letters refer to holes at Site U1302 unless otherwise indicated. A. 0–70 mcd. (Continued on next three pages.)

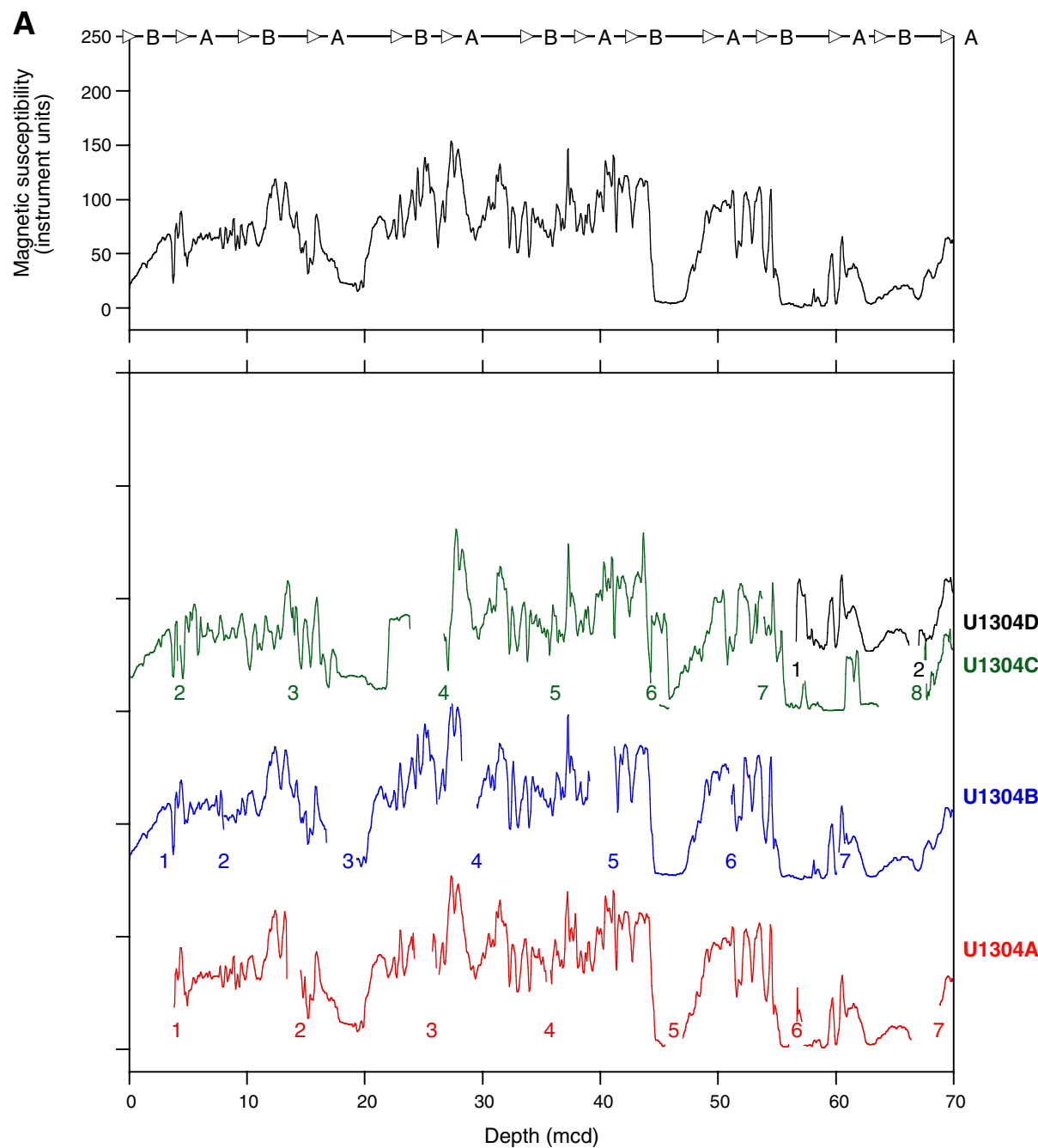


Figure F21 (continued). B. 70–140 mcd.

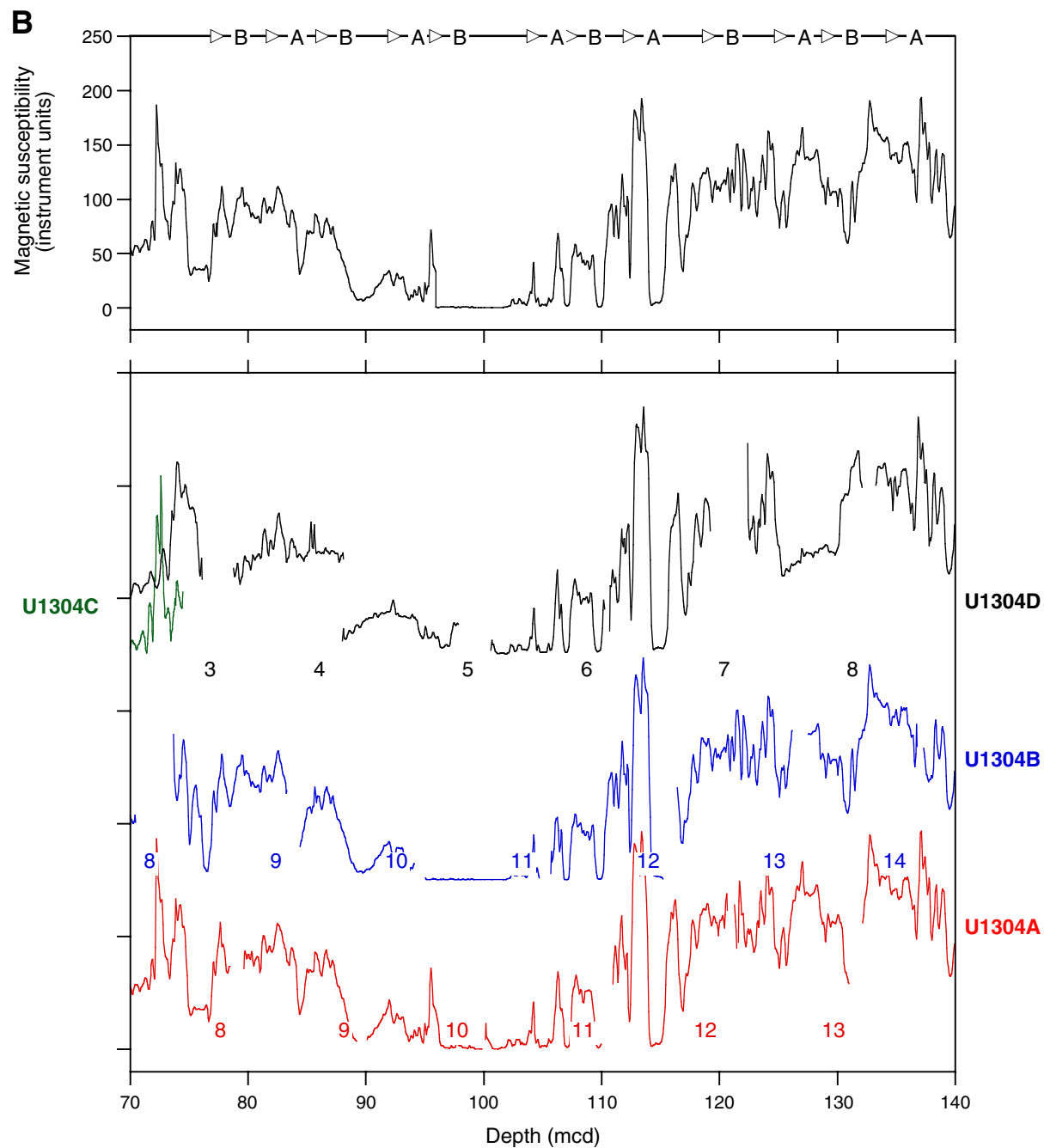


Figure F21 (continued). C. 140–210 mcd.

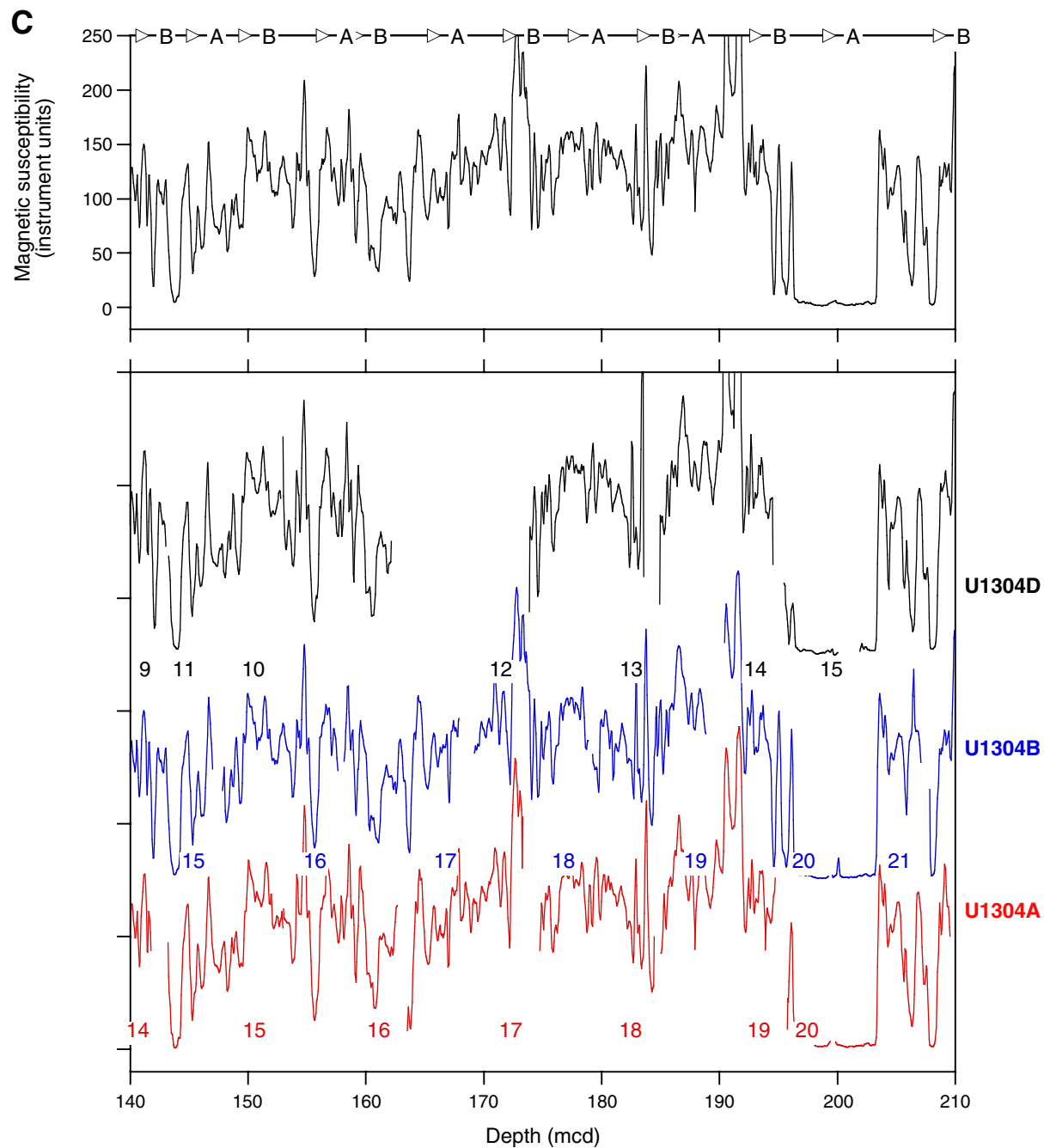
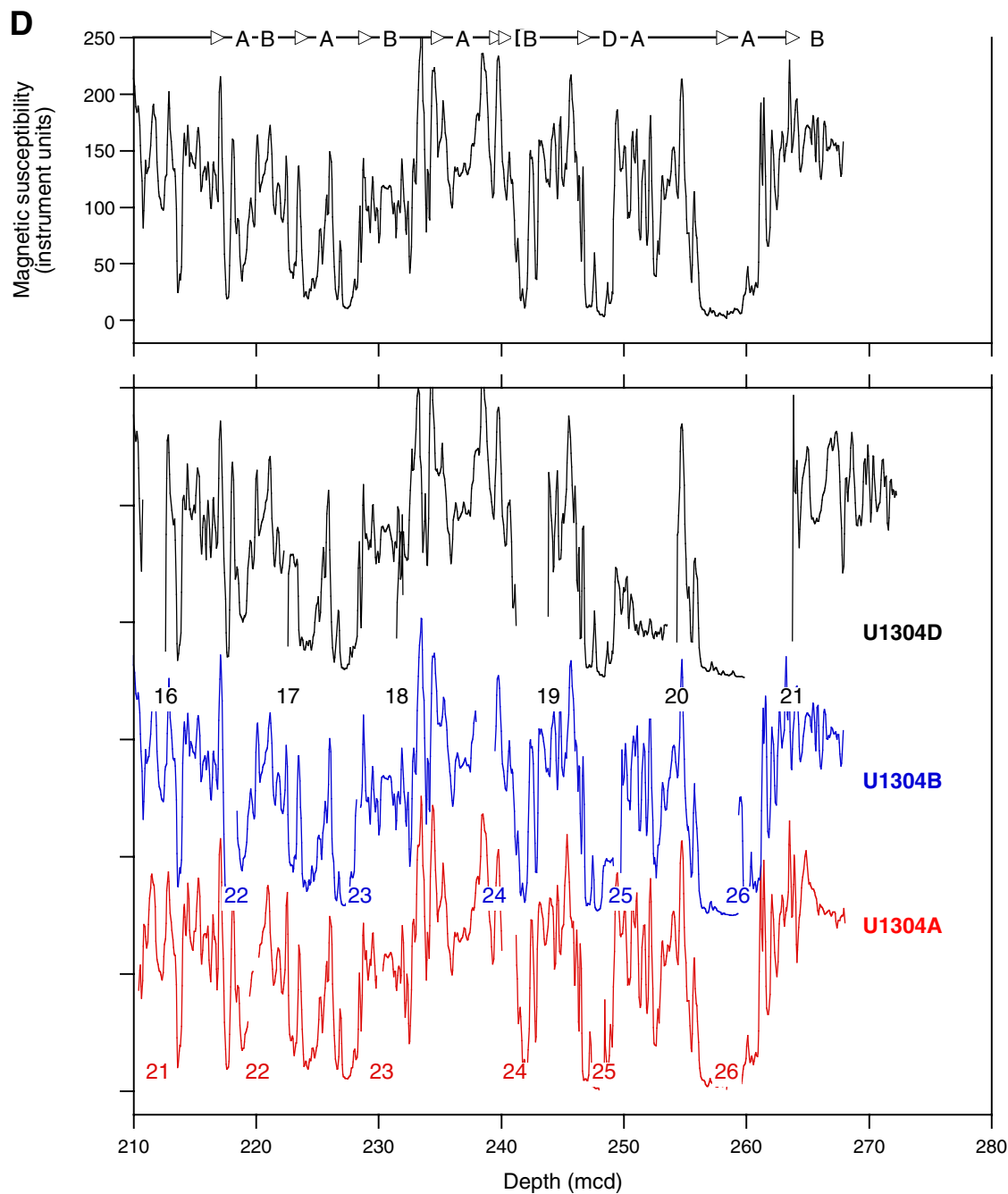
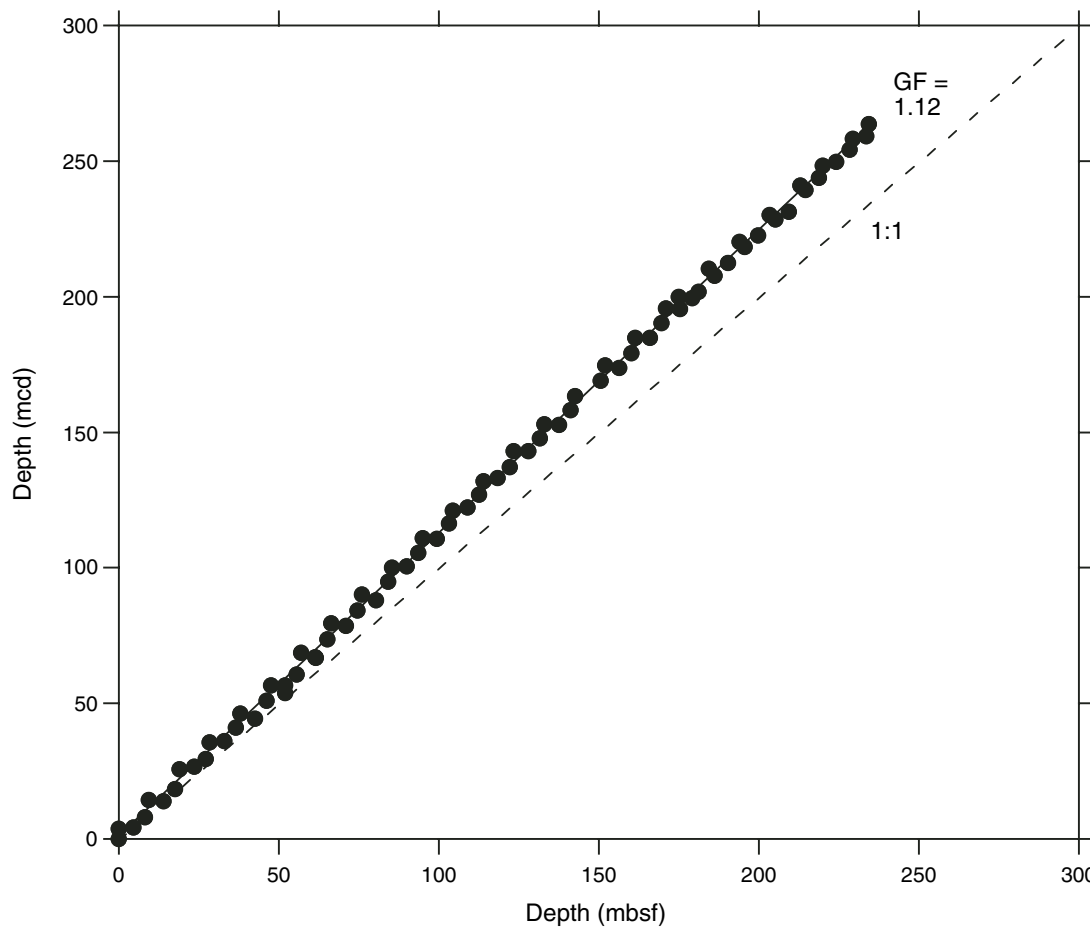


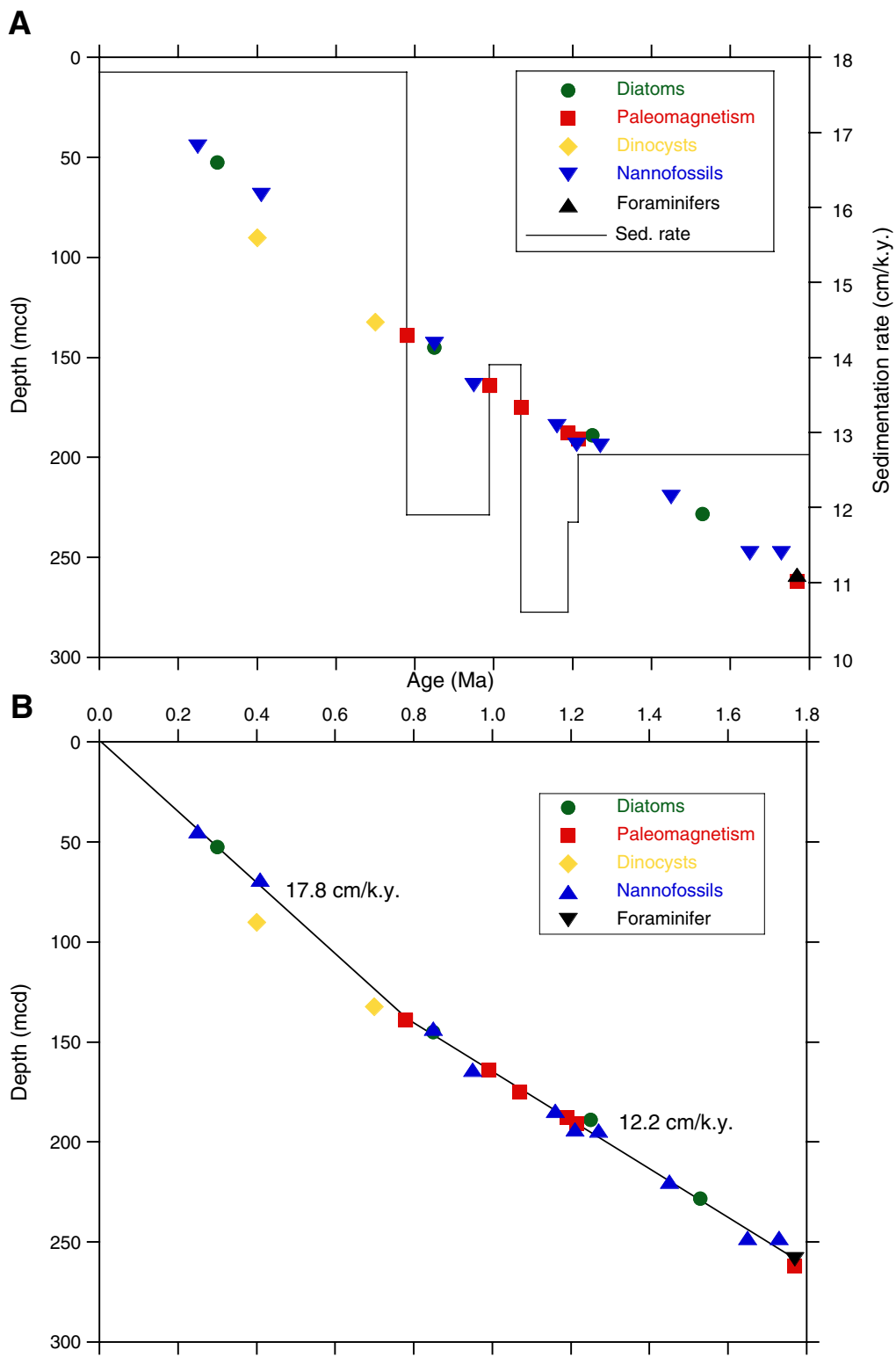
Figure F21 (continued). D. 210–280 mcd.

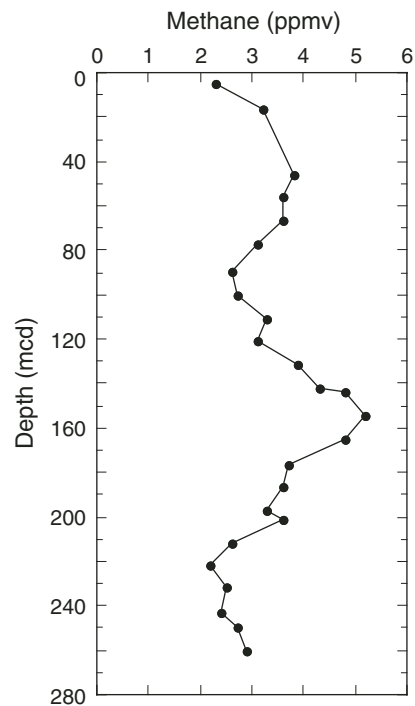


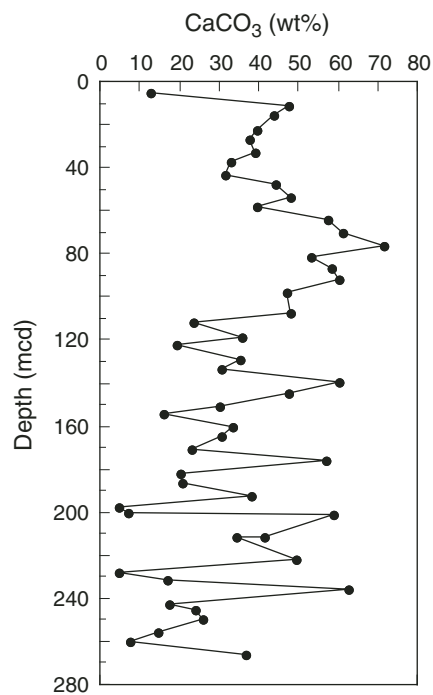
**Figure F22.** Meters composite depth versus meters below seafloor depth for tops of cores at Site U1304. The growth factor (GF) is the slope of the regression line for Sites U1302 and U1303 and for both sites combined. On average, the mcd of the spliced section is 12% greater than meters below seafloor.



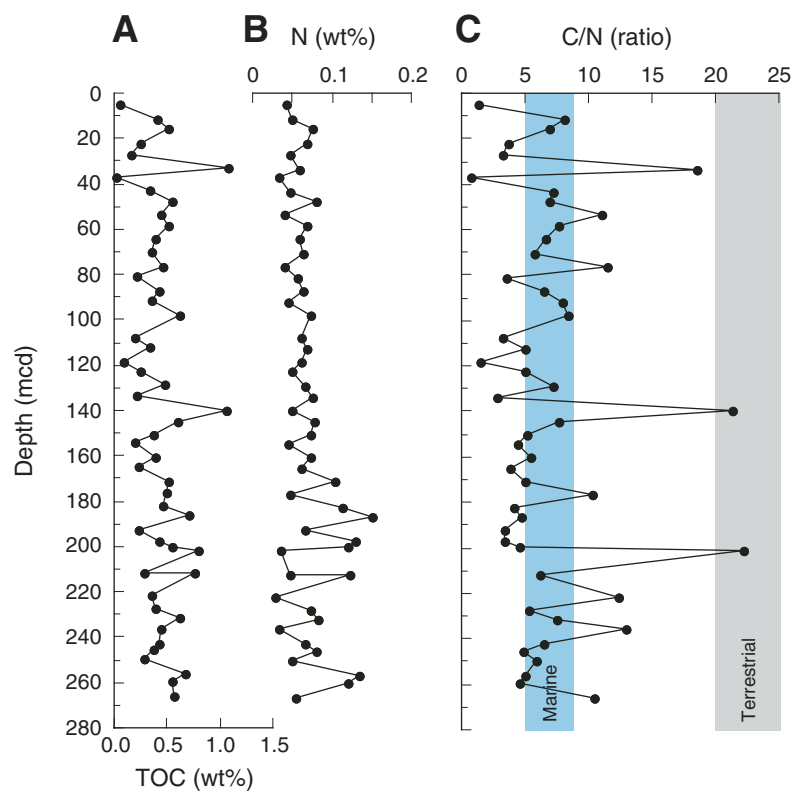
**Figure F23.** A. Age versus depth of paleomagnetic and biostratigraphic datums at Site U1304. Mean sedimentation rates were calculated by linear regression for the Brunhes Chron (0–0.78 Ma) and from the Brunhes/Matuyama boundary (0.78 Ma) to the top of the Olduvai Subchron (1.77 Ma). B. Datums shown with the interval sedimentation rates derived from the paleomagnetic datums only.



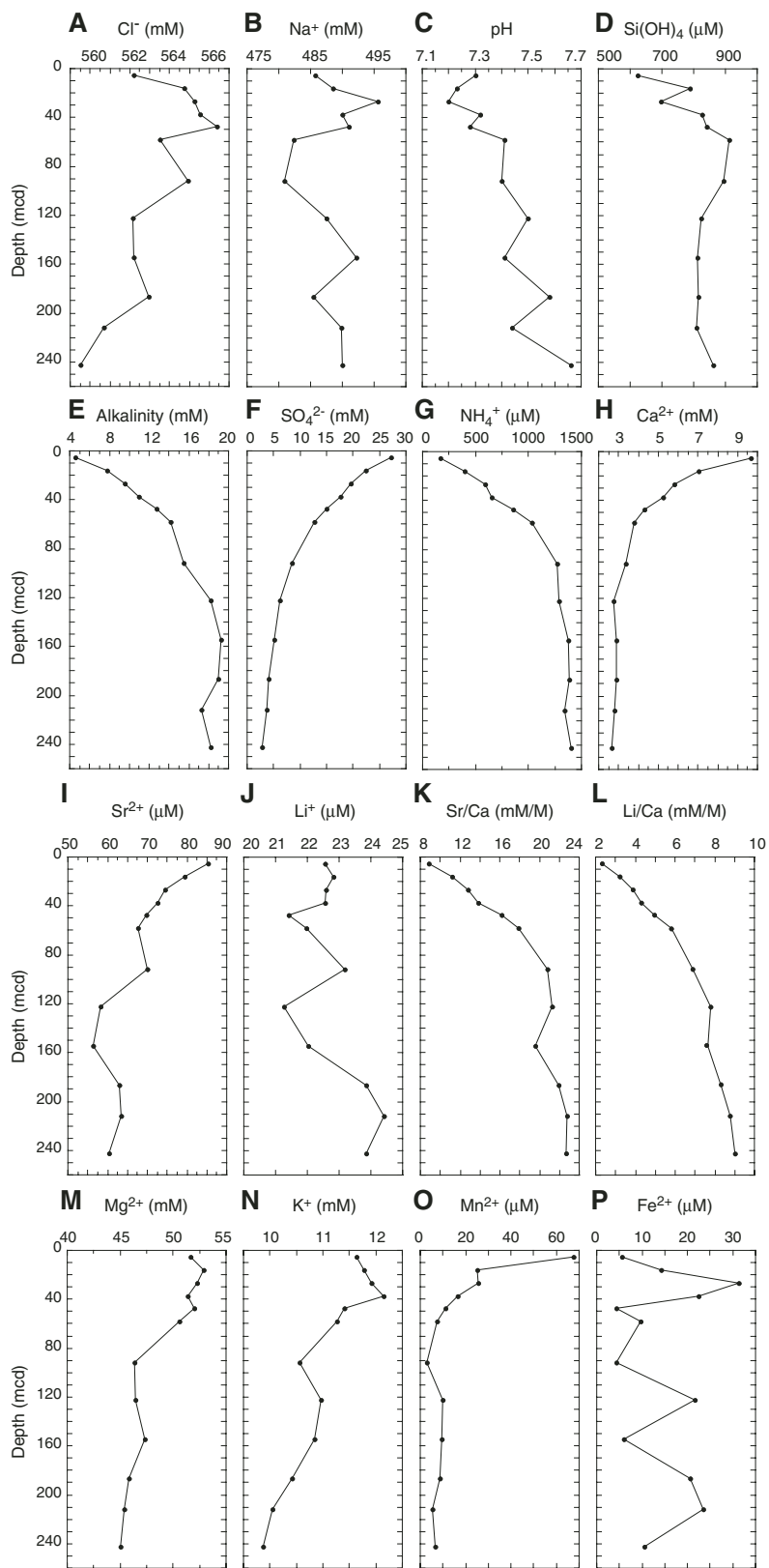
**Figure F24.** Headspace methane concentration, Hole U1304A.

**Figure F25.** Calcium carbonate content for Hole U1304A.

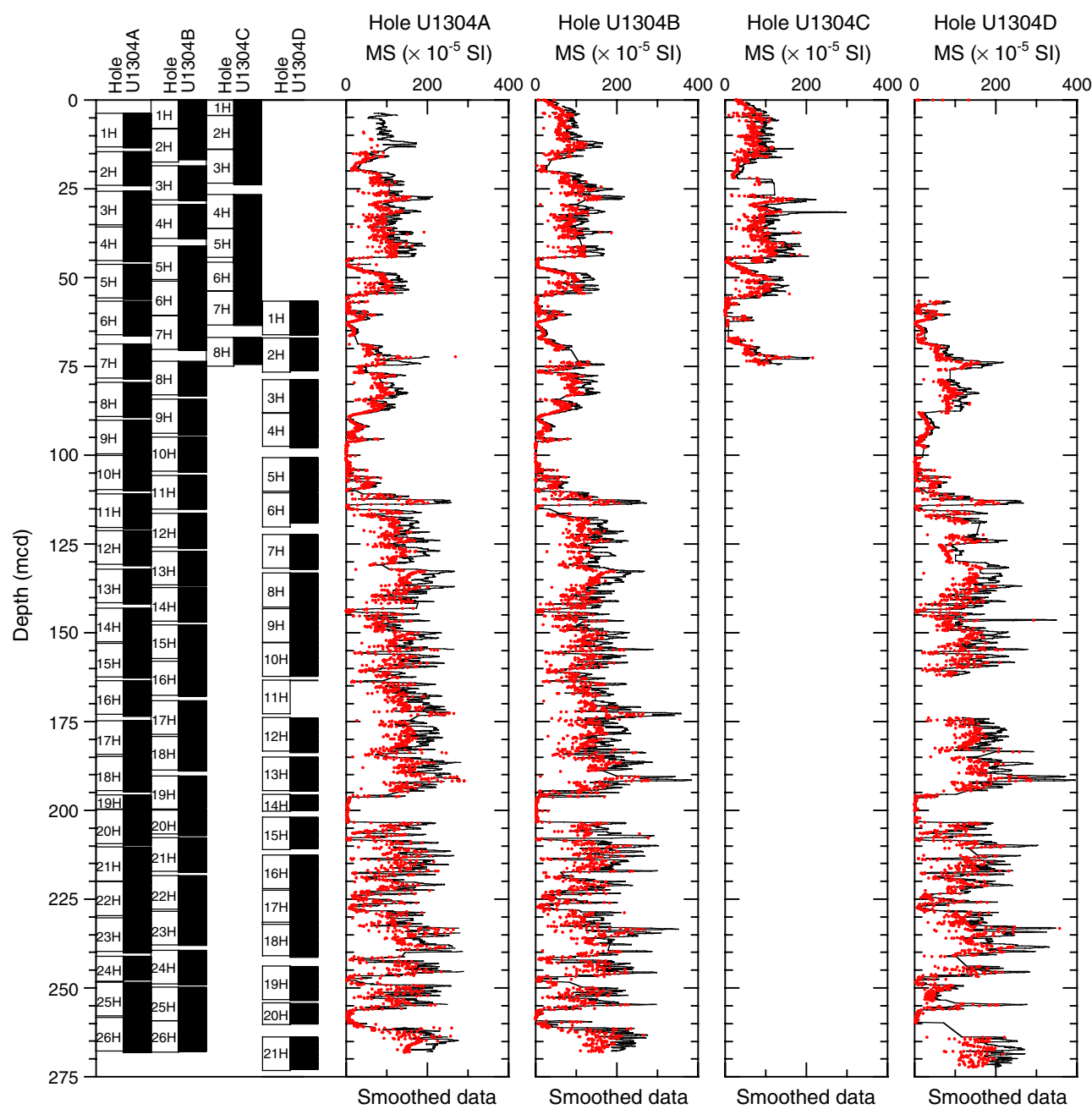
**Figure F26.** Hole U1304A carbonate contents and elemental compositions. A. Total organic carbon (TOC). B. Total nitrogen. C. Organic C/N ratio.



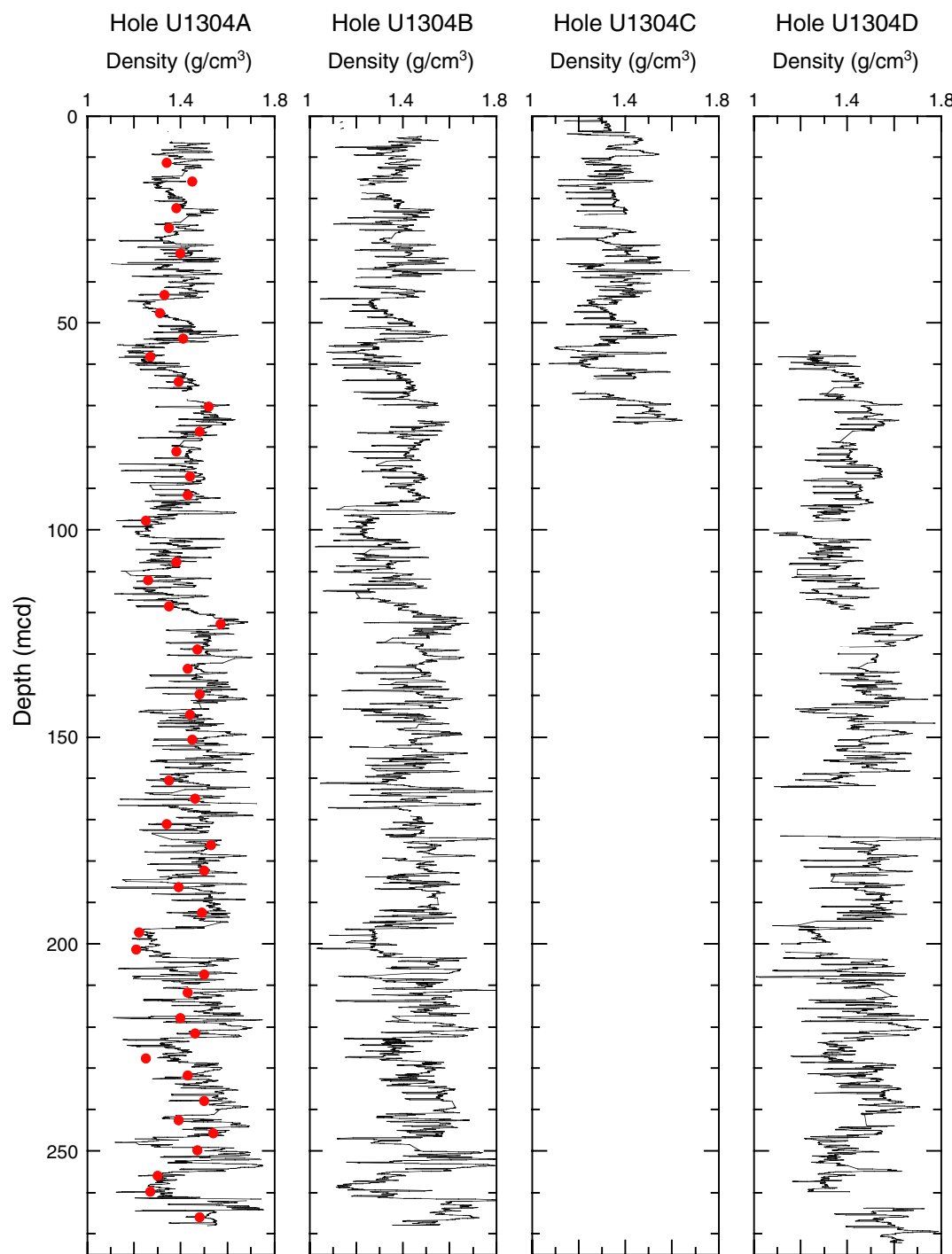
**Figure F27.** Profiles of chemical constituents in interstitial waters from Hole U1304A. A. Chlorinity. B. Sodium. C. pH. D. Silica. E. Alkalinity. F. Sulfate. G. Ammonium. H. Calcium. I. Strontium. J. Lithium. K. Sr/Ca and Li/Ca ratio. L. Magnesium. M. Potassium. N. Manganese. O. Iron.



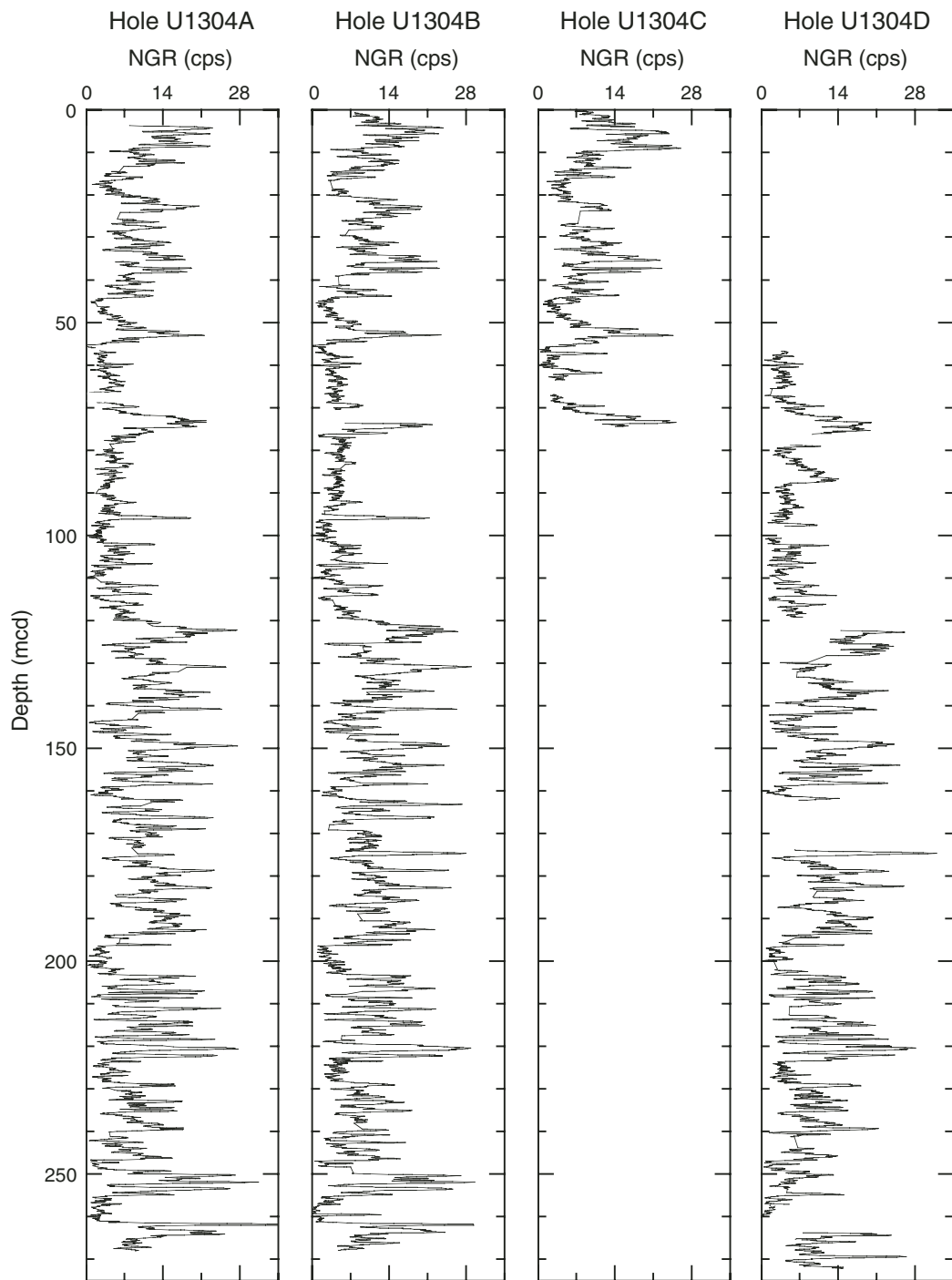
**Figure F28.** Site U1304 magnetic susceptibility (MS) records. Core recovery columns are represented on the left side. Black = multisensor track record, red = magnetic susceptibility core logger record.

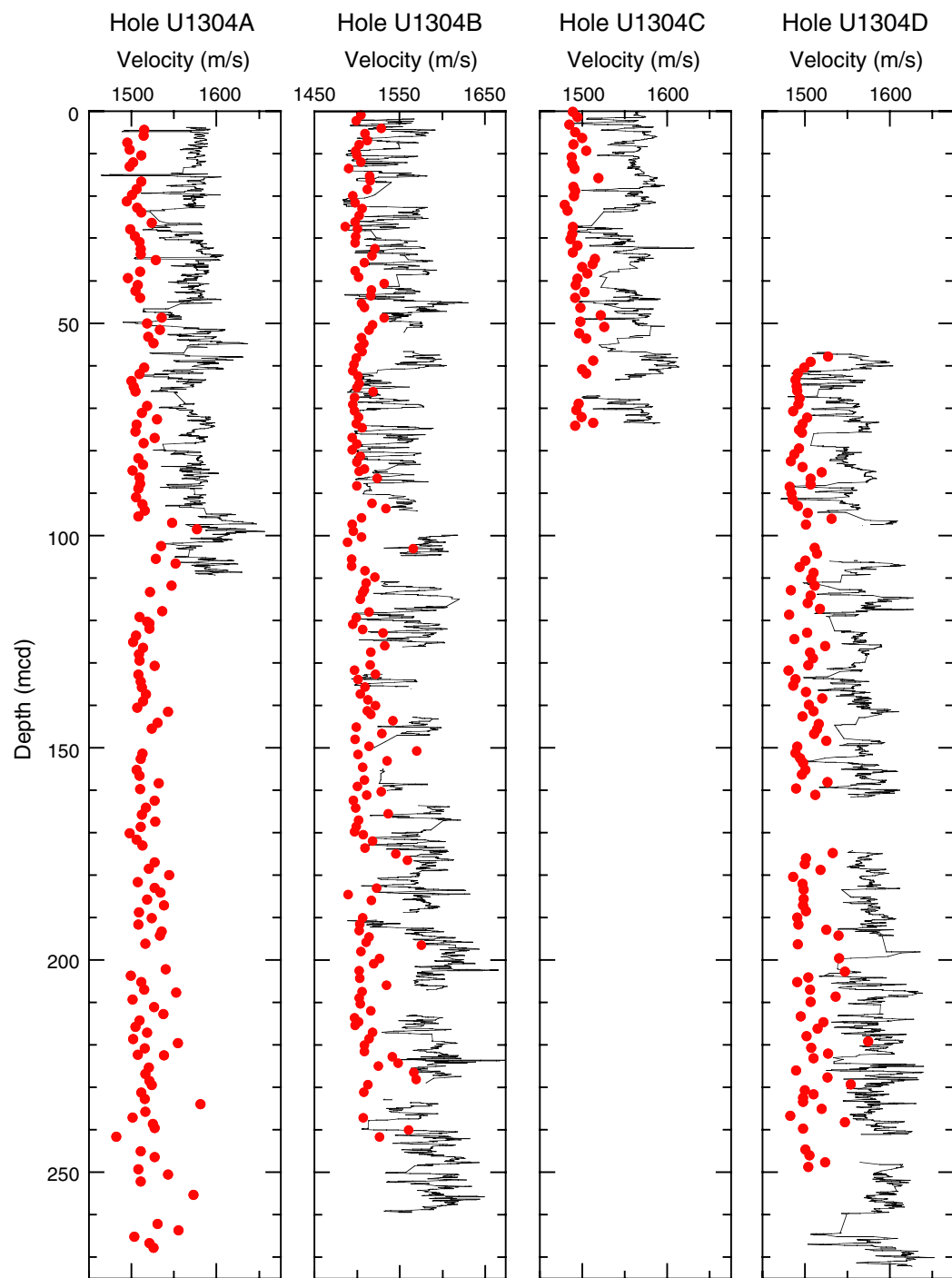


**Figure F29.** Combined gamma ray attenuation density measurements from the multisensor track (MST) and bulk density from discrete measurements (red circles), Site U1304.



**Figure F30.** Natural gamma ray (NGR) counts from the multisensor track, Site U1304.



**Figure F31.** Downcore *P*-wave velocity records, Site U1304.

**Figure F32.** Downcore gamma ray attenuation-derived porosity calculations and discrete porosity measurements (red circles), Site U1304.

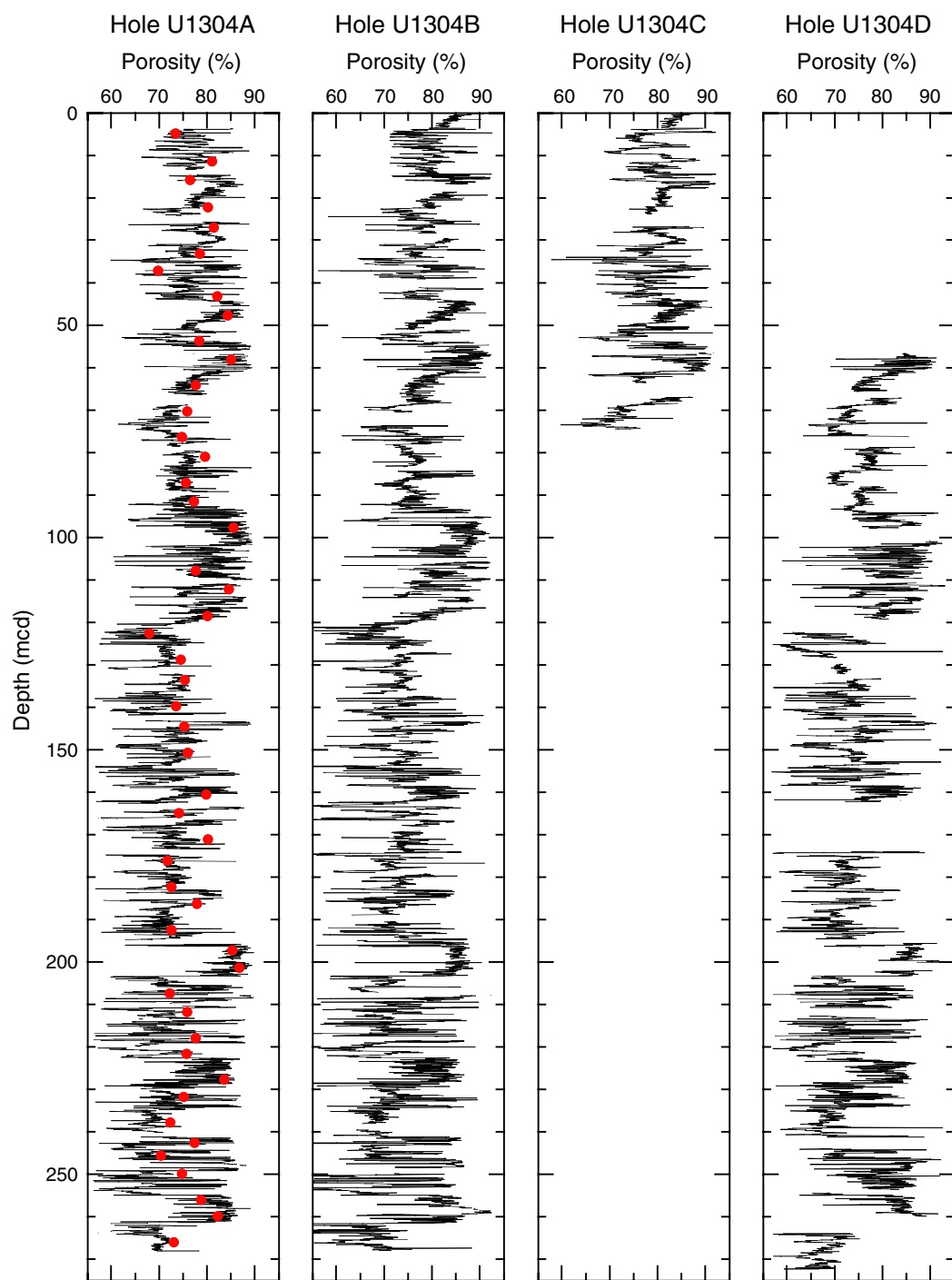


**Figure F33.** Combined plots of the smoothed spliced records of MSCL magnetic susceptibility (MS), gamma ray attenuation (GRA) density, and natural gamma ray (NGR), Site U1304.

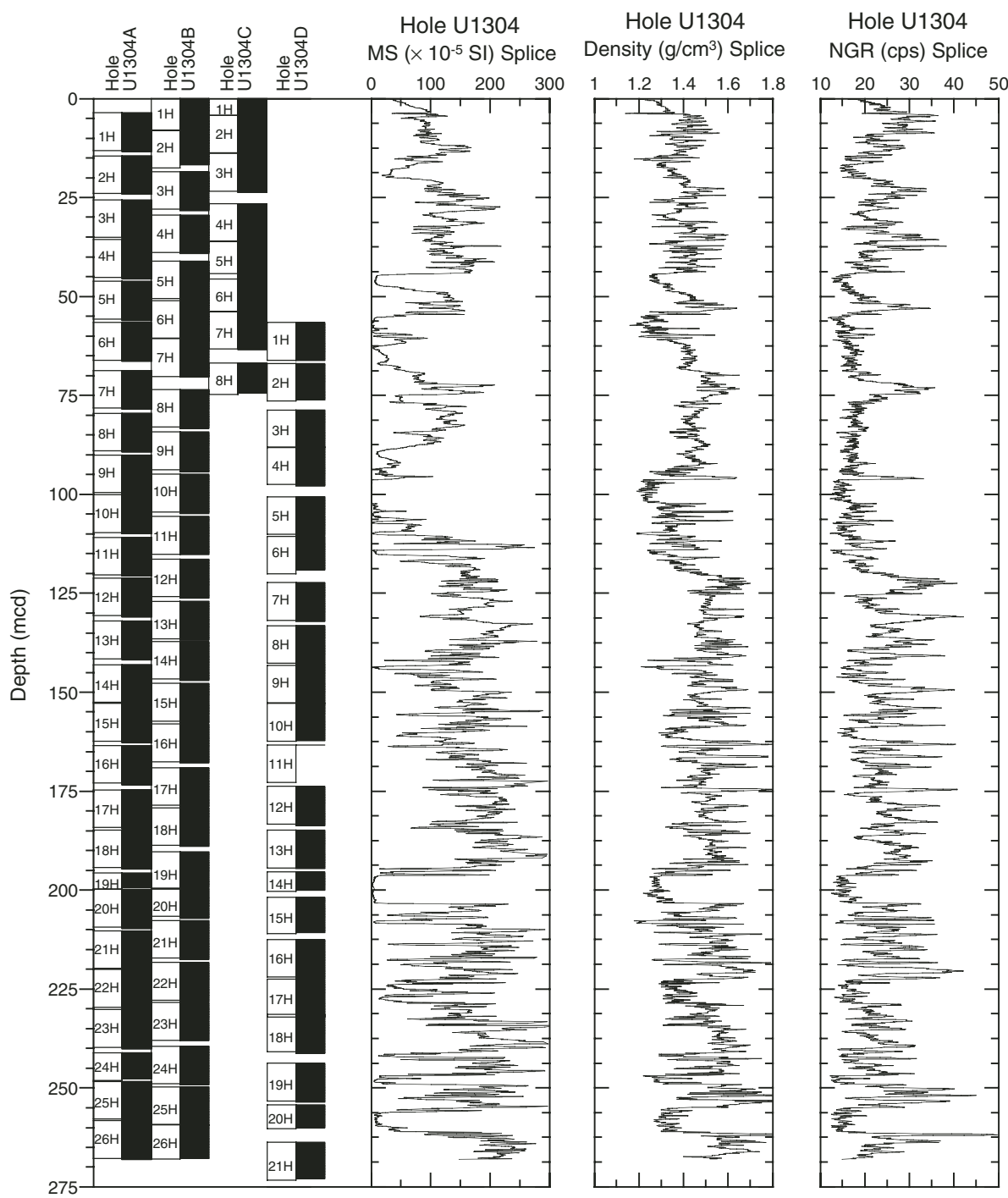


**Table T1.** Coring summary, Site U1304. (Continued on next two pages.)**Hole U1304A**

Latitude: 53°3.4007'N  
 Longitude: 33°31.7814'W  
 Time on site (h): 124.5 (0800 h, 9 October 2004–1230 h, 14 October 2004)  
 Time on hole (h): 35.75 (0800 h, 9 October 2004–1945 h, 10 October 2004)  
 Seafloor (drill pipe measurement from rig floor, mbrf): 3080.0  
 Distance between rig floor and sea level (m): 10.9  
 Water depth (drill pipe measurement from sea level, m): 3069.1  
 Total depth (drill pipe measurement from rig floor, mbrf): 3319.0  
 Total penetration (meters below seafloor, mbsf): 239  
 Total length of cored section (m): 239  
 Total core recovered (m): 251.37  
 Core recovery (%): 105.2  
 Total number of cores: 26

**Hole U1304B**

Latitude: 53°3.3929'N  
 Longitude: 33°31.7681'W  
 Time on hole (h): 30.50 (1945 h, 10 October 2004–0215 h, 12 October 2004)  
 Seafloor (drill pipe measurement from rig floor, mbrf): 3076.3  
 Distance between rig floor and sea level (m): 10.9  
 Water depth (drill pipe measurement from sea level, m): 3065.4  
 Total depth (drill pipe measurement from rig floor, mbrf): 3318.7  
 Total penetration (meters below seafloor, mbsf): 242.4  
 Total length of cored section (m): 242.4  
 Total core recovered (m): 252.15  
 Core recovery (%): 104.0  
 Total number of cores: 26

**Hole U1304C**

Latitude: 53°3.3841'N  
 Longitude: 33°31.7510'W  
 Time on hole (h): 12.17 (0215 h, 12 October 2004–1425 h, 12 October 2004)  
 Seafloor (drill pipe measurement from rig floor, mbrf): 3075.4  
 Distance between rig floor and sea level (m): 10.9  
 Water depth (drill pipe measurement from sea level, m): 3064.5  
 Total depth (drill pipe measurement from rig floor, mbrf): 3145.0  
 Total penetration (meters below seafloor, mbsf): 69.6  
 Total length of cored section (m): 69.6  
 Total core recovered (m): 71.82  
 Core recovery (%): 103.2  
 Total number of cores: 8  
 Comments: Coring operation suspended after 8 h. Pulled out of hole for waiting for weather (WOW).

**Hole U1304D**

Latitude: 53°3.3781'N  
 Longitude: 33°31.7411'W  
 Time on hole (h): 46.08 (1425 h, 12 October 2004–1230 h, 14 October 2004)  
 Seafloor (drill pipe measurement from rig floor, mbrf): 3075.4  
 Distance between rig floor and sea level (m): 10.9  
 Water depth (drill pipe measurement from sea level, m): 3064.5  
 Total depth (drill pipe measurement from rig floor, mbrf): 3319.3  
 Total penetration (meters below seafloor, mbsf): 243.9  
 Total length of cored section (m): 190.9  
 Total length of drilled intervals (m): 53  
 Total core recovered (m): 185.67  
 Core recovery (%): 97.3  
 Total number of cores: 21  
 Total number of drilled intervals: 2

Core	Date (Oct 2004)	Local time (h)	Depth (mbsf)		Length (m)		Recovery (%)	Comments
			Top	Bottom	Cored	Recovered		
<b>303-U1304A-</b>								
1H	9	1400	0.0	9.50	9.50	9.91	104.3	Nonmagnetic barrel
2H	9	1500	9.5	19.00	9.50	9.88	104.0	Nonmagnetic barrel
3H	9	1550	19.0	28.50	9.50	9.96	104.8	Oriented; nonmagnetic barrel
4H	9	1640	28.5	38.00	9.50	10.03	105.6	Oriented; nonmagnetic barrel
5H	9	1740	38.0	47.50	9.50	10.04	105.7	Oriented; nonmagnetic barrel
6H	9	1840	47.5	57.00	9.50	9.94	104.6	Oriented; nonmagnetic barrel
7H	9	1930	57.0	66.50	9.50	9.97	105.0	Oriented; nonmagnetic barrel



Table T1 (continued).

Core	Date (Oct 2004)	Local time (h)	Depth (mbsf)		Length (m)		Recovery (%)	Comments
			Top	Bottom	Cored	Recovered		
8H	9	2030	66.5	76.00	9.50	9.96	104.8	Oriented; nonmagnetic barrel
9H	9	2125	76.0	85.50	9.50	10.23	107.7	Oriented; nonmagnetic barrel
10H	9	2225	85.5	95.00	9.50	10.09	106.2	Oriented; nonmagnetic barrel
11H	9	2330	95.0	104.50	9.50	9.98	105.1	Oriented; nonmagnetic barrel
12H	10	0025	104.5	114.00	9.50	10.07	106.0	Oriented; nonmagnetic barrel
13H	10	0120	114.0	123.50	9.50	9.98	105.1	Oriented; nonmagnetic barrel
14H	10	0220	123.5	133.00	9.50	10.08	106.1	Oriented; nonmagnetic barrel
15H	10	0315	133.0	142.50	9.50	10.02	105.5	Oriented; nonmagnetic barrel
16H	10	0400	142.5	152.00	9.50	10.12	106.5	Oriented; nonmagnetic barrel
17H	10	0500	152.0	161.50	9.50	10.00	105.3	Oriented; nonmagnetic barrel
18H	10	0610	161.5	171.00	9.50	10.09	106.2	Oriented; nonmagnetic barrel
19H	10	0740	171.0	175.00	4.00	3.85	96.3	Oriented; nonmagnetic barrel; drillover core barrel
20H	10	0930	175.0	184.50	9.50	10.12	106.5	Liner shattered due to expansion
21H	10	1100	184.5	194.00	9.50	9.97	105.0	Drillover core barrel
22H	10	1230	194.0	203.50	9.50	10.06	105.9	Drillover core barrel
23H	10	1405	203.5	213.00	9.50	10.08	106.1	
24H	10	1515	213.0	220.00	7.00	6.88	98.3	Drillover core barrel; split liner Section 4
25H	10	1640	220.0	229.50	9.50	10.10	106.3	Shattered liner; liner patch used
26H	10	1800	229.5	239.00	9.50	9.96	104.8	Drillover core barrel
			Totals:		239.00	251.37	105.2	
303-U1304B-								
1H	10	2125	0.0	8.2	8.2	8.14	99.3	Nonmagnetic barrel
2H	10	2200	8.2	17.7	9.5	8.96	94.3	Nonmagnetic barrel
3H	10	2255	17.7	27.2	9.5	9.90	104.2	Oriented; nonmagnetic barrel
4H	11	0005	27.2	36.7	9.5	9.87	103.9	Oriented; nonmagnetic barrel
5H	11	0100	36.7	46.2	9.5	10.12	106.5	Oriented; nonmagnetic barrel
6H	11	0150	46.2	55.7	9.5	9.90	104.2	Oriented; nonmagnetic barrel
7H	11	0245	55.7	65.2	9.5	9.85	103.7	Oriented; nonmagnetic barrel
8H	11	0335	65.2	74.7	9.5	9.90	104.2	Oriented; nonmagnetic barrel
9H	11	0430	74.7	84.2	9.5	10.25	107.9	Oriented; nonmagnetic barrel
10H	11	0520	84.2	93.7	9.5	10.10	106.3	Oriented; nonmagnetic barrel
11H	11	0620	93.7	103.2	9.5	9.72	102.3	Oriented; nonmagnetic barrel
12H	11	0710	103.2	112.7	9.5	10.07	106.0	Oriented; nonmagnetic barrel
13H	11	0800	112.7	122.2	9.5	9.98	105.1	Oriented; nonmagnetic barrel
14H	11	0850	122.2	131.7	9.5	9.95	104.7	Oriented; nonmagnetic barrel
15H	11	0945	131.7	141.2	9.5	10.13	106.6	Oriented; nonmagnetic barrel
16H	11	1140	141.2	150.7	9.5	9.95	104.7	Oriented; nonmagnetic barrel
17H	11	1255	150.7	160.2	9.5	10.08	106.1	Oriented; nonmagnetic barrel
18H	11	1350	160.2	169.7	9.5	9.96	104.8	Oriented; nonmagnetic barrel
19H	11	1530	169.7	179.2	9.5	9.18	96.6	Drillover core barrel
20H	11	1645	179.2	186.2	7.0	7.78	111.1	Drillover core barrel
21H	11	1835	186.2	195.7	9.5	9.96	104.8	Drillover core barrel
22H	11	2015	195.7	205.2	9.5	10.04	105.7	
23H	11	2145	205.2	214.7	9.5	9.78	103.0	
24H	11	2225	214.7	224.2	9.5	9.99	105.2	Drillover core barrel
25H	11	2330	224.2	233.7	9.5	9.84	103.6	Drillover core barrel
26H	12	0030	233.7	242.4	8.7	8.75	100.6	
			Totals:		242.4	252.15	104.0	
303-U1304C-								
1H	12	0510	0.0	4.6	4.6	4.58	99.6	Nonmagnetic barrel
2H	12	0600	4.6	14.1	9.5	9.88	104.0	Nonmagnetic barrel
3H	12	0710	14.1	23.6	9.5	10.10	106.3	Oriented; nonmagnetic barrel
4H	12	0825	23.6	33.1	9.5	9.93	104.5	Oriented; nonmagnetic barrel
5H	12	0945	33.1	42.6	9.5	9.98	105.1	Oriented; nonmagnetic barrel
6H	12	1100	42.6	52.1	9.5	9.68	101.9	Oriented; nonmagnetic barrel
7H	12	1210	52.1	61.6	9.5	9.89	104.1	Oriented; nonmagnetic barrel
8H	12	1320	61.6	69.6	8.0	7.78	97.3	Oriented; nonmagnetic barrel
			Totals:		69.6	71.82	103.2	
303-U1304D-								
*****Drilled 0.0 to 52.0 mbsf *****								
1H	12	2140	52.0	61.5	9.5	9.76	102.7	Drilled with center bit
2H	12	2250	61.5	71.0	9.5	9.33	98.2	Oriented; nonmagnetic barrel
3H	13	0005	71.0	80.5	9.5	9.69	102.0	Oriented; nonmagnetic barrel
4H	13	0235	80.5	90.0	9.5	10.02	105.5	Oriented; nonmagnetic barrel
5H	13	0400	90.0	99.5	9.5	9.95	104.7	Oriented; nonmagnetic barrel
6H	13	0525	99.5	109.0	9.5	8.64	91.0	Oriented; nonmagnetic barrel
7H	13	0710	109.0	118.5	9.5	9.95	104.7	Oriented; nonmagnetic barrel

Table T1 (continued).

Core	Date (Oct 2004)	Local time (h)	Depth (mbsf)		Length (m)		Recovery (%)	Comments
			Top	Bottom	Cored	Recovered		
8H	13	1000	118.5	128.0	9.5	10.08	106.1	Oriented; nonmagnetic barrel
9H	13	1110	128.0	137.5	9.5	9.92	104.4	Oriented; nonmagnetic barrel
10H	13	1225	137.5	147.0	9.5	9.56	100.6	Oriented; nonmagnetic barrel
11H	13	1340	147.0	156.5	9.5	0.14	1.5	Oriented; nonmagnetic barrel
12H	13	1530	156.5	166.0	9.5	10.00	105.3	Oriented; nonmagnetic barrel
13H	13	1635	166.0	175.5	9.5	9.88	104.0	Oriented; nonmagnetic barrel
14H	13	1735	175.5	180.3	4.8	4.73	98.5	Oriented; nonmagnetic barrel; crushed liner
*****Drilled 180.3 to 181.3 mbst*****								
15H	13	2010	181.3	190.4	9.1	9.09	99.9	
16H	13	2135	190.4	199.9	9.5	10.04	105.7	
17H	13	2320	199.9	209.4	9.5	9.67	101.8	
18H	14	0020	209.4	218.9	9.5	10.03	105.6	
19H	14	0135	218.9	228.4	9.5	9.94	104.6	
20H	14	0330	228.4	234.4	6.0	5.91	98.5	Crushed liner
21H	14	0430	234.4	243.9	9.5	9.34	98.3	Crushed liner
			Cored:	190.9	185.67	97.3		
			Drilled:	53				
			Total:	243.9				



**Table T2.** Distribution of calcareous nannofossils, Hole U1304A.

Core, section, interval (cm)	Age (Ma)	Abundance	Preservation	Calcareous nannofossils, Hole U1304A												Reworked species	MIS
				M. nannofoossilia (Ma)	M. nannofoossilia (Ma)	M. nannofoossilia (Ma)	M. nannofoossilia (Ma)	M. nannofoossilia (Ma)	M. nannofoossilia (Ma)	M. nannofoossilia (Ma)	M. nannofoossilia (Ma)	M. nannofoossilia (Ma)	M. nannofoossilia (Ma)	M. nannofoossilia (Ma)	M. nannofoossilia (Ma)		
303-U1304A-1H-CC	0~0.25	A	G	R	R	R	R	R	R	R	R	R	R	R	R	+	0.25
2H-CC	0~0.25	A	G	R	R	R	R	R	R	R	R	R	R	R	R	+	0.41
3H-CC	0~0.25	P	M	F	F	F	F	F	F	F	F	F	F	F	F	+	0.85
4H-CC	0~0.25	C	G	F	F	F	F	F	F	F	F	F	F	F	F	+	0.95
5H-CC	0.25~0.41	A	G	F	F	F	F	F	F	F	F	F	F	F	F	+	1.16
6H-CC	0.25~0.41	A	G	R	C	R	R	R	R	R	R	R	R	R	R	+	1.21
7H-CC	0.41~0.85	A	G	R	C	C	+	R	R	R	R	R	R	R	R	+	1.27
8H-CC	0.41~0.85	A	G	R	C	C	+	R	R	R	R	R	R	R	R	+	1.45
9H-CC	0.41~0.85	C	G	+ F	R	R	+	R	R	R	R	R	R	R	R	+	1.65
10H-CC	0.41~0.85	A	G	R	R	R	R	R	R	R	R	R	R	R	R	+	1.73
11H-CC	0.41~0.85	C	M	+	R	R	R	R	R	R	R	R	R	R	R	+	
12H-CC	0.41~0.85	C	M	R	+	R	R	R	R	R	R	R	R	R	R	+	
13H-CC	0.41~0.85	A	G	R	+	R	R	R	R	R	R	R	R	R	R	+	
14H-CC	0.85~0.95	A	G	R	R	R	R	R	R	R	R	R	R	R	R	+	
15H-CC	0.85~0.95	A	G	R	R	R	R	R	R	R	R	R	R	R	R	+	
16H-CC	0.95~1.16	C	G	R	R	R	R	R	R	R	R	R	R	R	R	+	
17H-CC	0.95~1.16	C	M	C	R	R	R	R	R	R	R	R	R	R	R	+	
18H-1, 0~1	1.16~1.21	R	M	F	R	R	R	R	R	R	R	R	R	R	R	+	
18H-3, 0~1	1.16~1.21	A	G	F	R	R	R	R	R	R	R	R	R	R	R	+	
18H-5, 0~1	1.16~1.21	A	M	F	R	R	R	R	R	R	R	R	R	R	R	+	
18H-6, 0~1	1.16~1.21	A	M	R	C	R	R	R	R	R	R	R	R	R	R	+	
18H-7, 0~1	1.16~1.21	C	M	R	C	R	R	R	R	R	R	R	R	R	R	+	
18H-7, 50~51	1.21~1.27	A	M	F	C	R	R	R	R	R	R	R	R	R	R	+	
18H-CC	1.27~1.45	C	M	R	C	+	R	R	R	R	R	R	R	R	R	+	
19H-CC	?	B	G	F	F	R	+	R	F	A	C	+	A	R	R	+	
20H-CC	1.27~1.45	A	G	F	F	R	+	R	F	A	C	+	A	R	R	+	
21H-CC	?	B	G	F	C	+	R	R	C	C	A	C	F	F	C	+	
22H-CC	1.45~1.65	A	G	R	A	R	R	R	R	R	A	C	F	F	A	+	
23H-CC	1.45~1.65	A	G	R	C	+	R	R	F	R	F	C	F	F	C	+	
24H-CC	1.45~1.65	C	M	R	C	+	R	R	F	R	F	+	F	F	C	+	
25H-CC	1.73~1.97	C	M	+	C	R	+	R	R	R	F	+	F	F	C	+	
26H-CC	1.73~1.97	A	G	+	A	R	+	R	R	R	+	F	F	F	C	+	

Notes: Abundance: A = abundant, C = common, F = few, R = rare, + = present, r = reworked. Preservation: G = good, M = moderate. MIS = marine isotope stage (per Wei, 1993; Sato et al., 1999).

**Table T3.** Distribution of calcareous nannofossils, Hole U1304B.

Core, section	Age (Ma)	Abundance	Preservation	MIS																		Reworked species	
				Nanofossil datum age (Ma)						Marine isotope stage						Cretaceous							
303-U1304B-																							
1H-CC	0-0.25	A	G	C	F	R	R	R	R	R	R	R	R	R	R	R	R	R	R	R	R	R	
2H-CC	0-0.25	A	G	F	F	F	R	R	R	R	R	R	R	R	R	R	R	R	R	R	R	R	
3H-CC	0-0.25	A	G	+G	R	R	R	R	R	R	R	R	R	R	R	R	R	R	R	R	R	R	
4H-CC	0-0.25	A	G	R	R	R	R	R	R	R	R	R	R	R	R	R	R	R	R	R	R	R	
5H-CC	0.25-0.41	A	G	R	R	R	R	R	R	R	R	R	R	R	R	R	R	R	R	R	R	R	r
6H-CC	0.25-0.41	A	G	R	R	R	R	R	R	R	R	R	R	R	R	R	R	R	R	R	R	R	r
7H-CC	0.25-0.41	A	G	R	R	R	R	R	R	R	R	R	R	R	R	R	R	R	R	R	R	R	r
8H-CC	0.41-0.85	A	G	R	R	R	R	R	R	R	R	R	R	R	R	R	R	R	R	R	R	R	r
9H-CC	0.41-0.85	A	G	+G	R	R	R	R	R	R	R	R	R	R	R	R	R	R	R	R	R	R	r
10H-CC	0.41-0.85	A	G	R	R	R	R	R	R	R	R	R	R	R	R	R	R	R	R	R	R	R	r
11H-CC	0.41-0.85	A	G	R	R	R	R	R	R	R	R	R	R	R	R	R	R	R	R	R	R	R	r
12H-CC	0.41-0.85	A	G	R	R	R	R	R	R	R	R	R	R	R	R	R	R	R	R	R	R	R	r
13H-CC	0.41-0.85	R	M	F	R	R	R	R	R	R	R	R	R	R	R	R	R	R	R	R	R	R	r
14H-CC	0.41-0.85	A	G	F	R	R	R	R	R	R	R	R	R	R	R	R	R	R	R	R	R	R	r
15H-CC	0.85-0.95	A	G	F	R	R	R	R	R	R	R	R	R	R	R	R	R	R	R	R	R	R	r
16H-CC	0.85-0.95	C	G	R	R	R	R	R	R	R	R	R	R	R	R	R	R	R	R	R	R	R	r
17H-CC	0.95-1.16	C	M	R	R	R	R	R	R	R	R	R	R	R	R	R	R	R	R	R	R	R	r
18H-CC	0.95-1.16	C	G	R	R	R	R	R	R	R	R	R	R	R	R	R	R	R	R	R	R	R	r
19H-CC	1.21-1.27	C	M	R	R	R	R	R	R	R	R	R	R	R	R	R	R	R	R	R	R	R	1.21
20H-CC	1.27-1.45	C	G	R	R	R	R	R	R	R	R	R	R	R	R	R	R	R	R	R	R	R	1.27
21H-CC	1.27-1.45	C	M	R	F	R	R	R	R	R	R	R	R	R	R	R	R	R	R	R	R	R	1.45
22H-CC	1.45-1.65	A	G	+G	F	R	R	R	R	R	R	R	R	R	R	R	R	R	R	R	R	R	1.65
23H-CC	1.45-1.65	A	G	+G	F	R	R	R	R	R	R	R	R	R	R	R	R	R	R	R	R	R	1.73
24H-CC	1.45-1.65	C	M	R	R	R	R	R	R	R	R	R	R	R	R	R	R	R	R	R	R	R	1.73
25H-CC	1.73-1.97	C	M	+G	R	R	R	R	R	R	R	R	R	R	R	R	R	R	R	R	R	R	
26H-CC	1.73-1.97	A	M	+G	A	R	R	R	R	R	R	R	R	R	R	R	R	R	R	R	R	R	

Notes: Abundance: A = abundant, C = common, F = few, R = rare, + = present, r = reworked. Preservation: G = good, M = moderate, P = poor. MIS = marine isotope stage (per Wei, 1993; Sato et al., 1999).



**Table T4.** Distribution of calcareous nannofossils, Hole U1304C.

Core, section	Age (Ma)	Abundance	Preservation													Reworked species							
				<i>Calcidiscus leptoporus</i>	<i>Coccolithus pelagicus</i>	<i>Coccolithus streckerii</i>	<i>Discolithina japonica</i>	<i>Discolithina</i> spp.	<i>Emiliania huxleyi</i>	<i>Gephyrocapsa caribbeana</i>	<i>Gephyrocapsa oceanica</i>	<i>Gephyrocapsa parallela</i>	<i>Gephyrocapsa</i> spp. (large)	<i>Gephyrocapsa</i> spp. (small)	<i>Helicosphaera carteri</i>	<i>Helicosphaera hyalina</i>	<i>Helicosphaera inversa</i>	<i>Pseudoeumiliania lacunosa</i>	<i>Reticulofenestra</i> spp. (small)	<i>Rhabdosphaera clavigera</i>	<i>Rhabdosphaera stylifera</i>	<i>Scapholithus fossilis</i>	<i>Syracosphaera pulchra</i>
303-U1304C-1H-CC	0~0.25	C	M	F R +		A	F F		C R														
2H-CC	0~0.25	A	G	R R +		A	C R		C F														
3H-CC	0~0.25	A	G	R F R +		F	R R		A F														
4H-CC	0~0.25	R	M	F C +	R	F	R R		A F														
5H-CC	0~0.25	A	G	F F		+	+ +		A R +														
6H-CC	0.25~0.41	A	G	R F + +			+ +		A +														
7H-CC	0.25~0.41	A	G	R C R			+ +		A F +														
8H-CC	0.41~0.85	C	G	F F			R R +		C R		F												

Notes: Abundance: A = abundant, C = common, F = few, R = rare, + = present, r = reworked. Preservation: G = good, M = moderate.



**Table T5.** Distribution of calcareous nannofossils, Hole U1304D.

Core, section	Age (Ma)	Abundance	Preservation	MIS											
				12	0.41	0.85	0.85	0.95	0.95	1.16	1.21	1.45	1.45	1.65	1.73
303-U1304D-1H-CC	0-0.41	A	G	R	R	R	R	R	R	R	R	R	R	R	R
2H-CC	0.41-0.85	A	G	R	R	R	R	R	R	R	R	R	R	R	R
3H-CC	0.41-0.85	A	G	R	R	R	R	R	R	R	R	R	R	R	R
4H-CC	0.41-0.85	A	G	R	R	R	R	R	R	R	R	R	R	R	R
5H-CC	0.41-0.85	A	G	R	R	R	R	R	R	R	R	R	R	R	R
6H-CC	0.41-0.85	A	G	R	R	R	R	R	R	R	R	R	R	R	R
7H-CC	0.41-0.85	A	G	R	R	R	R	R	R	R	R	R	R	R	R
8H-CC	0.41-0.85	A	G	R	R	R	R	R	R	R	R	R	R	R	R
9H-CC	0.85-0.95	A	G	R	R	R	R	R	R	R	R	R	R	R	R
10H-CC	0.85-0.95	A	G	R	R	R	R	R	R	R	R	R	R	R	R
11H-CC	0.95-1.16	A	G	F	+ +	R	R	R	R	R	R	R	R	R	R
12H-CC	0.95-1.16	A	G	F	+ +	R	R	R	R	R	R	R	R	r	r
13H-CC	1.21-1.45	C	G	F	+ +	R	R	R	R	R	R	R	R	r	r
14H-CC	1.21-1.45	F	P	+ +	+ +	R	R	R	R	R	R	R	R	r	r
15H-CC	1.21-1.45	R	M	+ +	+ +	R	R	R	R	R	R	R	R	r	r
16H-CC	1.45-1.65	A	G	R	F	+ R	F	C	C	F	+ R	R	C	r	r
17H-CC	1.45-1.65	A	G	R	F	+ +	R	F	F	R	R	R	C	+ +	+ +
18H-CC	1.45-1.65	A	G	R	F	+ +	R	R	R	R	R	R	F	+ +	+ +
19H-CC	1.45-1.65	C	M	+ +	+ R	+ +	R	R	C	F	R	C	R	1.65	1.73
20H-CC	1.73-1.97	F	M	+ +	+ R	+ +	R	R	F	R	R	C	A	R	
21H-CC	1.73-1.97	C	G	+ +	+ C	+ R									

Notes: Abundance: A = abundant, C = common, F = few, R = rare, + = present, r = reworked. Preservation: G = good, M = moderate, P = poor. MIS = marine isotope stage (as per Wei, 1993; Sato et al., 1999).



**Table T6.** Distribution of planktonic foraminifers, Hole U1304A.

Core, section	Overall abundance	Preservation	<i>Globigerina bulloides</i>	<i>Globigerina decorapta</i>	<i>Globigerina falconensis</i>	<i>Globigerinella calida</i>	<i>Globigerinella siphonifera</i>	<i>Globigerinella glutinata</i>	<i>Globigerinella uvula</i>	<i>Globigerinoides ruber</i>	<i>Globigerinoides crassiformis</i>	<i>Globorotalia crassula</i>	<i>Globorotalia hirsuta</i>	<i>Globorotalia inflata</i>	<i>Globorotalia punctulata</i>	<i>Globorotalia scitula</i>	<i>Globorotalia truncatulinoides</i>	<i>Neogloboquadrina atlantica</i> (s)	<i>Neogloboquadrina dutertrei</i>	<i>Neogloboquadrina incompta</i>	<i>Neogloboquadrina pachyderma</i> (d)	<i>Neogloboquadrina pachyderma</i> (s)	<i>Orbulina universa</i>	<i>Turborotalita quinqueloba</i> (d)	<i>Turborotalita quinqueloba</i> (s)	Biozone
303-U1304A-																										
1H-CC	A	VG	F				P						P								R	D	P	R		
2H-CC	A	VG	D				P						P							F	F	A	R	R		
3H-CC	A	VG	A										P							R	D					
4H-CC	A	VG	A				P						R							D	A		A	F		
5H-CC	A	VG	D				R						P							A	A		A	A		
6H-CC	A	G	A				F	R					F							D	D		A	F		
7H-CC	A	G	A					P					P	D			R			A	P		P			
8H-CC	A	VG	A				P	P					P	D		P				D	F		F	R		
9H-CC	A	VG					F						R							R	D		R	R		
10H-CC	A	VG	A										A							F	D		F	A		
11H-CC	A	VG	R										R							R	D		P			
12H-CC	A	G	R																	R	D		P			
13H-CC	A	VG	R				R	P					R							R	D		F	A		N. pachyderma (s)
14H-CC	A	G	F				R						P							P	A	D	R	F		
15H-CC	R	G	R																	R	A	D				
16H-CC	A	VG	A				R						R							P	A	D	R			
17H-CC	A	VG	R				R						A							P	A	D	F	F		
18H-CC	A	G	F				R		P				R							A	D	F	A			
19H-CC	R	VG											P							P	A	D	P	P		
20H-CC	A	G	F										D							P	A	D	P			
21H-CC	R	G	F				F						A				P			A	A		P			
22H-CC	A	VG	F				P	P	R	P			D							F	F	P	R	R		
23H-CC	A	G	R				A	F					P			P				F	D	R	R			
24H-CC	A	G					R	P					P			P				A	D	A	A			
25H-CC	A	G	R		R		R	P					R			R				F	D	F	A			
26H-CC	A	G	R		P		F	R					R		R	P				D	F	F	A			G. inflata

Notes: Abundance: D = dominant, A = abundant, C = common, F = few, R = rare, P = present, B = barren. Preservation: VG = very good, G = good, M = moderate, P = poor (see “**Foraminifers**” in the “Site U1302–U1308 methods” chapter). d = dextral, s = sinistral.



Table T7. Distribution of planktonic foraminifers, Hole U1304B.

Core	Overall abundance	Preservation	Biozone																			
			<i>Globigerina bulloides</i>	<i>Globigerina decorapta</i>	<i>Globigerina falconensis</i>	<i>Globigerinella calida</i>	<i>Globigerinella siphonifera</i>	<i>Globigerinella glutinata</i>	<i>Globigerinella uvula</i>	<i>Globigerinoides ruber</i>	<i>Globigerinoides crassiformis</i>	<i>Globorotalia crassula</i>	<i>Globorotalia hirsuta</i>	<i>Globorotalia inflata</i>	<i>Globorotalia punctulata</i>	<i>Globorotalia scitula</i>	<i>Globorotalia truncatulinoides</i>	<i>Neogloboquadrina atlantica</i> (d)	<i>Neogloboquadrina atlantica</i> (s)	<i>Neogloboquadrina dutertrei</i>	<i>Neogloboquadrina incincta</i>	<i>Neogloboquadrina pachyderma</i> (d)
303-U1304B-																						
1H	A	VG	F															D	R	R		
2H	A	VG	A														F	P	F	F		
3H	A	VG	A														A	R	P	R		
4H	A	VG	A														D	R	P	P		
5H	C	VG	R														D	A	F	R		
6H	C	G	P														D	D	R	R		
7H	A	VG	D		P												F	R				
8H	A	VG	A														R	D	F	R		
9H	R	VG	A														A	D	R	R		
10H	R	VG	A														R	A	P	A	R	
11H	R	G	P														A	A	A	D		
12H	A	M	A														D	A	F	F		
13H	A	G	R														F	D	R			
14H	A	G	A		P												R	A	R	R		
15H	A	G	F														A	A	R	R		
16H	A	VG	A														F	D	P	R		
17H	R	VG	F														A	D	P	P		
18H	R	G	P	P													F	D	F	F		
19H	R	G															D	A	A	F		
20H	R	G	R	P													A	F	R	F		
21H	R	G	P														R	D	F	A		
22H	A	VG	R		R												F	A	R	F		
23H	A	VG	D		P												A	D	P	R		
24H	R	VG	F														R	D	R	A		
25H	C	VG	A														A	D	P	A		
26H	A	VG	A														D		R			

Notes: Abundance: D = dominant, A = abundant, C = common, F = few, R = rare, P = present. Preservation: VG = very good, G = good, M = moderate (see "Foraminifers" in the "Site U1302–U1308 methods" chapter). d = dextral, s = sinistral.



**Table T8.** Distribution of planktonic foraminifers, Hole U1304C.

Core	Overall abundance	Preservation	<i>Globigerina bulloides</i>	<i>Globigerina decorapta</i>	<i>Globigerina decorata</i>	<i>Globigerina falconensis</i>	<i>Globigerinella calida</i>	<i>Globigerinella siphonifera</i>	<i>Globigerinita glutinata</i>	<i>Globigerinita uvula</i>	<i>Globigerinoides ruber</i>	<i>Globigerinoides crassiformis</i>	<i>Globorotalia crassula</i>	<i>Globorotalia hirsuta</i>	<i>Globorotalia inflata</i>	<i>Globorotalia puncticulata</i>	<i>Globorotalia scitula</i>	<i>Globorotalia truncatulinoides</i>	<i>Neogloboquadrina atlantica (d)</i>	<i>Neogloboquadrina atlantica (s)</i>	<i>Neogloboquadrina dutertrei</i>	<i>Neogloboquadrina incompta</i>	<i>Neogloboquadrina pachyderma (d)</i>	<i>Neogloboquadrina pachyderma (s)</i>	<i>Orbulina universa</i>	<i>Turborotalita quinqueloba (d)</i>	<i>Turborotalita quinqueloba (s)</i>	Biozone
303-U1304C-																												
1H	C	VG	R					P																				
2H	A	VG	R					P																				
3H	A	VG	A					R																				
4H	R	VG	A					R																				
5H	R	VG	D																									
6H	A	G	P					R	F																			
7H	A	VG	A					F	P																			
8H	R-C	VG																										

Notes: Abundance: D = dominant, A = abundant, C = common, F = few, R = rare, P = present. Preservation: VG = very good, G = good (see “Foraminifers” in the “Site U1302–U1308 methods” chapter). d = dextral, s = sinistral.

**Table T9.** Distribution of planktonic foraminifers, Hole U1304D.

Core	Overall abundance	Preservation	<i>Globigerina bulloides</i>	<i>Globigerina decorapta</i>	<i>Globigerina decorata</i>	<i>Globigerina falconensis</i>	<i>Globigerinella calida</i>	<i>Globigerinella siphonifera</i>	<i>Globigerinita glutinata</i>	<i>Globigerinita uvula</i>	<i>Globigerinoides ruber</i>	<i>Globigerinoides crassiformis</i>	<i>Globorotalia crassula</i>	<i>Globorotalia hirsuta</i>	<i>Globorotalia inflata</i>	<i>Globorotalia puncticulata</i>	<i>Globorotalia scitula</i>	<i>Globorotalia truncatulinoides</i>	<i>Neogloboquadrina atlantica (d)</i>	<i>Neogloboquadrina atlantica (s)</i>	<i>Neogloboquadrina dutertrei</i>	<i>Neogloboquadrina incompta</i>	<i>Neogloboquadrina pachyderma (d)</i>	<i>Neogloboquadrina pachyderma (s)</i>	<i>Orbulina universa</i>	<i>Turborotalita quinqueloba (d)</i>	<i>Turborotalita quinqueloba (s)</i>	Biozone		
303-U1304D-																														
1H	R	G	F					P																						
2H	A	G	A						R	F																				
3H	A	VG	A						R	R																				
4H	R	D																												
5H	C	VG	A																											
6H	A	VG	D						P	R																				
7H	A	VG	A						P	R																				
8H	A	G	F						P	R																				
9H	A	G	A						P	R																				
10H	A	G	D						P	R																				
11H	C	G	R						R	R																				
12H	R	M	R						R	R																				
13H	C	M	A						R	R																				
14H	B																													
15H	R	G																												
16H	C	VG	P																											
17H	R	VG	F						P	R																				
18H	R	VG	F						R	R																				
19H	R	VG	R						R	R																				
20H	R	VG	F						R	R																				
21H	C	G	R						R	R																				

Notes: Abundance: D = dominant, A = abundant, C = common, F = few, R = rare, P = present, B = barren. Preservation: VG = very good, G = good, M = moderate (see “Foraminifers” in the “Site U1302–U1308 methods” chapter). d = dextral, s = sinistral.



**Table T10.** Distribution of benthic foraminifers, Holes U1304A, U1304B, U1304C, and U1304D. (See table note. Continued on next page.)

Core	1H	2H	3H	4H	5H	6H	7H	8H	9H	10H	11H	12H	14H	16H	17H	18H	20H	23H	25H	26H	1H	2H	3H	4H	5H	6H	7H	8H	9H	11H	12H	13H	14H	15H	16H	17H	18H	19H	20H	21H							
303-U1304A-																																															
1H	P																																														
2H		P																																													
3H			P																																												
4H				P																																											
5H					P																																										
6H						P																																									
7H							P																																								
8H								P																																							
9H									P																																						
10H										P																																					
11H											P																																				
12H												P																																			
14H													P																																		
16H														P																																	
17H															P																																
18H																P																															
20H																	P																														
23H																		P																													
25H																			P																												
26H																				P																											
303-U1304B-																					P																										
1H																						P																									
2H																							P																								
3H																								P																							
4H																									P																						
5H																										P																					
6H																											P																				
7H																												P																			
8H																													P																		
9H																														P																	
11H																															P																
12H																																P															
13H																																	P														
14H																																		P													
15H																																			P												
16H																																				P											
17H																																					P										
18H																																						P									
303-U1304B-																																															
19H																																															
20H																																															
21H																																															

**Table T10 (continued).**

		Core	Boring sp.	Boring calcite	Cassidulina reticulata	Cassidulina minima	Eggerelloides multilestorif	Globobulimina sp.	Globobulimina sp.	Globocassidulina sp.	Globocassidulina sp.	Hedgpethia elegans	Lagena sp.	Miliolid sp.	Nodosaria sp.	Nodogenerina sp.	Nobilis sp./Astartoconus sp.	Ondotoides uncinatus	Pulicella diutinella	Pulicella pulicella	Pygospio elegans	Sphaerodictina bulloides	Sphaerodictina cornuta	Terebellid sp.	Uvigerina peregrina
22H																									
24H																									
25H																									
303-U1304C-																									
1H		P																							
2H																									
3H																									
4H																									
5H																									
6H																									
7H																									
8H																									
303-U1304D-		P																							
1H																									
2H																									
3H																									
4H																									
6H																									
7H																									
8H																									
9H																									
10H																									
11H																									
13H																									
15H																									
17H																									
18H																									
19H																									
20H																									
21H					P	D	P	P																	

Note: P = present, D = dominant.

**Table T11.** Distribution of diatoms and silicoflagellates, Hole U1304A. (This table available in an [oversized format](#).)

**Table T12.** Distribution of diatoms and silicoflagellates, Hole U1304B. (Continued on next two pages.)

Core, section, interval (cm)	Zone	Abundance	Preservation	Diatoms																									
				<i>Actinocyclus curvatus</i>	<i>Actinocyclus octonarius</i>	<i>Actinocyclus sp.</i>	<i>Actinoptychus bipunctatus</i>	<i>Actinoptychus undulatus</i>	<i>Actinoptychus vulgaris</i>	<i>Alveus marinus</i>	<i>Azpeitia neorenulata</i>	<i>Azpeitia tabularis</i>	<i>Bacteriadrum sp.</i>	<i>Bacteriosa fragilis</i>	<i>Chaetoceros concavicornis</i>	<i>Chaetoceros spp.</i>	<i>RS Chaetoceros affinis</i>	<i>RS Chaetoceros cinctus</i>	<i>RS Chaetoceros compressus</i>	<i>RS Chaetoceros coronatus</i>	<i>RS Chaetoceros debilis</i>	<i>RS Chaetoceros diadema</i>	<i>RS Chaetoceros dydimus</i>	<i>RS Chaetoceros sp.</i>	<i>Chaetoceros setae</i>	<i>Coscinodiscus asteromorphalus</i>	<i>Coscinodiscus argus</i>	<i>Coscinodiscus marginatus</i>	<i>Coscinodiscus oculus-inferis</i>
303-U1304B-																													
1H-1, 13	A	G	T																										
1H-1, 23	A	G																											
1H-1, 146	A	M	T																										
1H-3, 55	A	G	T																										
1H-3, 92	A	G	R																										
1H-3, 113	A	M	T																										
1H-4, 40	A	M	R																										
1H-5, 102	A	G																											
1H-6, 30	A	M	F																										
1H-CC	F	P	T																										
2H-3, 20	C	M																											
2H-CC	A	G																											
3H-7, 5	C	M	T																										
3H-7, 50	A	M	T																										
3H-CC	A	M	T																										
4H-CC	A	G	T																										
5H-CC	Pc	C	G	T																									
6H-CC	A	M																											
7H-CC	A	M	T																										
8H-CC	A	G	T																										
9H-CC	C	G	T																										
10H-CC	C	M	T																										
11H-CC	F	M																											
12H-CC	Pc	A	G	T																									
13H-CC	R	M	T																										
14H-CC	Ns	F	M	T																									
15H-CC	Ns	C	G	*																									
16H-CC	Ns	C	M	T																									
17H-CC	Ns	A	G																										
18H-CC	C	M	T																										
19H-CC	A	M	T																										
20H-CC	C	G	T																										
21H-CC	A	G																											
22H-CC	C	M																											
23H-CC	F	P	T	T																									
24H-CC	A	G	T	T	T																								
25H-CC	A	T	P	T	T																								
26H-CC																												C	

Notes: Zone: Pc = *Proboscia curvirostris*, Ns = *Neodenticula seminae*. Abundance: A = abundant, C = common, F = few, R = rare, T = trace. Preservation: G = good, M = moderate, P = poor. RS = resting spore. \* = fragment present.



Table T12 (continued).

Core, section, interval (cm)	Zone	Abundance	Preservation	Diatoms																								
				<i>Fragilariaopsis pseudocylindrica</i>	<i>Fragilariaopsis reinholdii</i>	<i>Fragilariaopsis sp.</i>	<i>Hemidiscus cuneiformis</i>	<i>Merosira albicans</i>	<i>Neodenticula seminae</i>	<i>Nitzschia bicapitata</i>	<i>Nitzschia kolaczekii</i>	<i>Nitzschia interrupstiaria</i>	<i>Nitzschia porteri</i>	<i>Nitzschia punctiformis</i>	<i>Nitzschia sicula</i>	<i>Nitzschia sp.</i>	<i>Odontella aurita</i>	<i>Paralia sulcata</i>	<i>Planktoniella sol</i>	<i>Porosira gladialis</i>	<i>Proboscia alata</i>	<i>Proboscia curvirostris</i>	<i>Rhizosolenia aciculans</i>	<i>Rhizosolenia acuminata</i>	<i>Rhizosolenia bergenii</i>	<i>Rhizosolenia hebetata f. hiemalis</i>	<i>Rhizosolenia hebetata f. semispina</i>	<i>Rhizosolenia hebetata f. subacuta</i>
303-U1304B-	Pc	A	G	T																								
1H-1, 13		A	G																									
1H-1, 23		A	M																									
1H-1, 146		A	G																									
1H-3, 55		A	G																									
1H-3, 92		A	G																									
1H-3, 113		A	M																									
1H-4, 40		A	M																									
1H-5, 102		A	G																									
1H-6, 30		A	M																									
1H-CC		F	P																									
2H-3, 20		C	M																									
2H-CC		A	G																									
3H-7, 5		C	M																									
3H-7, 50		A	M																									
3H-CC		A	M																									
4H-CC		A	G																									
5H-CC		C	G																									
6H-CC		A	M																									
7H-CC		A	M																									
8H-CC		A	G																									
9H-CC		C	G																									
10H-CC		C	M																									
11H-CC		F	M																									
12H-CC		Pc	A	G																								
13H-CC		R	M																									
14H-CC		Ns	F	M	*																							
15H-CC		Ns	C	G	*																							
16H-CC		Ns	C	M																								
17H-CC		Ns	A	G																								
18H-CC		Ns	C	M																								
19H-CC		A	M																									
20H-CC		C	G																									
21H-CC		A	G																									
22H-CC		C	M																									
23H-CC		F	P																									
24H-CC		A	G																									
25H-CC		A	T	P	C																							
26H-CC																												

**Table T12** (continued).



**Table T13.** Distribution of diatoms and silicoflagellates, Hole U1304C. (Continued on next two pages.)

Notes: Zone: P<sub>c</sub> = *Proboscia curvirostris*, N<sub>s</sub> = *Neodenticula seminae*. Abundance: A = abundant, C = common, F = few, R = rare, T = trace, B = barren. Preservation: G = good, M = moderate, P = poor. RS = resting spore. \* = fragment present.



Table T13 (continued).

Core, section, interval (cm)	Zone	Abundance	Preservation	Diatoms																									
				Coscinodiscus oculus-iridis	Fragilariaopsis doliolus	Fragilariaopsis fossilis	Fragilariaopsis pseudocylindrica	Fragilariaopsis reinholzii	Fragilariaopsis sp.	Hemidiscus cuneiformis	Navicula sp.	Neodenticula seminae	Nitzschia bicapitata	Nitzschia interrupta	Nitzschia sicula	Nitzschia sp. aff. sicula	Paralia sulcata	Planktoniella sol	Pleurosigma sp.	Porosira gracilis	Proboscia alata	Proboscia alata f. indica	Proboscia curvirostris	Pseudosolenia calcar-avis	Rhizosolenia acicularis	Rhizosolenia bergenii	Rhizosolenia hebetata f. hibernalis	Rhizosolenia hebetata f. semispina	Rhizosolenia hebetata f. subacuta
303-U1304C-																													
1H-CC		A	G	T																									
2H-CC		A	G	T	*																								
3H-CC	Pc	F	M	*	T																								
4H-CC		C	M	*	T																								
5H-CC	Pc	C	G																										
6H-CC	Pc	C	G	T	*																								
7H-1, 10		T	M																										
7H-1, 40		F	P																										
7H-6, 2	Pc	A	G	R	F																								
7H-CC		A	M	T	T																								
8H-3, 55		A	M																										
8H-4, 5		R	M																										
8H-5, 130		A	M																										
8H-7, 33		A	M																										
8H-CC	Pc	C	M																										
9H-5, 93	Ns	A	G																										
9H-CC	Ns	A	G	T	T																								
10H-1, 88	Ns	C	M																										
10H-3, 140	Ns	A	M	T	T																								
10H-CC	Ns	A	G	*																									
11H-CC	Ns	A	G																										
12H-1, 50		R	P																										
12H-1, 70		B																											
12H-1, 78		B																											
12H-2, 45	Ns	A	G		F																								
12H-7, 50	Ns	C	M																										
12H-CC	Ns	A	M	*																									
13H-CC		A	G																										
14H-CC		A	G																										
15H-6, 3		A	M			T																							
15H-6, 87		A	G																										
15H-CC		C	M																										
16H-5, 50		C	M	T	T																								
16H-6, 40		R	P																										
16H-CC		A	G																										
17H-CC		A	G																										
18H-2, 3		A	M																										
18H-1, 100		F	P																										
18H-6, 34		F	M	T	R																								
18H-7, 12		B																											
18H-CC		F	M	*	*																								
19H-CC		C	M	*	*																								
20H-CC		C	M																										
21H-CC		T	P																										

Table T13 (continued).

Section	Zone	Diatoms																Silicoflagellates			
		Abundance		Preservation																	
		A	G	F	M	C	M	C	G	A	G	F	M	C	M	A	G	F	M		
303-U1304C-																					
1-CC	Pc	A	G																		
2-CC		A	G																		
3-CC	Pc	F	M																		
4-CC		C	M																		
5-CC	Pc	C	G																		
6-CC	Pc	C	G																		
7-1-10		T	M																		
7-1-40		F	P																		
7-6-2	Pc	A	G																		
7-CC	Pc	A	M																		
8-3-55		A	M																		
8-4-5		R	M																		
8-5-130		A	M																		
8-7-33		A	M																		
8-CC	Pc	C	M																		
9-5-93	Ns	A	G																		
9-CC	Ns	A	G	T	*		T		*												
10-1-88	Ns	C	M																		
10-3-140	Ns	A	M	T			T														
10-CC	Ns	A	G																		
11-CC	Ns	A	G																		
12-1-50		R	P																		
12-1-70		B	B																		
12-1-78		B	B																		
12-2-45	Ns	A	G																		
12-7-50	Ns	C	M																		
12-CC	Ns	A	M		*		*														
13-CC		A	G																		
14-CC		A	G																		
15-6-3		A	M																		
15-6-87		A	G																		
15-CC		C	M																		
16-5-50		C	M																		
16-6-40		R	P																		
16-CC		A	G																		
17-CC		A	G																		
18-2-3		A	M																		
18-1-100		F	P																		
18-6-34		F	M																		
18-7-12		B																			
18-CC		F	M		*		T		*							*					
19-CC		C	M																		
20-CC		C	M																		
21-CC		T	P																		

**Table T14.** Distribution of diatoms and silicoflagellates, Hole U1304D. (Continued on next page.)

Core, section, interval (cm)	Abundance	Preservation	Diatoms																										
			<i>Actinocyclus curvatus</i>	<i>Actinocyclus octonarius</i>	<i>Actinocyclus sp.</i>	<i>Actinoptychus vulgaris</i>	<i>Azpeitia tabularis</i>	<i>Bacteriosa fragilis</i>	<i>Chaetoceros bacteriastroides</i>	<i>Chaetoceros concavicornis</i>	<i>RS Chaetoceros cinctus</i>	<i>RS Chaetoceros compressus</i>	<i>RS Chaetoceros coronatus</i>	<i>RS Chaetoceros debilis</i>	<i>RS Chaetoceros diadema</i>	<i>RS Chaetoceros sp.</i>	<i>Chaetoceros setae</i>	<i>Coscinodiscus asteromphalus</i>	<i>Coscinodiscus des crescens</i>	<i>Coscinodiscus marginatus</i>	<i>Coscinodiscus oculus-iniris</i>	<i>Coscinodiscus radiatus</i>	<i>Fragilariaopsis doliolus</i>	<i>Hemidiscus cuneiformis</i>	<i>Neodenticula seminae</i>	<i>Nitzschia bicapitata</i>	<i>Nitzschia kolaczekii</i>	<i>Paralia sulcata</i>	<i>Proboscia alata</i>
303-U1304D-1H-3, 58	A	M																											
1H-3, 138	A	M																											
1H-CC	C	G	T	*																									
2H-4, 40	F	M	F																										
2H-6, 100	C	G	T																										
2H-7, 40	A	G																											
2H-CC	A	M																											
3H-CC	C	M	*																										
4H-5, 133	C	G	R																										
4H-6, 83	A	M	C																										
4H-CC	F	M																											
5H-1, 70	A	M																											
5H-1, 125	C	G	F	T																									
5H-CC	A	G																											
6H-CC	A	G	T																										
7H-CC	A	G	T																										
8H-CC	C	G	C																										

Notes: Abundance: A = abundant, C = common, F = few, R = rare, T = trace. Preservation: G = good, M = moderate, P = poor. RS = resting spore.  
 \* = fragment present.

Table T14 (continued).

Core, section, interval (cm)	Abundance	Preservation	Diatoms														Silicoflagellates											
			Rhizosolenia bergonii	Rhizosolenia hebetata f. <i>hiemalis</i>	Rhizosolenia hebetata f. <i>semispina</i>	Rhizosolenia hebetata f. <i>subacuta</i>	Rhizosolenia setigera	Rhizosolenia styliformis	Roperia tessellata	Stephanopyxis dimorpha	Stephanopyxis grunowii	Stephanopyxis turris	Thalassionema nitzschiooides var. <i>nitzschiooides</i>	Thalassiosira bipora	Thalassiosira eccentrica	Thalassiosira ferlineata	Thalassiosira gravida	Thalassiosira gracida spore	Thalassiosira grunowii	Thalassiosira leptopus	Thalassiosira lineata	Thalassiosira oestrupii var. <i>oestrupii</i>	Thalassiosira oestrupii" var. <i>vennickae</i>	Thalassiosira poroseriata	Thalassiosira trifilosa	Thalassiosira spp.	Thalassiothrix-Lioloma complex	Dyctiocha fibula
303-U1304D-1H-3, 58	A	M							T	T									T	T				T				
1H-3, 138	A	M							T	T									T	T				T				
1H-CC	C	G			T	T			T										T	T	R			C				
2H-4, 40	F	M																	T	T	R			T				
2H-6, 100	C	G				R													T	T	F			T				
2H-7, 40	A	G			T	T			T									T	T	R			T					
2H-CC	A	M			T														T	T	F			T				
3H-CC	C	M			T	T			R	T								T	T	R			T					
4H-5, 133	C	G																	T	T	T			T				
4H-6, 83	A	M			T	T	T	T	R									T	T	T			T					
4H-CC	F	M			T	F												T	T	F			T					
5H-1, 70	A	M				R													T	T	F			T				
5H-1, 125	C	G			T	T												T	T	R			T					
5-CC	A	G																	T	T	F			T				
6-CC	A	G																	T	T	C			T				
7-CC	A	G																	T	T	F			T				
8-CC	C	G			T	T												T	T	T			T	T				



Table T15. Distribution of radiolarians, Holes U1304A and U1304B. (Continued on next page.)

Core, section	Abundance	Preservation	Other collosphaerids	<i>Actinomma leptoderum</i>	<i>Actinomma</i> spp.	<i>Druppatractus</i> spp.	<i>Hexactinulum enthaecanthum</i>	<i>Stylotracus universus</i>	<i>Axoprunum angelinum</i>	Other actinommiids	<i>Heliodiscus asteriscus</i>	<i>Amphitropodium ypsilon</i> group	<i>Dicyocyme</i> spp.	<i>Hymenistrium euclides</i>	<i>Stylochlamidium venustum</i>	<i>Stylocidya multispina</i>	<i>Spongocore</i> spp.	<i>Spongodiscus</i> spp.	<i>Octopyle</i> spp.	<i>Larcpyle butschili</i> group	<i>Lithelius minor</i>	<i>Lithelius nautiloides</i>	<i>Pylospira octopyle</i>	<i>Pylospira</i> spp.	Acanthodesmiids	<i>Amphiplecta</i> spp.	<i>Arachnocalloium</i> spp.	<i>Ceratocyrtis</i> spp.	<i>Gondwanaria</i> spp.	<i>Lophophaena</i> spp.	<i>Lampronia</i> sp.	<i>Lipmanella</i> spp.	<i>Lithomelissa setosa</i>	<i>Peridium</i> spp.	<i>Pseudodictyophimus</i> spp.	Other plagoniids	<i>Bathyopyramis</i> spp.
303-U1304A-																																					
1H-CC	A	G	C	F	R	R		R						R	R	R		R	F		F	A		R	F	T	F			R	C	R	F				
2H-CC	B																																				
3H-CC	B																																				
4H-CC	C	G	F	F											F	R		R	F	F	C	C		R							F	F	R	R			
5H-CC	C	G	R	F											F	R	T	F	R	F	C			R													
6H-CC	A	G	T	C	C	T	R							R	R	R		R	R	C	F		T														
7H-CC	A	G	F	C	F	R		R	F	R				R	R	R		R	F	F	C	A		R													
8H-CC	A	G	R	F	F	F								R	F	F		R	R	C	C	A		R													
9H-CC	F	G	R	R																																	
10H-CC	C	G	F	C	R									C	F			C	R		R	F															
11H-CC	C	M	A	R	R									R				F	F		R	C															
12H-CC	T	M	T	T														T	T		T																
13H-CC	C	M	A	C														F	R	F	F	C															
14H-CC	C	M	A	C														T	R	C	F	A															
15H-CC	T	M												T																							
16H-CC	B																																				
17H-CC	C	G	A	A										R	F	T	R	C	F	R	C	A		T				T			R						
18H-CC	F	M	R	R	R	T								R	F	T	R	T	R	T	R	A															
19H-CC	R	G	R																																		
20H-CC	R	M	R																																		
21H-CC	C	M	F	C	R	R								F																							
22H-CC	B																																				
23H-CC	T	M	T											T																							
24H-CC	T	M	T																																		
25H-CC	C	M	F	F	R	T								F																							
26H-CC	R	M	R	R	T																																
303-U1304B-																																					
1H-CC	B													R				A	R	F	T	C	F	C	T	T	T		F	C	C	R	T				
2H-CC	C	G	T	F	R	R	R							R	A	R	A	R	A	R	A	C	R	F	T	T											
3H-CC	A	M	F	R	R	T								F	R		A	C	R	F	R	A	F														
4H-CC	C	M	F	R										R	C		F	R	R	C	R	F	A														
5H-CC	C	M	C	F										R	C		F	R	R	C	R	F	A														
6H-CC	C	G	C	T	F	F								C			F	R	R	F	F	A	A	R													
7H-CC	A	G	T	C	F	T	T							R	T	T	F	A	T	T	F	A	C	T													
8H-CC	C	G	C	T	T	T	T							F	T	T	C	F	F	R	R	F	T														
9H-CC	F	G	R											T																							
10H-CC	C	G	F											A	R	R	A	T	T	F	F	T	C	F	T	T	T	T	R	A	F						
11H-CC	F	G	R											R																							
12H-CC	A	M	A	F	F	T								F	R	T	A	R	A	T	A	T	A	C													
13H-CC	T	M												T																							
14H-CC	T	M	T	T																																	
15H-CC	A	M	A	F	T									F	R		C	R	C	R	F	A															
16H-CC	F	M	R	R										R			R	R	R	R	R	R	R														
17H-CC	R	M	R	T										R			R	R	R	R	R	R	R														
18H-CC	T	M	R											R			R	R	R	R	R	R	R														
19H-CC	T	G												R			R	R	R	R	R	R	R														
20H-CC	C	G	A	F										R			C																				
21H-CC	T	G																T			T																
22H-CC	A	M	F											F			C			F	T		R	R													
23H-CC	B																																				
24H-CC	C	G	T	F																																	
25H-CC	T	G																																			
26H-CC	B																																				

Notes: Abundance: A = abundant, C = common, F = few, R = rare, T = trace, B = barren (only in total abundance). Preservation: G = good, M = moderate, P = poor.



Table T15 (continued).

Sample	Abundance	Preservation	<i>Comulella</i> spp.	<i>Cycladophora davisiана</i>	<i>Cycladophora bicornis</i>	<i>Dicyophimus</i> spp.	<i>Euceyphalus</i> spp.	<i>Eucyrtidium acuminatum</i>	<i>Eucyrtidium cienkowskii</i>	<i>Eucyrtidium teucheri</i>	<i>Lithocampe punctatum</i>	<i>Litharachnium</i> spp.	<i>Pteracanium</i> spp.	Other theoperids	<i>Carpocanistrum</i> spp.	<i>Androcydias gamphonycha</i>	<i>Lamprocyclas maritatis</i>	<i>Pteracyclys zandaeus</i>	<i>Thecothyridium trachelium</i>	<i>Botryostrobus acutulanaris</i>	<i>Botryostrobus auritus/australis</i>	<i>Phormostichoartus</i> cf. <i>corbula</i>	<i>Siphocampe</i> spp.	<i>Stichocorys seriatia</i>	<i>Spirocyclis</i> spp.	Cannabotryids	Radiolarian zone
303-U1304A-																											
1H-CC	A	G	F	A		F			T		R	R	R	R	R				A					R		C. d. <i>davisiана</i>	
2H-CC	B																										
3H-CC	B																										
4H-CC	C	G	R	A																							
5H-CC	C	G	R	A					T		R	R	T	T	T												
6H-CC	A	G	F	R					R		R	F	R	T													
7H-CC	A	G	R	A					R		R	F	R	R													
8H-CC	A	G	R	F					T		R	F	F	T													
9H-CC	F	G	R	R																							
10H-CC	C	G	R	A		F																					
11H-CC	C	M	M	A						R																	
12H-CC	T	M	M	T																							
13H-CC	C	M	M	A						R																	
14H-CC	C	M	T	A						R																	
15H-CC	T	M	M	T																							
16H-CC	B																										
17H-CC	C	G	R	C																							
18H-CC	F	M	M	R																							
19H-CC	R	G	R	R																							
20H-CC	R	M	M	R																							
21H-CC	C	M	M	A																							
22H-CC	B																										
23H-CC	T	M	M	T																							
24H-CC	T	M	M	T																							
25H-CC	C	M	M	A																							
26H-CC	R	M	M	A																							
303-U1304B-																											
1H-CC	B																										
2H-CC	C	G	F	A					T		T																
3H-CC	A	M	T	C																							
4H-CC	C	M	M	A																							
5H-CC	C	M	F	A	T																						
6H-CC	C	G	R	F																							
7H-CC	A	G	R	A					T		R	T															
8H-CC	C	G	T	A	T				T		T	R	T														
9H-CC	F	G	T	T																							
10H-CC	C	G	T	F	R				T																		
11H-CC	F	G	T	R	C				T		T	R	T														
12H-CC	A	M	T	C	T																						
13H-CC	T	M	M	T	T																						
14H-CC	T	M	M	T	T																						
15H-CC	A	M	A	T																							
16H-CC	F	M	M	R																							
17H-CC	R	M	M	T																							
18H-CC	T	M	M	R																							
19H-CC	T	G	T	T																							
20H-CC	C	G	A	A	T																						
21H-CC	T	G	T	T																							
22H-CC	A	M	A	A																							
23H-CC	B																										
24H-CC	C	G	T	T																							
25H-CC	T	G	T	T																							
26H-CC	B																										

**Table T16.** Distribution of palynomorphs, Hole U1304A.

Core, section	Marine	Terrestrial	Reworked	Dinocyst assemblages																														
	Foraminifer ostracode limings	Taxanomy	Dinocysts	Preservation	Pollen	Spores of Paleodiopterytes	Palaeoflorula	Agglutinated pollen	Mesozoic-Paleogene dinocysts	Trilete pores	Bivalve pollen	Ammonia	Leptostyloidea	C. lisandrum brevispinosum	Selaphopeltina sp.	Oliniella sp.	Quinqueloculina pectinata	Impagidinium pallidum	Impagidinium schaeferiana	Impagidinium bicolorum	Impagidinium carterianum	Operculodinium centroconicum (short process form)	Operculodinium cf. taylorianum	Bivalvularia testaceanae	Neodiscotilium jardinei	Achniosphaera sp.	Parudinopsis reticulata	Spiniferites deliciosa	Spiniferites elongatus	Spiniferites membranaceus	Spiniferites ramosus	Spiniferites hypoplectanthus-mimulus	Spiniferites hypoplectanthus	Calymene labradorii
303-U1304A-																																		
1H-CC	G x r	G x	G	r r	G G	x r	r	r	P P										P															
2H-CC	G x	G	G	x	G G	x x	x	x	XXX XXX										o															
3H-CC	G r	G	G	x	G G	x x	x	x	XXX XXX										r															
4H-CC	G XX x	G	G	x x	G G	x x	x	x	XXX XXX										r															
5H-CC	G XXX XX	G	G	XX x	G G	x x	x	x	XXX XX										r															
6H-CC	G XXXX x	G	G	x x	G G	x x	x	x	XXX XX										r															
7H-CC	G XXXX XX	G	G	XX x	G G	x x	x	x	XXX XX										r															
8H-CC	G XXXX x	G	G	XX x	G G	x x	x	x	XXX XXX										x															
9H-CC	G XXXX	G	G	x	G G	x x	x	x	XXX XXX										r															
10H-CC	M XXXX r	M	G	x x	G G	x x	x	x	XXX x										r															
11H-CC	M XX x	M	G	x r r r	G G	x r r r	r	r x x	P P									P											P					
12H-CC	M x r	M	G	x	G G	x x	x	x	P P									P																
13H-CC	M XXX XX	M	M	XX	G G	x x	x	x	XXX x									P																
14H-CC	M XXX x	M	M	x	G G	x x	x	x	XXX x									x										x						
15H-CC	?	r	G	x	G G	x x	x	x	XXX x									x																
16H-CC	G XXX x	G	G	x x	G G	x x	x	x	XXX x									x										r	x					
17H-CC	G XX x	G	G	x x	G G	x x	x	x	XX x									XXX x XX										r	x					
18H-CC	G XX x	G	G	x x	G G	x x	x	x	XX x									P P o										P o						
19H-CC	G XX x	G	G	x x	G G	x x	x	x	XXX									XX x										r	x					
20H-CC	G XX x	G	G	x x	G G	x x	x	x	XX x									XX x										XX	X					
21H-CC	G XX	G	G	x x	G G	x x	r	r	x									r										XXX						
22H-CC	G XXX	G	G	XX r	G G	x x	r	r	x									x x										x XX r	X					
23H-CC	G XX	G	G	x	G G	x x	r	r	o									XX										r	r					
24H-CC	?	r	?	?	G	XX	r	r	o									XXX x																
25H-CC	G XX r r	G	G	XX r	G G	x x	r	r	o x									r										r	r					
26H-CC	G XX	G	G	x	G G	x x	r	r	XXX									XX										r	r					

Notes: Absolute abundances: XXXX = extremely abundant, XXX = abundant, XX = common, x = few, r = rare. Relative abundance of dinocyst taxa: XXX = dominant, XX = common, X = few, r = rare, P = present, o = single occurrence.

**Table T17.** Distribution of palynomorphs, Hole U1304D.

Core, section	Marine	Terrestrial	Reworked	Dinocyst assemblages																																																								
	Preservation	Foraminifer organic linings	Preservation	Pollen	Bisaccate pollen	Tritele spores	Brigantedinium spp.			Selenopempix nephroides			Impagidinium paradoxum			Impagidinium patulum			Impagidinium striatum			Impagidinium pallidum			Impagidinium cf. velorum			Bitectatodinium tepikeense			Operculodinium centrocarpum			Operculodinium centrocarpum (short process form)			Operculodinium janducurei			Nematospheopsis labyrinthus			Spiniferites elongatus			Spiniferites hyperbactus-mirabilis type			Spiniferites membranaceus			Spiniferites ramosus			Corndinium labradorii			Filisphaera filifera		
303-U1304D-																																																												
1H-CC	G	XXXX XX	G	XX		x	XXX XXX x		r	x																																																		
3H-CC	G	XXX x	G	x			XXX XX																																																					
4H-CC	G	XXX x	G	x																																																								
5H-CC	G	XXXX	G	x																																																								
6H-CC	G	XXXX XX	G	r																																																								
7H-CC	G	XXXX x	G	x		x	x	r	x	r																																																		
8H-CC	G	x	G	x																																																								
9H-CC	G	XXXX x	G	x		x	XXX x																																																					
10H-CC	G	XX	G	x		r	r	x	x																																																			
11H-CC	G	XXXX x	G	x																																																								
12H-CC	G	XXXX x	G	x																																																								
15H-CC	G	XX	G																																																									

Notes: Absolute abundances: XXXX = extremely abundant, XXX = abundant, XX = common, x = few, r = rare. Relative abundance of dinocyst taxa: XXX = dominant, XX = common, X = few, r = rare, P = present, o = single occurrence.

**Table T18.** Polarity zonation, Holes U1304A, U1304B, and U1304C.

Polarity chron interpretation	Age (Ma)	Interval	Hole U1304A			Hole U1304B			Hole U1304D		
			Core, section, interval (cm)	Depth (mbsf)	Depth (mcd)	Core, section, interval (cm)	Depth (mbsf)	Depth (mcd)	Core, section, interval (cm)	Depth (mbsf)	Depth (mcd)
		303-U1304A-				303-U1304B-			303-U1304D-		
C1n (b) Matuyama/Brunhes	0.78	Upper	13H-5, 30	120.30	138.42	14H-1, 80	123.0	138.08	8H-4, 80	123.8	138.53
		Lower	13H-6, 15	121.65	139.77	14H-2, 55	124.25	139.38	8H-5, 80	125.3	140.03
C1r.1n (t) Jaramillo	0.99	Upper	15H-7, 50	142.5	162.46	16H-4, 70	146.41	163.32			
		Lower	16H-2, 75	144.75	165.77	16H-5, 100	148.22	165.18			
C1r.1n (b) Jaramillo	1.07	Upper				17H-5, 40	157.14	175.60	12H-2, 65	158.65	176.04
		Lower				17H-6, 10	157.37	176.83	12H-3, 25	159.7	177.14
(t) Cobb Mountain	1.19	Upper	18H-2, 80	163.79	187.21	18H-6, 65	168.33	187.34	13H-2, 60	168.10	187.05
		Lower	18H-3, 40	164.9	188.31	18H-6, 140	169.08	188.09	13H-3, 105	170.05	189.00
(b) Cobb Mountain	1.215	Upper	18H-4, 10	166.10	189.51				13H-4, 10	170.6	189.55
		Lower	18H-5, 70	168.2	191.61				13H-6, 130	174.8	193.75
C2n (t) Olduvai	1.77	Upper	26H-2, 145	232.45	261.34	26H-2, 135	236.55	262.24	20H-3, 35	231.75	257.67
		Lower	26H-4, 30	234.3	263.19	26H-3, 110	237.8	263.49	21H-1, 80	235.2	264.59

Note: (b) = bottom, (t) = top.



**Table T19.** Age interpretation, Site U1304.

Polarity chron interpretation	Age (Ma)	Depth	
		(mcd)	± (m)
C1n (b) Matuyama/Brunhes	0.78	139.0	1
C1r1n (t) Jaramillo	0.99	164.0	1.5
C1r1n (b) Jaramillo	1.07	176.2	1
Cobb Mountain	1.2	189.7	2.5
C2n (t) Olduvai	1.77	262	1.5

Note: (b) = bottom, (t) = top.

**Table T20.** Shipboard composite and corrected composite depths, Holes U1304A, U1304B, U1304C, and U1304D.

Core	Top depth (mbsf)	Offset (m)	Top depth		Core	Top depth (mbsf)	Offset (m)	Top depth						
			(mcd)	(cmcd)				(mcd)	(cmcd)					
<b>303-U1304A-</b>														
1H	0.00	3.70	3.70	3.30	16H	141.20	16.91	158.11	141.17					
2H	9.50	5.02	14.52	12.96	17H	150.70	18.46	169.16	151.04					
3H	19.00	6.69	25.69	22.94	18H	160.20	19.01	179.21	160.01					
4H	28.50	7.20	35.70	31.88	19H	169.70	20.70	190.40	170.00					
5H	38.00	8.26	46.26	41.30	20H	179.20	20.41	199.61	178.22					
6H	47.50	9.20	56.70	50.63	21H	186.20	21.55	207.75	185.49					
7H	57.00	11.76	68.76	61.39	22H	195.70	22.69	218.39	194.99					
8H	66.50	13.10	79.60	71.07	23H	205.20	23.28	228.48	204.00					
9H	76.00	14.15	90.15	80.49	24H	214.70	24.76	239.46	213.80					
10H	85.50	14.66	100.16	89.43	25H	224.20	25.59	249.79	223.03					
11H	95.00	15.92	110.92	99.04	26H	233.70	25.46	259.16	231.39					
12H	104.50	16.75	121.25	108.26	<b>303-U1304C-</b>									
13H	114.00	18.12	132.12	117.96	1H	0.00	-0.30	-0.30	-0.27					
14H	123.50	19.60	143.10	127.77	2H	4.60	-0.30	4.30	3.84					
15H	133.00	19.96	152.96	136.57	3H	14.10	-0.17	13.93	12.44					
16H	142.50	21.02	163.52	146.00	4H	23.60	3.10	26.70	23.84					
17H	152.00	22.74	174.74	156.02	5H	33.10	3.05	36.15	32.28					
18H	161.50	23.41	184.91	165.10	6H	42.60	1.73	44.33	39.58					
19H	171.00	24.76	195.76	174.79	7H	52.10	1.73	53.83	48.06					
20H	175.00	24.87	199.87	178.46	8H	61.60	5.29	66.89	59.72					
21H	184.50	25.88	210.38	187.84	<b>303-U1304D-</b>									
22H	194.00	26.15	220.15	196.56	1H	52.00	4.64	56.64	50.57					
23H	203.50	26.79	230.29	205.62	2H	61.50	5.56	67.06	59.88					
24H	213.00	28.14	241.14	215.30	3H	71.00	7.74	78.74	70.30					
25H	220.00	28.40	248.40	221.79	4H	80.50	7.54	88.04	78.61					
26H	229.50	28.89	258.39	230.71	5H	90.00	10.65	100.65	89.87					
<b>303-U1304B-</b>														
1H	0.00	0.00	0.00	0.00	6H	99.50	11.21	110.71	98.85					
2H	8.20	-0.18	8.02	7.16	7H	109.00	13.36	122.36	109.25					
3H	17.70	0.87	18.57	16.58	8H	118.50	14.73	133.23	118.96					
4H	27.20	2.30	29.50	26.34	9H	128.00	15.22	143.22	127.88					
5H	36.70	4.43	41.13	36.72	10H	137.50	15.40	152.90	136.52					
6H	46.20	4.89	51.09	45.62	12H	156.50	17.39	173.89	155.26					
7H	55.70	5.10	60.80	54.29	13H	166.00	18.95	184.95	165.13					
8H	65.20	8.42	73.62	65.73	14H	175.50	20.02	195.52	174.57					
9H	74.70	9.62	84.32	75.29	15H	181.30	20.64	201.94	180.30					
10H	84.20	10.80	95.00	84.82	16H	190.40	22.20	212.60	189.82					
11H	93.70	11.99	105.69	94.37	17H	199.90	22.71	222.61	198.76					
12H	103.20	13.21	116.41	103.94	18H	209.40	22.08	231.48	206.68					
13H	112.70	14.38	127.08	113.46	19H	218.90	24.94	243.84	217.71					
14H	122.20	15.08	137.28	122.57	20H	228.40	25.92	254.32	227.07					
15H	131.70	16.10	147.80	131.96	21H	234.40	29.39	263.79	234.22					

**Table T21.** Sampling splice tie points, Site U1304.

Hole, core, section, interval (cm)	Depth		Hole, core, section, interval (cm)	Depth		
	mbsf	mcd		mbsf	mcd	
303-			303-			
1304B-1H-4, 0.00	4.53	4.53	Tie to	1304A-1H-1, 0.10	0.83	4.53
1304A-1H-5, 10.00	6.10	9.80	Tie to	1304B-2H-2, 27.00	9.98	9.80
1304B-2H-6, 15.00	15.85	15.67	Tie to	1304A-2H-1, 115.00	10.65	15.67
1304A-2H-6, 75.00	17.75	22.77	Tie to	1304B-3H-3, 120.00	21.90	22.77
1304B-3H-6, 100.00	26.20	27.07	Tie to	1304A-3H-1, 136.40	20.38	27.07
1304A-3H-6, 60.00	27.10	33.79	Tie to	1304B-4H-3, 129.50	31.49	33.79
1304B-4H-6, 135.00	36.04	38.35	Tie to	1304A-4H-2, 115.00	31.15	38.35
1304A-4H-5, 100.00	35.50	42.70	Tie to	1304B-5H-2, 5.50	38.27	42.70
1304B-5H-6, 65.00	44.85	49.28	Tie to	1304A-5H-3, 0.00	41.02	49.28
1304A-5H-6, 5.00	45.55	53.81	Tie to	1304B-6H-2, 120.50	48.92	53.81
1304B-6H-6, 140.00	55.10	59.99	Tie to	1304A-6H-3, 28.50	50.79	59.99
1304A-6H-5, 115.00	54.65	63.85	Tie to	1304B-7H-3, 5.00	58.75	63.85
1304B-7H-6, 120.00	64.37	69.47	Tie to	1304A-7H-1, 69.00	57.71	69.47
1304A-7H-6, 110.00	65.60	77.36	Tie to	1304B-8H-3, 73.50	68.94	77.36
1304B-8H-6, 100.00	73.70	82.12	Tie to	1304A-8H-2, 100.30	69.02	82.12
1304A-8H-5, 70.00	73.20	86.30	Tie to	1304B-9H-2, 46.50	76.68	86.30
1304B-9H-6, 0.60	82.80	92.42	Tie to	1304A-9H-2, 0.80	78.27	92.42
1304A-9H-4, 130.00	81.80	95.95	Tie to	1304B-10H-1, 95.00	85.15	95.95
1304B-10H-7, 20.00	93.39	104.19	Tie to	1304A-10H-3, 99.40	89.53	104.19
1304A-10H-5, 1.20	92.76	107.42	Tie to	1304B-11H-2, 0.20	95.43	107.42
1304B-11H-5, 70.00	100.41	112.40	Tie to	1304A-11H-1, 148.30	96.48	112.40
1304A-11H-6, 70.00	103.20	119.12	Tie to	1304B-12H-2, 119.00	105.91	119.12
1304B-12H-6, 130.00	111.99	125.20	Tie to	1304A-12H-3, 95.00	108.45	125.20
1304A-12H-6, 50.00	112.50	129.25	Tie to	1304B-13H-2, 65.50	114.87	129.25
1304B-13H-6, 15.00	120.32	134.70	Tie to	1304A-13H-2, 107.00	116.58	134.70
1304A-13H-6, 140.00	122.90	141.02	Tie to	1304B-14H-3, 75.00	125.94	141.02
1304B-14H-6, 60.00	130.27	145.35	Tie to	1304A-14H-2, 75.00	125.75	145.35
1304A-14H-5, 65.00	130.15	149.75	Tie to	1304B-15H-2, 45.00	133.65	149.75
1304B-15H-6, 105.00	140.23	156.33	Tie to	1304A-15H-3, 35.50	136.37	156.33
1304A-15H-5, 0.30	139.29	159.24	Tie to	1304B-16H-1, 0.40	142.33	159.24
1304B-16H-6, 15.00	148.87	165.78	Tie to	1304A-16H-2, 74.00	144.76	165.78
1304A-16H-6, 120.00	151.20	172.22	Tie to	1304B-17H-3, 5.00	153.76	172.22
1304B-17H-6, 100.00	159.27	177.73	Tie to	1304A-17H-2, 149.00	154.99	177.73
1304A-17H-6, 140.00	160.87	183.61	Tie to	1304B-18H-3, 139.00	164.60	183.61
1304B-18H-5, 100.00	167.18	186.19	Tie to	1304A-18H-1, 127.00	162.78	186.19
1304A-18H-6, 70.00	169.70	193.11	Tie to	1304B-19H-2, 120.00	172.41	193.11
1304B-19H-6, 140.00	178.61	199.31	Append to	1304A-20H-1, 0.00	175.00	199.87
1304A-20H-6, 135.00	183.85	208.72	Tie to	1304B-21H-1, 95.50	187.17	208.72
1304B-21H-7, 10.00	195.32	216.87	Tie to	1304A-21H-5, 48.50	190.99	216.87
1304A-21H-6, 105.00	193.05	218.93	Tie to	1304B-22H-1, 53.00	196.24	218.93
1304B-22H-4, 85.00	201.05	223.74	Tie to	1304A-22H-3, 58.90	197.59	223.74
1304A-22H-6, 1.30	202.74	228.90	Tie to	1304B-23H-1, 0.30	205.62	228.90
1304B-23H-5, 35.00	211.55	234.83	Tie to	1304A-23H-3, 148.70	208.04	234.83
1304A-23H-7, 0.20	212.79	239.58	Tie to	1304D-18H-6, 59.70	217.50	239.58
1304D-18H-6, 137.90	218.28	240.36	Tie to	1304B-24H-1, 0.90	215.60	240.36
1304B-24H-5, 1.30	222.01	246.78	Tie to	1304D-19H-2, 143.80	221.84	246.78
1304D-19H-4, 78.70	224.18	249.12	Tie to	1304A-25H-1, 0.70	220.72	249.12
1304A-25H-7, 74.00	229.75	258.15	Append to	1304A-26H-1, 0.00	229.50	258.39
1304A-26H-2, 1.20	232.19	261.08	Tie to	1304B-26H-2, 0.50	235.62	261.08
1304B-26H-6, 115.00	242.35	267.82				



**Table T22.** Depth ranges and sedimentation rates, Site U1304.

Depth interval (mcd)	Sedimentation rate (cm/k.y.)
0–139.1	17.8
139.1–164.1	11.9
164.1–175.3	13.9
175.3–187.9	10.6
187.9–190.9	11.8
190.9–262.3	12.7

**Table T23.** Headspace hydrocarbon gases, Hole U1304A.

Core, section, interval (cm)	Depth (mbsf)	Depth (mcd)	C <sub>1</sub> (ppmv)
303-U1304A-			
1H-2, 0–5	1.5	5.20	2.3
2H-2, 0–5	11.0	16.02	3.2
5H-2, 0–5	39.5	46.19	3.8
6H-2, 0–5	49.0	56.20	3.6
7H-2, 0–5	58.5	66.76	3.6
8H-2, 0–5	68.0	77.20	3.1
9H-2, 0–5	77.5	89.26	2.6
10H-2, 0–5	87.0	100.10	2.7
11H-2, 0–5	96.5	110.65	3.3
12H-2, 0–5	106.0	120.66	3.1
13H-2, 0–5	115.5	131.42	3.9
14H-2, 0–5	125.0	141.75	4.3
14H-2, 50–51	125.5	143.62	4.8
15H-2, 0–5	134.5	154.46	5.2
16H-2, 0–5	144.0	165.02	4.8
17H-2, 0–5	153.5	176.24	3.7
18H-2, 0–5	163.0	186.41	3.6
19H-2, 0–5	172.5	197.27	3.3
20H-2, 0–5	176.5	201.37	3.6
21H-2, 0–5	186.0	211.88	2.6
22H-2, 0–5	195.5	221.65	2.2
23H-2, 0–5	205.0	231.80	2.5
24H-2, 0–5	214.5	242.64	2.4
25H-2, 0–5	221.5	249.90	2.7
26H-2, 0–5	231.0	259.89	2.9



**Table T24.** Bulk sedimentary carbon, nitrogen, and hydrogen, Hole U1304A.

Core, section, interval (cm)	Depth		Carbon (wt%)			Nitrogen (wt%)	Organic C/N
	(mbsf)	(mcd)	Inorganic	CaCO <sub>3</sub>	Total	Organic	
303-U1304A-							
1H-1, 108–109	1.08	4.78	1.5	12.7	1.6	0.1	0.0 1.3
1H-6, 18–19	7.68	11.38	5.7	47.6	6.1	0.4	0.0 8.1
2H-1, 124–125	10.74	15.76	5.3	44.0	5.8	0.5	0.1 6.9
2H-6, 18–19	17.18	22.20	4.7	39.3	5.0	0.2	0.1 3.6
3H-1, 141–142	20.41	27.10	4.5	37.7	4.7	0.2	0.0 3.3
3H-6, 8–9	26.58	33.27	4.7	38.9	5.7	1.1	0.1 19.0
4H-1, 143–144	29.93	37.13	3.9	32.7	4.0	0.0	0.0 0.7
4H-6, 1–2	36.01	43.21	3.8	31.7	4.1	0.3	0.0 7.2
5H-1, 144–145	39.44	47.70	5.3	44.1	5.8	0.5	0.1 6.9
5H-6, 1–2	45.51	53.77	5.7	47.8	6.2	0.4	0.0 11.0
6H-1, 143–144	48.93	58.13	4.7	39.4	5.2	0.5	0.1 7.6
6H-6, 1–2	55.01	64.21	6.9	57.4	7.3	0.4	0.1 6.6
7H-1, 149–150	58.49	70.25	7.3	61.1	7.7	0.4	0.1 5.7
7H-6, 1–2	64.51	76.27	8.6	71.3	9.0	0.5	0.0 12.0
8H-1, 148–149	67.98	81.08	6.4	53.4	6.6	0.2	0.1 3.5
8H-6, 1–2	74.01	87.11	7.0	58.1	7.4	0.4	0.1 6.5
9H-1, 142–143	77.42	91.57	7.3	60.4	7.6	0.4	0.0 8.0
9H-6, 1–2	83.54	97.69	5.7	47.2	6.3	0.6	0.1 8.4
10H-6, 3–4	93.11	107.77	5.8	48.0	6.0	0.2	0.1 3.2
11H-1, 133–134	96.33	112.25	2.8	23.5	3.2	0.3	0.1 5.0
11H-6, 3–4	102.53	118.45	4.3	35.8	4.4	0.1	0.1 1.5
12H-1, 141–142	105.91	122.66	2.3	19.3	2.6	0.3	0.1 5.0
12H-6, 3–4	112.03	128.78	4.3	35.5	4.7	0.5	0.1 7.2
13H-1, 146–147	115.46	133.58	3.7	30.5	3.9	0.2	0.1 2.8
13H-6, 3–4	121.53	139.65	7.3	60.4	8.3	1.1	0.0 21.0
14H-1, 146–147	124.96	144.56	5.7	47.6	6.3	0.6	0.1 7.6
14H-6, 3–4	131.04	150.64	3.6	30.1	4.0	0.4	0.1 5.1
15H-1, 138–139	134.38	154.34	1.9	15.8	2.1	0.2	0.0 4.4
15H-6, 1–2	140.51	160.47	4.0	33.2	4.4	0.4	0.1 5.4
16H-1, 142–143	143.92	164.94	3.7	30.8	3.9	0.2	0.1 3.8
16H-6, 3–4	150.03	171.05	2.8	23.2	3.3	0.5	0.1 5.0
17H-1, 143–144	153.43	176.17	6.8	56.7	7.3	0.5	0.0 10.0
17H-6, 3–4	159.50	182.24	2.5	20.4	2.9	0.5	0.1 4.1
18H-1, 142–143	162.92	186.33	2.5	20.7	3.2	0.7	0.1 4.7
18H-6, 2–3	169.02	192.43	4.6	38.2	4.8	0.2	0.1 3.4
19H-1, 149–150	172.49	197.25	0.6	4.66	1.0	0.4	0.1 3.3
20H-1, 149–150	176.49	201.36	0.9	7.25	1.4	0.6	0.1 4.6
20H-6, 1–2	182.51	207.38	7.1	59.0	7.9	0.8	0.0 22.0
21H-1, 142–143	185.92	211.80	5.0	41.4	5.3	0.3	0.0 6.2
21H-6, 1–2	192.01	217.89	4.1	34.5	4.9	0.8	0.1 6.2
22H-1, 149–150	195.49	221.64	6.0	49.6	6.3	0.3	0.0 12.0
22H-6, 0–1	201.49	227.64	0.6	4.58	0.9	0.4	0.1 5.3
23H-1, 149–150	204.99	231.78	2.0	16.7	2.6	0.6	0.1 7.5
23H-4, 114–115	209.20	235.99	7.5	62.4	7.9	0.4	0.0 13.0
24H-1, 144–145	214.44	242.58	2.1	17.3	2.5	0.4	0.1 6.4
24H-4, 1–2	217.51	245.65	2.9	23.9	3.2	0.4	0.1 4.8
25H-1, 143–144	221.43	249.83	3.1	25.9	3.4	0.3	0.0 5.9
25H-6, 3–4	227.54	255.94	1.8	14.6	2.4	0.7	0.1 4.9
26H-1, 143–144	230.93	259.82	0.9	7.66	1.5	0.6	0.1 4.6
26H-6, 3–4	237.03	265.92	4.4	36.5	4.9	0.6	0.1 10.0



**Table T25.** Interstitial water geochemistry, Hole U1304A.

Core, section, interval (cm)	Depth (mbsf) (mcd)		Anions (mM)		Alkalinity (mM)	Salinity (g/kg)	Major cations (mM)				Minor and trace constituents ( $\mu\text{M}$ )						
	SO <sub>4</sub> <sup>2-</sup>	Cl <sup>-</sup>	pH	Na <sup>+</sup>	K <sup>+</sup>	Mg <sup>2+</sup>	Ca <sup>2+</sup>	NH <sub>4</sub> <sup>+</sup>	B	Ba <sup>2+</sup>	Fe <sup>2+</sup>	Li <sup>+</sup>	Mn <sup>2+</sup>	H <sub>4</sub> SiO <sub>4</sub>	Sr <sup>2+</sup>		
303-U1304A-																	
1H-1, 145–150	1.45	5.15	27.25	562	7.30	4.53	36	486	11.60	51.70	9.68	169	460	0.2	5.5	22.6	
2H-1, 145–150	10.95	15.97	22.34	565	7.23	7.76	36	489	11.80	52.90	7.06	395	505	0.2	14.2	22.8	
3H-1, 145–150	20.45	27.14	19.62	565	7.20	9.55	36	496	11.90	52.30	5.82	593	523	0.3	31.3	22.6	
4H-1, 145–150	29.95	37.15	17.71	566	7.32	10.95	35	490	12.10	51.40	5.25	654	561	0.3	22.5	22.5	
5H-1, 145–150	39.45	47.71	15.08	566	7.28	12.74	35	491	11.40	52.00	4.31	853	535	0.3	4.3	21.4	
6H-1, 145–150	48.95	58.15	12.69	564	7.41	14.13	34	482	11.30	50.60	3.78	1029	565	0.4	9.8	22.0	
9H-1, 145–150	77.45	91.60	8.53	565	7.40	15.46	35	481	10.60	46.30	3.37	1267	583	0.5	4.3	23.2	
12H-1, 145–150	105.95	122.70	6.17	562	7.50	18.24	35	488	11.00	46.40	2.74	1291	607	0.8	21.6	21.3	
15H-1, 145–150	134.45	154.41	5.18	562	7.41	19.27	34	492	10.80	47.30	2.88	1372	556	1.0	6.1	22.0	
18H-1, 145–150	162.95	186.36	4.07	563	7.58	18.97	35	485	10.40	45.80	2.87	1387	500	1.2	20.5	23.9	
21H-1, 145–150	185.95	211.83	3.68	561	7.44	17.32	34	490	10.00	45.40	2.78	1341	536	1.3	23.5	24.4	
24H-1, 145–150	214.45	242.59	2.81	560	7.66	18.21	33	490	9.87	45.00	2.65	1400	518	1.6	10.6	23.9	



**Table T26.** Thermal conductivity, Hole U1304A.

Core, section	Depth (mbsf)	Thermal conductivity (W/[m·K])
303-U1304A-		
1H-4	5.25	0.771
2H-4	14.75	0.8323
3H-4	24.25	0.814
4H-4	33.75	0.781
5H-4	43.25	0.7343
6H-4	52.75	0.8373
7H-4	62.25	0.946
8H-4	71.75	0.876
9H-4	81.25	0.738
10H-4	90.79	0.753
11H-4	100.25	0.8503
12H-4	109.75	0.8617
13H-4	119.25	1.028
14H-4	128.75	0.8237
15H-4	138.25	0.9783
16H-4	147.75	0.8887
17H-4	157.24	0.9307
18H-4	166.75	0.8217
19H-2	173.26	0.761
20H-4	180.25	0.9237
21H-4	189.74	0.9383
22H-4	199.32	0.718
23H-4	208.8	0.9303
24H-4	218.25	0.691
25H-3	223.75	0.9203
26H-4	234.75	1.071